AD-A127 456 LAMINAR BOUNDARY LAYERS BEHIND BLAST AND DETONATION WAVES(U) TORONTO UNIV DOWNSVIEW (ONTARIO) INST FOR AEROSPACE STUDIES X DU ET AL. AUG 82 UTIAS-259 1/

UNCLASSIFIED AFOSR-TR-83-0271 AFOSR-82-0096 F/G 19/4 NL

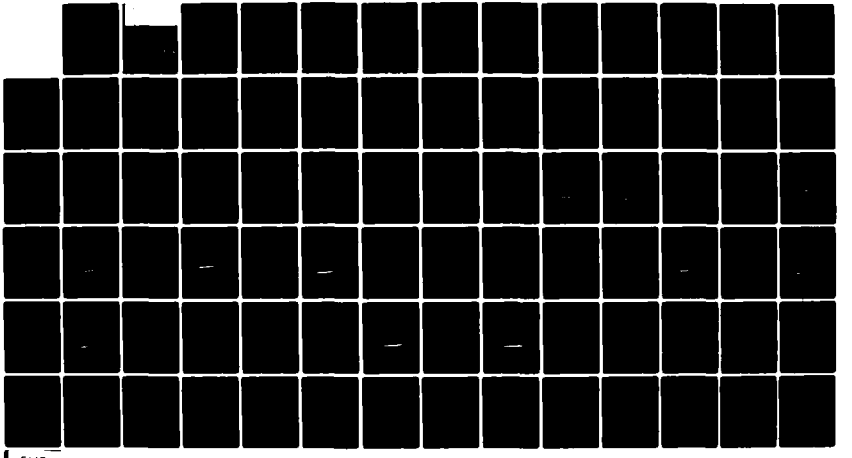

END
DATE FILMED
6-83
DTIC

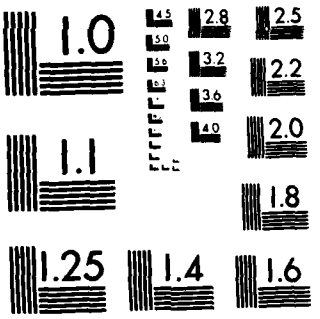

INSTITUTE
FOR
AEROSPACE STUDIES

UNIVERSITY OF TORONTO

AFOSR-TR- 83-0271

LAMINAR BOUNDARY LAYERS BEHIND BLAST AND DETONATION WAVES

by

Xixing Du, W. S. Liu and I. I. Glass

August, 1982

UTIAS Report No. 259
CN ISSN 0082-5255

UNCLASSIFIED

SECURITY CLASSIFICATION OF THIS PAGE *(When Data Entered)*

REPORT DOCUMENTATION PAGE	READ INSTRUCTIONS BEFORE COMPLETING FORM
1. REPORT NUMBER: AFOSR-TR- 83-0271 / 2. GOVT ACCESSION NO.: AD-A127456	3. RECIPIENT'S CATALOG NUMBER
4. TITLE *(and Subtitle)*: LAMINAR BOUNDARY LAYERS BEHIND BLAST AND DETONATION WAVES	5. TYPE OF REPORT & PERIOD COVERED: INTERIM
	6. PERFORMING ORG. REPORT NUMBER
7. AUTHOR(s): XIXING DU; W S LIU; I I GLASS	8. CONTRACT OR GRANT NUMBER(s): AFOSR-82-0096
9. PERFORMING ORGANIZATION NAME AND ADDRESS: UNIVERSITY OF TORONTO, DEPT OF AEROSPACE SCIENCE & ENGINEERING, 4925 DUFFERIN ST - DOWNSVIEW, ONTARIO, CN M3H 5T6	10. PROGRAM ELEMENT, PROJECT, TASK AREA & WORK UNIT NUMBERS: 61102F; 2307/A1
11. CONTROLLING OFFICE NAME AND ADDRESS: AIR FORCE OFFICE OF SCIENTIFIC RESEARCH/NA, BOLLING AFB, DC 20332	12. REPORT DATE: August 1982
	13. NUMBER OF PAGES: 78
14. MONITORING AGENCY NAME & ADDRESS*(if different from Controlling Office)*	15. SECURITY CLASS. *(of this report)*: Unclassified
	15a. DECLASSIFICATION DOWNGRADING SCHEDULE

16. DISTRIBUTION STATEMENT *(of this Report)*

Approved for Public Release; Distribution Unlimited.

17. DISTRIBUTION STATEMENT *(of the abstract entered in Block 20, if different from Report)*

18. SUPPLEMENTARY NOTES

19. KEY WORDS *(Continue on reverse side if necessary and identify by block number)*

BLAST WAVES
DETONATION WAVES
LAMINAR WALL-BOUNDARY-LAYERS
COMPARISON WITH EXPERIMENTAL DATA

20. ABSTRACT *(Continue on reverse side if necessary and identify by block number)*

The transformed coordinates devised by Mirels and Hamman have been modified in such a way that the transformed nonstationary-boundary-layer equations become applicable to boundary-layer flows induced by both blast and detonation waves moving with a power-law trajectory in planar, cylindrical and spherical geometries. Investigations were made of boundary-layer flows in air behind nonuniform strong blast waves and in the burned gas of a stoichiometric mixture of hydrogen and oxygen behind uniform Chapmar-Jouguet detona-

DD FORM 1 JAN 73 1473 EDITION OF 1 NOV 65 IS OBSOLETE

UNCLASSIFIED

SECURITY CLASSIFICATION OF THIS PAGE *(When Data Entered)*

tion waves. The results show tht the Prandtl number has a profound influence on boundary-layer flow. For a blast wave and Pr less than unity it controls a boundary-layer velocity-overshoot as one moves away from the wave. The overshoot decreases with increasing Prandtl number. For a Chapman-Jouguet detonation wave similar results are obtained for a Pr = 0.72. However, for an actual Pr = 2.26, a flow reversal occurs away from the wave where the inviscid flow velocity approaches a small value. The results also show that the viscous exponent has a significant effect on the wall shear stresses and heat transfer, and that the effect of the wall temperature is small. In order to show some of the physical features of the various boundary layers, actual velocity profiles were computed for spherical and planar detonation waves in stoichiometric hydrogen-oxygen and for blast waves in air. It is shown that owing to the rapid decrease in density behind a blast wave the boundary layer thickness becomes very much larger than their detonation-wave counterparts at the same wave velocity (but different physical conditions). In addition, the velocity-boundary-layer thickness in air behind a quasistationary planar shock wave is somewhat more than for a planar detonation wave at the same wave velocity (but in different gases). In order to test the validity of the analysis, the heat transfer to the wall behind a planar detonation wave was calculated. The profile of the variation of the heat transfer with time at any given position behind a C-J detonation wave is in good agreement with the experimental data, and adds confidence to the present analyses for cylindrical and spherical flows as well.

13

LAMINAR BOUNDARY LAYERS BEHIND BLAST AND DETONATION WAVES

by

Xixing Du, W. S. Liu and I. I. Glass

Submitted February, 1982

August, 1982

UTIAS Report No. 259
CN ISSN 0082-5255

Acknowledgements

One of us (X. X. Du) would like to express his gratitude to The Aerodynamics Research and Development Centre, Beijing, People's Republic of China, for providing this opportunity to work at UTIAS. The assistance he received from his fellows at UTIAS is very much appreciated.

We thank Dr. T. Saito for providing the random-choice computer program for solving the flow profiles behind a spherical Chapman-Jouguet detonation wave.

The financial support received from AFOSR (82-0092), the U.S. ARO and the Natural Sciences and Engineering Research Council of Canada is acknowledged with thanks.

Summary

The transformed coordinates devised by Mirels and Hamman have been modified in such a way that the transformed nonstationary-boundary-layer equations become applicable to boundary-layer flows induced by both blast and detonation waves moving with a power-law trajectory in planar, cylindrical and spherical geometries. Investigations were made of boundary-layer flows in air behind nonuniform strong blast waves and in the burned gas of a stoichiometric mixture of hydrogen and oxygen behind uniform Chapman-Jouguet detonation waves. The results show that the Prandtl number has a profound influence on boundary-layer flow. For a blast wave and Pr less than unity it controls a boundary-layer velocity-overshoot as one moves away from the wave. The overshoot decreases with increasing Prandtl number. For a Chapman-Jouguet detonation wave similar results are obtained for a Pr = 0.72. However, for an actual Pr = 2.26, a flow reversal occurs away from the wave where the inviscid flow velocity approaches a small value. The results also show that the viscous exponent has a significant effect on the wall shear stresses and heat transfer, and that the effect of the wall temperature is small.

In order to show some of the physical features of the various boundary layers, actual velocity profiles were computed for spherical and planar detonation waves in stoichiometric hydrogen-oxygen and for blast waves in air. It is shown that owing to the rapid decrease in density behind a blast wave the boundary layer thickness becomes very much larger than their detonation-wave counterparts at the same wave velocity (but different physical conditions). In addition, the velocity-boundary-layer thickness in air behind a quasistationary planar shock wave is somewhat more than for a planar detonation wave at the same wave velocity (but in different gases).

In order to test the validity of the analysis, the heat transfer to the wall behind a planar detonation wave was calculated. The profile of the variation of the heat transfer with time at any given position behind a C-J detonation wave is in good agreement with the experimental data, and adds confidence to the present analyses for cylindrical and spherical flows as well.

CONTENTS

Notation

a_∞	speed of sound ahead of the wave front
A	constant used in the transformed coordinate η
b	molecular-weight ratio $\gamma(\gamma_\infty-1)C_{p_\infty}/\gamma_\infty(\gamma-1)C_p$
B	ratio $\rho\mu/\rho_e\mu_e$
C	constant used in $x_s = Ct^m$
C_f	skin friction coefficient defined as $C_f = \tau_w/\frac{1}{2}\rho_e u_e^2$
C_p	specific heat at constant pressure
D	heat diffusivity defined as $D = K/\rho C_p$
E	internal energy
f	nondimensional stream function
F	similarity parameter, $F = p/\rho_\infty u_s^2$, for inviscid flow
g	enthalpy ratio, $g = h/h_e$ $(= T/T_e)$
h	specific enthalpy
H_1, H_2	boundary-layer-thickness coefficients
I	integral quantity defined by Eq. (14)
K	thermal conductivity
K_1	energy coefficient defined by Eq. (22)
K_2	invariant defined by Eq. (31)
m	exponent used in $x_s = Ct^m$
M_s	wave Mach number
M_{CJ}	C-J wave Mach number
n	number of chemical species
N	mole fraction of species
p	pressure
Q	chemical energy released during combustion
q	nondimensional chemical energy, $= Q/a_\infty^2$
q_w	heat flux on the wall
R	gas density ratio behind and ahead of the wave front, $R = \rho/\rho_\infty$
S	quantity defined by Eq. (21)
S_o	integral quantity defined in Eq. (66)
t	time variable
T	temperature
u	velocity component in x-direction
v	velocity component in y-direction

w	velocity ratio across the boundary layer, $w = f_\eta(\xi,\eta) = u/u_e$
x	direction along the wall surface
y	direction normal to the wall surface
α	$= (m-1)/m$
β	nondimensional speed of sound
γ	specific-heat ratio or isentropic exponent
δ	boundary-layer thickness
λ	geometric step-size ratio in η-direction
μ	viscosity
ρ	density
η	transformed coordinate
ξ	transformed coordinate
φ	velocity ratio, $\varphi = u/u_s$
χ	scalar stream function
$\bar{\sigma}$	geometric parameter for inviscid flow
σ	geometric parameter for viscous flow
ω	viscous exponent
τ	time-transformed variable
τ_w	wall shear stress

Subscripts

o	value just behind wave front, or at $\xi = 0$
∞	conditions ahead of wave front
r	reference condition
w	wall condition
e	edge of boundary layer
s	wave front

1. INTRODUCTION

This study was motivated by the existence of a unique explosive-driven-implosion facility at the Institute. Stable focussed implosions can be produced in this reliable facility yielding extremely high-pressure and temperature conditions at the focus. This facility has been used successfully for the generation of hypervelocity projectile flight and intense shock waves as well as the production of diamonds from graphite and neutrons and γ rays from deuterium fusion [Ref. 1]. The performance of the implosion chamber was investigated extensively [Refs. 2-8]. In all these investigations it was assumed that effects of viscosity and heat conductivity were negligible. However, it is important for a complete assessment of performance for the implosion chamber to evaluate the effects of the viscous boundary layer on the implosion focus. It is necessary to consider these aspects of flow in several stages. The first stage concerns the induced boundary layer behind the gaseous detonation wave in a hydrogen-oxygen mixture and is the subject of the present report.

In general, all detonations or explosions fall into two categories: structure-independent and structure-dependent. For the former, the chemical-reaction zone is very narrow immediately behind the wave front and its structure has no effect on the characteristics of the flow field behind it. For the latter the relatively long chemical-reaction zone and its structure dominate the properties of the flow field. Both types of detonation were studied extensively [Refs. 9-17]. In this study of $2H_2+O_2$ detonations only the structure-independent wave applies.

Mirels and Hamman [Ref. 18] made the first attempt to solve the laminar boundary layer behind a strong blast wave moving in a power-law path. They used a series-expansion method which was also employed later by Chen and Chung [Ref. 19]. This method is only applicable in the region near the wave front. Sichel and David [Ref. 29] made a modification of the shock-tube boundary-layer solution by Mirels [Ref. 21] and Hartunian et al [Ref. 22] to calculate the heat transfer to the wall behind a detonation wave with the assumption that the pressure, temperature and velocity behind the detonation remain constant and are equal to the C-J values. These assumptions are restrictive in describing the actual physics of the problem. Later on, numerical solutions were obtained by Liu and Mirels [Ref. 23] for different one-dimensional flows (planar, cylindrical and spherical) over the entire flow region.

In previous analyses [Refs. 18, 19, 23] for boundary-layer flows behind strong blast waves, four major assumptions were made in order to simplify the analysis: (1) The explosion wave moves with a power-law path in the time-distance plane. Consequently, similarity solutions exist for the inviscid and viscous flow fields. (2) The specific-heat ratios behind and ahead of the wave front are assumed constant and equal. This assumption is not applicable to a chemically-reacting flow where the specific-heat ratios for the unburned and burned gases are different. For example, the specific-heat ratio behind a Chapman-Jouguet (C-J) detonation wave is smaller than that of the unburned gas. Therefore, the previous analyses are not applicable to actual boundary layers behind detonation waves. (3) The dynamic viscosity coefficient of the gas behind the wave front was assumed proportional to temperature. This assumption affects the wall skin-friction and heat-transfer coefficient but not the boundary-layer structure. (4) The Prandtl number is assumed constant across the boundary layer. This assumption is reasonable since the temperature dependence of the gas thermal-conductivity is similar to the dynamic-viscosity coefficient. Some of these assumptions must be removed and the characteristics of the flow field must be taken into account for a more realistic analysis of nonstationary boundary-layer flows behind detonation waves. It will be shown subsequently that the available experimental heat-transfer data agree very well with the present analysis for planar flow. Consequently this agreement also adds confidence to the analyses of cylindrical and spherical detonation boundary-layer flows.

In this work, the last three assumptions were removed. The transformed coordinates of Mirels and Hamman [Ref. 18] were modified in such a way that their equations become applicable to flows behind blast waves as well as detonation waves.

It has been shown that direct initiation of a detonation wave requires the instantaneous release of a finite amount of ignition energy to guarantee a sufficiently strong shock wave for auto-ignition in the shocked medium. When it is ignited by an exploding wire, the detonation wave is, at least initially, overdriven, then it decays rapidly to a Chapman-Jouguet (C-J) detonation wave with a constant velocity. When such a hemispherical C-J detonation wave propagates outward along the major diameter, as shown in Fig. 1, a boundary layer forms behind it.

For C-J detonation waves, similarity solutions exist. A complete description of the method for solving C-J detonation waves is given in Ref. 13. The detailed calculations are given by Saito [Ref. 8] for detonation waves in $2H_2+O_2$ mixtures for various initial conditions. For the present application, it was necessary to recalculate the inviscid flow functions and their derivatives. In doing so, the compatibility of the solution with the boundary conditions at the outer edge of the boundary layer was ensured.

As pointed out in Refs. 8 and 13 the detonation wave is followed by a rarefaction wave and therefore all the properties of the inviscid flow behind the wave front decrease until the velocity approaches a very small value very near the half-distance that the detonation wave has travelled. Beyond that point the pressure and density remain constant and a uniform stationary state results. However, in the viscous flow behind a detonation wave the velocity boundary layer and the thermal boundary layer are both stable and grow with time in the entire region, except at the origin, where the boundary-layer equations become singular. As, according to the inviscid flow, three regions exist for the flow behind a C-J detonation wave, the solution for the boundary-layer equations must be divided into three parts corresponding to the foregoing three regions. Investigations were made, therefore, of boundary layers in air behind strong blast waves and in burned gases of stoichiometric mixtures of hydrogen-oxygen behind C-J detonation waves for different

geometries.

The effects of Prandtl number, the viscous exponent and the wall surface temperature on the flow structure are considered and discussed in detail. Comparisons have also been made between planar and spherical boundary-layer growths behind blast waves. It is shown that owing to the rarefaction wave profile behind the shock fronts the densities drop very rapidly and the boundary layers become very thick. The spherical boundary layer is thicker owing to the more rapid expansion. This phenomenon does not exist behind detonation waves (or constant speed shock waves) as the densities have finite values.

This is only a first step in trying to understand the viscous effects which exist in the UTIAS implosion facility at the focus of an implosion. As noted previously, the effects of viscosity, heat conduction and radiation are important for obtaining fusion in deuterium. However, since neutrons and γ rays have already been obtained in this facility the foregoing effects cannot be too limiting.

Although the motivation was primarily for this purpose, the present analytical-numerical results are general and can be applied to many boundary-layer flow problems behind blast and detonation waves.

2. INVISCID FLOW FIELD

2.1 Basic Equations

In a mixture of chemical species of a reacting gas, a great simplification can be made in the analysis of the inviscid flow by assuming momentum and thermal equilibria in the system. The governing equations are then reduced to three-flow equations for the mixture. The only difference in the governing equations between the unburned and burned gases is the equation of state. The basic equations describing the one-dimensional flow for the mixture are,

Mass:

$$\frac{\partial \rho}{\partial t} + \frac{1}{x^{\bar{\sigma}}} \frac{\partial}{\partial X} (\rho u x^{\bar{\sigma}}) = 0 \tag{1}$$

Momentum:

$$\frac{\partial u}{\partial t} + u \frac{\partial u}{\partial x} + \frac{1}{\rho} \frac{\partial p}{\partial x} = 0 \tag{2}$$

Energy:

$$\rho \left(\frac{\partial h}{\partial t} + u \frac{\partial h}{\partial x} \right) - \left(\frac{\partial p}{\partial t} + u \frac{\partial p}{\partial x} \right) = 0 \tag{3}$$

where $\bar{\sigma}$ is a numerical constant with values of 0, 1, 2 for planar, cylindrical and spherical symmetric inviscid flows, respectively, ρ is the mixture density, u is the flow velocity, p is the mixture pressure, h is the mixture specific enthalpy, t is the time and x is the flow direction. The wall shear stress, radiation-energy transfer and the wall heat transfer are neglected for inviscid flows.

If the chemical reaction is assumed to occur within a thin layer near the wave front, the unburned and burned gases can be treated as a perfect gas with constant specific-heat ratios γ_∞ and constant isentropic exponent γ, then

State:
$$p = \frac{\gamma - 1}{\gamma} \rho h \tag{4}$$

The isentropic exponent γ of the burnt $2H_2+O_2$ is about 1.3 at a temperature of 2,000 K and 1.04 at a temperature of 20,000 K. The pressure effect on γ is small and can be neglected when the pressure is below 10^4 atmosphere [Ref. 24].

From similarity considerations, it was shown [Refs.11,13] that for a self-similar motion the expanding wave front must either be a power law of time or an exponential function of time. For most explosion problems, the power-law form is of interest. Assume that the density ahead of the wave front, ρ_∞, is uniform and the wave front position x_s satisfies

$$x_s = Ct^m \tag{5}$$

where C and m are constants and C is determined from the energy integral equation. The following values of m are applied for explosive waves:

$$\left.\begin{aligned} m &= \frac{2}{\bar{\sigma} + 3}, \text{ for a strong blast wave} \\ m &= 1, \text{ for a Chapman-Jouguet wave} \end{aligned}\right\} \tag{6}$$

Define the following dimensionless coordinate,

$$\xi = 1 - \frac{x}{x_s} \tag{7}$$

and the dimensionless variables,

$$\left.\begin{aligned} F &= \frac{p}{\rho_\infty u_s^2} \\ R &= \frac{\rho}{\rho_\infty} \\ \varphi &= \frac{u}{u_s} \end{aligned}\right\} \tag{8}$$

where u_s is the wave front velocity which is a function of time. The following self-similarity equations result:

$$[\varphi - 1 + \xi] R_\xi + R\varphi_\xi - \frac{\bar{\sigma}\varphi R}{1-\xi} = 0 \tag{9}$$

$$[\varphi - 1 + \xi] \varphi_\xi + \frac{F_\xi}{R} - \alpha\varphi = 0 \tag{10}$$

$$[\varphi - 1 + \xi] F_\xi + \gamma F \varphi_\xi - 2\alpha F - \gamma\bar{\sigma} \frac{F\varphi}{1-\xi} = 0 \tag{11}$$

where $\xi = 0$ corresponds to the wave front and $\xi = 1$ corresponds to the origin and γ is the isentropic exponent of the gas behind the wave front. The subscript ξ denotes the derivative with respect to ξ. The parameter α is defined by

$$\alpha = \frac{m-1}{m} \tag{12}$$

where $\alpha = 0$ for a uniform wave front and $\alpha < 0$ for a decaying wave front.

Initially, we assume that a finite amount of energy E_o is released at time zero in a finite volume of dimension x_o in a medium at rest. From the energy integral, the constant C in Eq. (5) is given by [Ref.11]

$$C = \left(\frac{E_o}{m^2 \rho_\infty K_j I} \right)^{m/2} \tag{13}$$

where K_j is 1, 2π and 4π for planar, cylindrical and spherical symmetry, respectively, and I is defined by

$$I = \int_0^1 \left(\frac{F}{\gamma-1} + \frac{R\varphi^2}{2} \right) (1-\xi)^{\bar{\sigma}} d\xi \tag{14}$$

2.2 Boundary Conditions

To solve Eqs. (9)-(11), the boundary conditions immediately behind a shock or detonation wave front have to be determined. Consider the case where the shock wave moves to the right with the velocity u_s. The gas on the left side of the shock, which was stationary before being traversed by the shock, is given a velocity u_o to the right. The situation illustrated above may be transformed to the case where the shock wave is stationary. In the new frame of reference, the shock wave appears to be stationary, while the gas on the left side of the shock appears to be flowing to the left with the velocity $(u_o - u_s)$. In this frame of reference, the conservation equations across the shock front are given by:

Mass:

$$\rho_\infty u_s = \rho_o (u_s - u_o) \tag{15}$$

Momentum:

$$p_\infty + \rho_\infty u_s^2 = p_o + \rho_o (u_s - u_o)^2 \tag{16}$$

Energy:

$$h_\infty + \frac{1}{2} u_s^2 + Q = h_o + \frac{1}{2} (u_s - u_o)^2 \tag{17}$$

where Q is the chemical energy per unit mass released at the shock front. With given initial states (i.e., p_∞, ρ_∞, h_∞, γ_∞ and Q) the state immediately behind the shock front can be expressed conveniently in terms of the shock Mach number as:

$$\frac{\rho_o}{\rho_\infty} = \frac{\gamma_\infty(\gamma+1)}{\gamma\left(\gamma_\infty + \frac{1}{M_s^2} - S\right)} \tag{18}$$

$$\varphi_o = \frac{u_o}{u_s} = \frac{\gamma_\infty - \gamma\left(\frac{1}{M_s^2} - S\right)}{\gamma_\infty(\gamma+1)} \tag{19}$$

$$F_o = \frac{p_o}{\rho_\infty u_s^2} = \frac{\gamma_\infty + \frac{1}{M_s^2} + \gamma S}{\gamma_\infty(\gamma+1)} \tag{20}$$

where

$$S = \left\{ \left(\frac{\gamma_\infty}{\gamma} - \frac{1}{M_s^2} \right)^2 - K_1 \frac{1}{M_s^2} \right\}^{1/2} \tag{21}$$

$$K_1 = 2 \left\{ \frac{\gamma_\infty(\gamma-\gamma_\infty)(\gamma+1)}{\gamma^2(\gamma_\infty-1)} + \frac{\gamma_\infty^2(\gamma^2-1)}{\gamma^2} q \right\} \tag{22}$$

$$q = \frac{Q}{a_\infty^2} \tag{23}$$

$$a_\infty^2 = \gamma_\infty \frac{p_\infty}{\rho_\infty} \tag{24}$$

For a strong blast wave ($M_s \to \infty$), the boundary conditions at the wave front ($\xi = 0$) are

$$\left.\begin{aligned} \varphi_o = F_o = \frac{2}{\gamma+1} \\ R_o = \frac{\gamma+1}{\gamma-1} \end{aligned}\right\} \tag{25}$$

For a C-J detonation wave, we have $M_s = M_{CJ}$, which is defined by

$$M_{CJ}^2 = \left[\frac{\gamma_\infty}{\gamma} + \frac{K_1}{2} - K_1 \left(\frac{\gamma_\infty}{\gamma} + \frac{K_1}{4} \right)^{1/2} \right]^{-1} \tag{26}$$

and $s = 0$. The boundary conditions at the wave front are,

$$\left.\begin{aligned} \varphi_o = \frac{\gamma_\infty - \gamma M_{CJ}}{\gamma_\infty(\gamma+1)} \\ F_o = \frac{\gamma_\infty + M_{CJ}^{-2}}{\gamma_\infty(\gamma+1)} \\ R_o = \frac{\gamma_\infty(\gamma+1)}{\gamma(\gamma_\infty + M_{CJ}^{-2})} \end{aligned}\right\} \tag{27}$$

2.3 Similarity Solutions

For a strong blast wave the shock speed is time-dependent, hence the entropy change across the shock front decreases with time. The similarity conditions require an infinite strength wave. However, in practice the strong-shock approximation is adequate for shock strengths above three. The solutions for a strong blast wave can be obtained by integrating Eqs. (9)-(11) with the boundary conditions at the wave front, Eq. (25). Table 1 and Fig. 2 show the dimensionless flow profiles for a strong spherical wave with $\gamma = \gamma_\infty = 1.4$. Their corresponding derivatives are shown in Table 2 and Fig. 3. The flow is stationary only at the origin ($\xi = 1$), which is a singular point. These similarity solutions are valid because the pressure ahead of the blast wave can be neglected compared with that behind an intense explosion wave. The energy released by the explosion and the undisturbed gas density play major roles in a strong blast wave. It is noted that the pressure immediately behind the wave front decreased inversely as its radius cubed. The total energy contained in the region behind the blast wave is constant only if $p \sim x^{-3}$. For powers less than or greater than 3, energy is being added or removed continuously with time. As seen in Fig. 2, the pressure is highest immediately behind the wave front. It then decays as ξ increases, levels off, and remains approximately constant for $\xi > 0.5$. The particle velocity varies in an almost linear fashion from the wave front to the origin and vanishes at the origin. The density approaches zero for $\xi > 0.5$.

For the C-J detonation wave, it is more convenient to introduce a new variable β defined as

$$\beta = \left(\frac{\gamma F}{R} \right)^{1/2} \tag{28}$$

Then the three similarity equations (9)-(11) can be reduced to two equations in terms of Φ and β as follows [Ref.13]:

$$\Phi_\xi = - \frac{\tilde{\sigma}\Phi\beta^2}{[(\Phi-1+\xi)^2-\beta^2](1-\xi)} \tag{29}$$

$$\beta_\xi = \frac{\gamma-1}{2} \frac{\tilde{\sigma}\Phi\beta(\Phi-1+\xi)}{[(\Phi-1+\xi)^2-\beta^2](1-\xi)} \tag{30}$$

In the C-J detonation wave, the shock front propagates at a constant velocity and the entropy increase is identical for all gas particles across the wave front. The invariant then reduces to the following form:

$$\frac{R^\gamma}{F} = K_2 = \text{constant} \tag{31}$$

K_2 can be evaluated using the boundary conditions at the front, $\xi = 0$.

For the planar motion $\tilde{\sigma}$ equals zero. We can see that two solutions exist: (1) $(\Phi-1+\xi)^2-\beta^2 \neq 0$, hence both Φ_ξ and β_ξ are zero, which corresponds to a planar piston with constant speed driving a constant velocity shock or detonation wave. (2) $(\Phi-1+\xi)^2-\beta^2 = 0$, then both Φ_ξ and β_ξ are finite. Integrating Eqs. (29) and (30) we obtain the solution for $\Phi(\xi)$ and $\beta(\xi)$ with the proper signs as follows:

$$\Phi(\xi) = - \frac{2}{\gamma+1} \xi + \Phi_o \tag{32}$$

$$\beta(\xi) = - \frac{\gamma-1}{\gamma+1} \xi + \beta_o \tag{33}$$

where (for the C-J condition)

$$\Phi_o + \beta_o = 1 \tag{34}$$

The subscript o denotes the value at $\xi = 0$. Using Eqs. (28) and (31), we get

$$R = \left(\frac{\beta^2 K_2}{\gamma} \right)^{\gamma-1} \tag{35}$$

$$F = \frac{\beta^2}{\gamma} R \tag{36}$$

If Φ_o and β_o are known, using Eqs. (32), (33), (35) and (36), Φ, R, F can be calculated; Φ_o and β_o are determined from Eqs. (27) and (28).

For the cylindrical and spherical detonation wave, $\tilde{\sigma} \neq 0$, $\Phi_o + \beta_o = 1$. This results in $\Phi_\xi \to -\infty$ and $\beta_\xi \to -\infty$ at the front, $\xi = 0$. Therefore, we cannot integrate Eqs. (29) and (30) directly from the boundary of the C-J detonation wave front. To overcome this difficulty, the perturbation method is used [Ref.13]. The solution, in the form of a perturbation series, in the immediate neighbourhood of the C-J front is given by the following expressions (with proper signs):

$$\Phi(\xi) = \Phi_o - \left(\frac{2\tilde{\sigma}\Phi_o\beta_o}{\gamma+1} \right)^{1/2} \xi^{1/2} + \ldots \tag{37}$$

$$\beta(\xi) = \beta_o - \frac{(\gamma-1)}{2} \left(\frac{2\tilde{\sigma}\Phi_o\beta_o}{\gamma+1} \right)^{1/2} \xi^{1/2} + \ldots \tag{38}$$

With Eqs. (37) and (38) the values $\Phi(o+\Delta\xi)$ and $\beta(o+\Delta\xi)$ can be calculated from the values Φ_o and β_o, where $\Delta\xi$ is very small. From these values, $\Phi(o+\Delta\xi)$ and $\beta(o+\Delta\xi)$, Eqs. (29) and (30) can then be integrated to obtain $\Phi(\xi)$ and $\beta(\xi)$. Using Eqs. (35) and (36), $R(\xi)$ and $F(\xi)$ are also obtained.

A stoichiometric mixture of hydrogen and oxygen was used. The specific heats, specific-heat ratios, isentropic exponent and equilibrium sound speed for the unburned and burned gases are given by Benoit [Ref. 24].

In the Chapman-Jouguet detonation wave the shock front propagates at a constant velocity and the entropy increase for all gas particles across the

wave front are identical. Table 3 and Figs. 4-6 show the dimensionless pressure, velocity and density profiles behind the planar, cylindrical and spherical C-J detonation waves with initial conditions of p_∞ = 13.6 atm, γ_∞ = 1.4 and T_∞ = 300 K. The corresponding derivatives which are needed in the boundary-layer analysis are shown in Table 4 and Figs. 7-9. It is noted that there are three regions. From the wave front (ξ = 0) to ξ = 0.48 is the expansion region and from ξ = 0.48 to the origin is the stationary zone. The particle velocity decreases sharply from its maximum value at ξ = 0 to zero at ξ = 0.48. Similar to the blast wave, the pressure behind the wave front decreases as ξ increases and then remains constant for ξ > 0.48. However, the gas density resembles the pressure profile and does not approach zero close to the wave midpoint. It can be seen from Figs. 7-9 that a discontinuity exists in the flow derivatives at the position where the particle velocity is zero. The flow derivatives also approach an infinite value at the detonation-wave front. As mentioned previously, at the origin the basic equations are singular.

3. VISCOUS FLOW FIELD

3.1 Governing Equations for Laminar Boundary-Layer Flows

The laminar boundary layer behind a strong blast wave moving with nonuniform velocity was investigated by Mirels et al [Refs.18, 23] and Chen and Chang [Ref. 19]. The laminar boundary layer behind a detonation wave has not been solved as yet. As mentioned in the Introduction, the last three assumptions made by Mirels et al [Ref. 18] are not applicable to a detonation-wave induced boundary layer. In order to generalize the analysis, these assumptions are modified: (1) The specific heats and the specific-heat ratios behind and ahead of the wave front are different, but constant in each region. (2) The Prandtl number may be variable across the boundary layer. (3) The temperature dependence of the dynamic-viscosity coefficient of the gas behind the wave front has a power law variation with temperature. Other assumptions are made that the chemical reaction takes place only at the C-J detonation-wave front and that the gases behind and ahead of the detonation wave are perfect. Therefore, the equations governing the laminar boundary-layer flow induced by a wave front are as follows:

$$\frac{\partial \rho}{\partial t} + \frac{1}{x^\sigma}\frac{\partial}{\partial x}(\rho u x^\sigma) + \frac{\partial}{\partial y}(\rho v) = 0 \tag{39}$$

$$\rho\frac{Du}{Dt} + \frac{\partial p}{\partial x} = \frac{\partial}{\partial y}\left(\mu\frac{\partial u}{\partial y}\right) \tag{40}$$

$$\rho\frac{Dh}{Dt} - \frac{Dp}{Dt} = \frac{\partial}{\partial y}\left(\frac{\mu}{Pr}\frac{\partial h}{\partial y}\right) + \mu\left(\frac{\partial u}{\partial y}\right)^2 \tag{41}$$

where

$$\frac{D}{Dt} = \frac{\partial}{\partial t} + u\frac{\partial}{\partial x} + v\frac{\partial}{\partial y}$$

and σ is a boundary-layer-type parameter, with a value 0 for plane flow and 1 for axisymmetric flow. The pressure p is constant in the y-direction, which is normal to the surface or flow-direction x. The velocities u and v are along the x and y-directions, respectively, and Pr is the Prandtl number. The temperature dependence of the dynamic-viscosity coefficient μ is assumed to be of the form:

$$\mu = \mu_r\left(\frac{T}{T_r}\right)^\omega \tag{42}$$

where the subscript r denotes a reference value and ω is the viscous exponent.

3.2 Transformed Boundary-Layer Equations

The following transformed coordinates were used by Mirels et al.

$$\xi = 1 - \frac{x}{x_s} \tag{43}$$

$$\eta = \frac{x^\sigma\int_0^y \frac{\rho}{\rho_\infty}\,dy}{[At^{2m(\sigma+1)-1}\xi]^{1/2}} \tag{44}$$

where $A = 2mF_0C^{2(\sigma+1)}\nu_\infty\rho_\infty/p_\infty$, $\nu_\infty = \mu_\infty/\rho_\infty$. As mentioned previously this set of transformed coordinates cannot be used in chemical-reacting flows. By defining the transformed coordinate η as

$$\eta = \frac{x^\sigma\int_0^y \frac{\rho}{\rho_\infty}\,dy}{[At^{2m\sigma+2\omega(m-1)+1}\xi]^{1/2}} \tag{45}$$

where $A = 2C^{2(\sigma+\omega)}m^{2\omega-1}\mu_\infty(bF_0\rho_\infty/p_\infty)^\omega/\rho_\infty$, C is given by Eq. (13), F_0 is given by Eqs. (25) or (27) and $b = [\gamma(\gamma_\infty-1)/\gamma_\infty(\gamma-1)]C_{p_\infty}/C_p$ is the molecular weight ratio of the gases behind and ahead of the wave front, then η is applicable to chemical-reacting flows as well as non-reacting flows. It can be shown that when ω = 1, b = 1 and $\gamma = \gamma_\infty$ then A and η become identical to those given by Mirels and Hamman [Ref.18].

Define the following dimensionless variables:

$$f(\xi,\eta) = \int_0^\eta \frac{u}{u_e}\,d\eta$$
$$g(\xi,\eta) = \frac{h}{h_e} \tag{46}$$

where the subscript e denotes the edge of the boundary layer. Since the pressure is constant in the y-direction, the density ratio is given by

$$\frac{\rho_e}{\rho} = g(\xi,\eta) \tag{47}$$

If a scalar stream function ψ is now introduced such that

$$u = \frac{\rho_\infty}{\rho x^\sigma}\frac{\partial\psi}{\partial y} \tag{48}$$

$$v = \frac{\nu_\infty}{\rho x^\sigma}\left[\frac{\partial\psi}{\partial x} + \frac{\partial}{\partial t}\left(x^\sigma\int_0^y\frac{\rho}{\rho_\infty}\,dy\right)\right] \tag{49}$$

The continuity equation is then satisfied automatically. It is not difficult to show that the relationship between the scalar stream function ψ and the dimensionless variable $f(\xi, \eta)$ is given by

$$\psi = u_e \left[A t^{2m\omega+2m(\omega-1)+1} \xi \right]^{1/2} f(\xi, \eta)$$

Applying the transformed coordinates, dimensionless variables and the relationship between ψ and f to Eqs. (39) to (41), the transformed boundary-layer equations are then obtained,

$$(1-\xi)^{2\sigma} R^{1-\omega} \left\{ \frac{F}{F_o} \right\}^{\omega} (Bf_{\eta\eta})_{\eta} + (\eta-\varphi f) f_{\eta\eta}$$
$$= 2\xi \left\{ \left[f\varphi_{\xi} + \varphi f_{\xi} - \frac{n}{2} [2\sigma + \alpha(2\omega-1)] \right] f_{\eta\eta} \right.$$
$$\left. + \alpha + (1-\xi-\varphi f_{\eta}) \left\{ \frac{\varphi_{\xi}}{\varphi} + \frac{f_{\eta\xi}}{f_{\eta}} \right\} \right] f_{\eta} - \frac{F_{\xi} g}{R\varphi} \Bigg\} \qquad (50)$$

$$(1-\xi)^{2\sigma} \left\{ R^{1-\omega} \left\{ \frac{F}{F_o} \right\}^{\omega} \left\{ \frac{B}{Pr} g_{\eta} \right\}_{\eta} \right.$$
$$+ \frac{\gamma-1}{\gamma} \frac{R\varphi^2}{F} R^{1-\omega} \left\{ \frac{F}{F_o} \right\}^{\omega} Bf_{\eta\eta}^2 \Bigg\} + (\eta-\varphi f) g_{\eta}$$
$$= 2\xi \left\{ \left[f\varphi_{\xi} + \varphi f_{\xi} - \frac{n}{2} [2\sigma + \alpha(2\omega-1)] \right] g_{\eta} \right.$$
$$\left. + \left[\frac{2\alpha}{\gamma} + (1-\xi-\varphi f_{\eta}) \left\{ \frac{g_{\xi}}{g} + \frac{F_{\xi}}{\gamma F} - \frac{R_{\xi}}{R} \right\} \right] g \right\} \qquad (51)$$

where α is defined by Eq. (12), the values F, R, φ and their derivatives F_{ξ}, R_{ξ} and φ_{ξ} are obtained from Eqs. (9) to (11), the subscripts η and ξ denote the derivatives with respect to η and ξ, and B is defined by

$$B \equiv \frac{\rho\mu}{\rho_e \mu_e} = g^{\omega-1} \qquad (52)$$

It can be shown that if $\omega = 1$ (i.e., $B = 1$) and Pr = constant, Eqs. (50) and (51) reduce to those derived by Mirels and Hamman [Ref.18]. (The details can be found in Appendix A.)

The required boundary conditions are given by

$y = 0$: $u(x, 0, t) = 0$

$v(x, 0, t) = 0$

$h(x, 0, t) = h_{\omega}(x, t)$ (53)

$y = \infty$: $u(x, \infty, t) = u_e(x, t)$

$h(x, \infty, t) = h_e(x, t)$ (54)

After the transformation, they become

$\eta = 0$: $f(\xi, 0) = f_{\eta}(\xi, 0) = 0$

$g(\xi, 0) = g_w(\xi)$ (55)

$\eta = \infty$: $f_{\eta} = 1$

$g = 1$ (56)

where the subscript w denotes the wall surface. It should be noted that from the definition of g_w

$$g_w \equiv \frac{h_w}{h_e} = \frac{T_w}{T_{\infty}} \left[\frac{RP_{\infty}}{bF\rho_{\infty} u_s^2} \right] = \frac{T_w}{T_{\infty}} \left(\frac{R}{b\gamma_{\infty} F M_s^2} \right) \qquad (57)$$

the value

$$\frac{T_w}{T_{\infty}} \cdot \frac{1}{u_s^2} \quad \text{or} \quad \frac{T_w}{T_{\infty}} \cdot \frac{1}{M_s^2}$$

should be a function of ξ only, for a self-similar boundary-layer flow. Therefore, two cases exist:

(1) For a strong blast wave, according to its definition, we have

$$\frac{1}{M_s^2} \to 0$$

so that $g_w = 0$.

(2) For the C-J detonation wave, we have $M_s^2 = M_{CJ}^2 =$ constant. Consequently, g_w is a function of ξ only.

It should be noted that for the strong blast wave or for the so-called cold-wall model (i.e., $T_w = 0$) the viscous exponent ω has to be unity. Otherwise, Eqs. (50) and (51) will be singular at the wall.

3.3 Numerical Method and Procedure

The nonlinear equations, (50) and (51), with the boundary conditions given by Eqs. (55) and (56), were solved numerically by an implicit six-point finite-difference scheme developed in Ref. 25. The initial profiles are required for a finite-difference method. Consequently, the solution at the start of the boundary layer has to be obtained first. At $\xi = 0$, the partial-differential equations, Eqs. (50) and (51), become a set of ordinary-differential equations as follows:

$$R^{(1-\omega)} (F/F_o)^{\omega} (Bf_{\eta\eta})_{\eta} + (\eta-\varphi f) f_{\eta\eta} = 0 \qquad (58)$$

$$R^{(1-\omega)} (F/F_o)^{\omega} \left[\left[\frac{B}{P_r} g_{\eta} \right]_{\eta} + \frac{\gamma-1}{\gamma} \frac{R\varphi^2}{F} Bf_{\eta\eta}^2 \right]$$
$$+ (\eta-\varphi f) g_{\eta} = 0 \qquad (59)$$

Equations (58) and (59) were solved using the Newton-Raphson method, or a shooting method.

Equations (50) and (51) are linearized in a form suitable for an iteration scheme by introducing the following function

$$W = \frac{\partial f}{\partial \eta} \qquad (60)$$

It is really only required for the momentum equa-

tion and not for the energy equation. The momentum equation in terms of W can be written as

$$(1-\xi)^{2\sigma_R^{1-\omega}}(F/F_o)BW_{\eta\eta}^{(p)}$$

$$+\left\{(1-\xi)^{2\sigma_R^{1-\omega}}(F/F_o)^{\omega}B_{\eta}+(\eta-\varphi f)\right.$$

$$\left.-2\xi\left[f\varphi_{\xi}+\Phi f_{\xi}-\frac{\eta}{2}\left[2\sigma+\alpha(2\omega-1)\right]\right]\right\}W_{\eta}^{(p)}$$

$$-2\xi\left[\alpha+(1-\xi-\varphi W)\frac{\Phi_{\xi}}{\Phi}\right]W^{(p)}$$

$$=2\xi(1-\xi-\varphi W)W_{\xi}^{(p)}-2\xi\frac{F_{\xi}g}{R\Phi} \qquad (61)$$

and the energy equation in the linearized form is

$$(1-\xi)^{2\sigma_R^{1-\omega}}(F/F_o)^{\omega}\frac{B}{P_r}g_{\eta\eta}^{(p)}$$

$$+(1-\xi)^{2\sigma_R^{1-\omega}}(F/F_o)^{\omega}\left(\frac{B}{P_r}\right)_{\eta}+(\eta-\varphi f)$$

$$-2\xi\left[f\varphi_{\xi}+\Phi f_{\xi}-\frac{\eta}{2}\left[2\sigma+\alpha(2\omega-1)\right]\right]g_{\eta\eta}^{(p)}$$

$$-2\xi\left[\frac{2\alpha}{\gamma}+(1-\xi-\varphi W)\left(\frac{F_{\xi}}{\gamma F}-\frac{R_{\xi}}{R}\right)\right]g^{(p)}$$

$$=2\xi(1-\xi-\varphi W)g_{\xi}^{(p)}-(1-\xi)^{2\sigma}\frac{\gamma-1}{\gamma}\frac{R\Phi^2}{F}R^{1-\omega}(F/F_o)^{\omega}BW_{\eta}^2 \qquad (62)$$

where superscript p denotes the order of the iteration process and the quantities without the superscript denote those evaluated at the (P-1) iteration order.

A computer program was written based on the numerical scheme outlined in Ref. 25 and Eqs. (61) and (62) were solved for four cases of practical interest. The results are presented in Section 4. In this method, either equal intervals or nonequal intervals can be used in the η-direction. The interval in the η-direction is increased in a geometric progression as

$$\frac{\Delta\eta_{i+1}}{\Delta\eta_i}=\lambda$$

where λ is a constant set with a value slightly greater than unity and i is the index of the η-coordinate for the difference net. There are two differences in the numerical procedure between the present work and Liu and Mirels [Ref. 23]. First, in this work the momentum equation (50) is transformed into a second-order differential equation through a function defined by Eq. (60). The numerical method of Blottner [Ref. 26], which was applied by them, introduced a transformed normal velocity and retained the continuity equation in order to avoid third-order derivatives in the momentum equation. Second, Liu and Mirels used an interpolation method in the inviscid flow values which appear in the coefficients of the boundary-layer equations. Consequently, the compatibility conditions at the edge of the boundary layer are not satisfied. In order to avoid a discontinuity in the gradients of the dependent variables at the edge of the boundary layer, they were forced to select a curve for η_e in their numerical procedure. The boundary-layer profiles were then recalculated using the selected η_e distribution. However, in the present work the inviscid flow equations, Eqs. (9)-(11), and the boundary-layer equations, Eqs. (50) and (51), are solved simultaneously with the same step size $\Delta\xi$. No interpolation errors are introduced and the compatibility conditions are satisfied. The selection of an η_e distribution is not necessary in this work. The advantage of the present numerical procedure is the reduction of the number of convergent iterations for the nonlinear differential equations and the consequent computation costs.

In the calculations, 80 mesh points were used in the η-direction with $\lambda = 1.02$ and an initial step size $\Delta\eta = 0.026$. The step size $\Delta\xi = 0.002$ was applied. Normally two or three iterations were required to converge the solution within an error of 10^{-5}.

3.4 Boundary-Layer Characteristics

The relations between the transformed coordinates (ξ, η) and the physical coordinates (x,y,t) are given by Eqs. (43) and (45),

$$x = x_s(1-\xi)$$

$$y = H_1(t)H_2(\xi)S_o(\xi,\eta) \qquad (63)$$

where

$$H_1=\left[\frac{u_s^{2\omega-1}x_s}{\rho_{\infty}}\mu_{\infty}\left(b\frac{\rho_{\infty}}{p_{\infty}}F_o\right)^{\omega}\right]^{1/2} \qquad (64)$$

$$H_2=\frac{(2\xi)^{1/2}}{(1-\xi)^{\sigma_R}} \qquad (65)$$

$$S_o=\int_o^{\eta}g\,d\eta \qquad (66)$$

The boundary-layer thickness δ_e, displacement thickness δ^* and the momentum thickness θ are expressed by

$$\delta_e=H_1H_2\int_o^{\eta_e}g\,d\eta \qquad (67)$$

$$\delta^*=\int_o^{\infty}\left(1-\frac{\rho u}{\rho_e u_e}\right)dy=H_1H_2S_1 \qquad (68)$$

$$\theta=\int_o^{\infty}\frac{\rho u}{\rho_e u_e}\left(1-\frac{u}{u_e}\right)dy=H_1H_2S_2$$

where

$$S_1=\int_o^{\eta_e}(g-f_{\eta})d\eta \qquad (69)$$

$$S_2=\int_o^{\eta_e}f_{\eta}(1-f_{\eta})d\eta \qquad (70)$$

and η_e is the value of η at the edge of the boundary layer.

From the definition of the shear stress τ_w and the skin-friction coefficient c_f:

$$\tau_w = \mu_w \left(\frac{\partial u}{\partial y} \right)_w \tag{71}$$

$$C_f = \frac{\tau_w}{\frac{1}{2} \rho_e u_e^2} \tag{72}$$

the dimensionless skin friction coefficient is expressed by

$$C_f \sqrt{Re} = \left(\frac{2}{\Phi} \right)^{\frac{1}{2}} \left(\frac{F}{F_o} \right)^{\frac{\omega}{2}} R^{\frac{1}{2}(1-\omega)} (1-\xi)^{\sigma} B_w f_{\eta\eta}(\xi,0) \tag{73}$$

where the Reynolds number Re is given by

$$Re = \left(\frac{p_\infty R}{b \rho_\infty u_s^2 F} \right)^{\omega} \frac{\rho_\infty}{\mu_\infty} R u_e x_s \xi \tag{74}$$

The heat transfer at the wall is given by

$$q_w = -K_w \left(\frac{\partial T}{\partial y} \right)_w = - \frac{1}{Pr_w} \mu_w \left(\frac{\partial \eta}{\partial y} \right)_w h_e g_\eta(\xi,0) \tag{75}$$

where K is the thermal conductivity of gas. With the definition of Stanton number St:

$$St = \frac{q_w}{\rho_e u_e H_e} \tag{76}$$

where $H_e = h_e + (1/2)u_e^2$. The normalized expression for wall heat transfer is

$$St \sqrt{Re} = - \frac{1}{Pr_w} \left(\frac{F}{F_o} \right)^{\frac{\omega}{2}} \left(\frac{R^{1-\omega}}{2} \right)^{\frac{1}{2}} \frac{(1-\xi)^{\sigma}}{\Phi \left(1 + \frac{\gamma-1}{2\gamma} \frac{R\Phi^2}{F} \right)} B_w g_\eta(\xi,0) \tag{77}$$

3.5 Properties of Hydrogen-Oxygen Stoichiometric Mixtures

A stoichiometric mixture of hydrogen and oxygen is taken as the working fluid. The properties of the unburned and burned gases, i.e., the gases behind and ahead of the detonation wave, are taken from Ref. 24. The chemical-reaction equation is as follows:

$$2H_2 + O_2 \rightleftarrows N_1 H_2O + N_2 OH + N_3 H_2 + N_4 O_2 + N_5 H + N_6 O$$

where N_1, N_2, ..., denote molar concentrations of H_2O, OH, ..., in the burned gases.

The initial conditions of the stoichiometric mixture of hydrogen and oxygen are $p_\infty = 13.6$ atm, $T_\infty = 298.15°K$, $\gamma_\infty = 1.4$ and $u_s = 2.9815 \times 10^5$ cm/sec.

The thermal conductivity and kinetic viscosity for the unburned and burned gases are calculated using the semi-empirical relations outlined in Ref. 30:

$$K = \sum_{i=1}^{n} \frac{N_i K_i}{\sum_{j=1}^{n} N_j \Phi_{ij}} \tag{78}$$

for the thermal conductivity of the burned gas, and

$$\mu = \sum_{i=1}^{n} \frac{N_i \mu_i}{\sum_{j=1}^{n} N_j \Phi_{ij}} \tag{79}$$

for the viscosity of burned gas, where

$$\Phi_{ij} = \frac{\left[1 + \left(\frac{\mu_i}{\mu_j} \right)^{1/2} \left(\frac{M_j}{M_i} \right)^{1/4} \right]^2}{\sqrt{8} \left(1 + \frac{M_i}{M_j} \right)^{1/2}} \tag{80}$$

and N, μ, K, M are the mole fraction, viscosity, conductivity and molecular weight of the species, respectively. Subscripts i and j denote the ith and jth species. The details of the calculation are given in Appendix B.

3.6 Discussion of Boundary-Layer Equations

As stated before, three regions are considered in treating the boundary layer behind a C-J detonation wave. For the expansion region from $\xi = 0$ to $\xi \cong 0.5$, the inviscid flow plays a significant role in the development of the boundary layer. Equations (50) and (51) are applied directly. For the stagnation region from $\xi \cong 0.5$ to $\xi \cong 0.95$, because the velocity approaches a very small value, Eqs. (50) and (51) become

$$(1-\xi)^{2\sigma} R^{1-\omega} \left(\frac{F}{F_o} \right)^{\omega} (B f_{\eta\eta})_\eta + \eta f_{\eta\eta}$$

$$= 2\xi \left\{ - \frac{\eta}{2} [2\sigma + \alpha(2\omega-1)] f_{\eta\eta} + \alpha f_\eta + (1-\xi) f_{\eta\xi} \right\} \ldots \tag{81}$$

$$(1-\xi)^{2\sigma} R^{1-\omega} \left(\frac{F}{F_o} \right)^{\omega} \left(\frac{B}{Pr} g_\eta \right)_\eta + \eta g_\eta$$

$$= 2\xi \left\{ - \frac{\eta}{2} [2\sigma + \alpha(2\omega-1)] g_\eta + \frac{2\alpha}{\gamma} g + (1-\xi) g_\xi \right\} \ldots \tag{82}$$

In the region from $\xi = 0.95$ to $\xi = 1$, the solution is given by

$$T(y,t) = (T_e - T_w) \operatorname{erf}(y/\sqrt{4Dt}) + T_w \tag{83}$$

where T is temperature, $\operatorname{erf}(y/\sqrt{4Dt})$ is the error function and

$$D = \frac{K}{\rho C_p} \tag{84}$$

where C_p is the specific heat of the gas. The temperature gradient at the wall decreases in proportion to $t^{-1/2}$. In the initial phase, the temperature gradient is so large that a temperature jump exists at the wall. Details of the derivation of Eq. (83) are given in Appendix C.

Three interesting observations may be made regarding Eqs. (50) and (51). First, as mentioned above, the equations are singular at $\xi = 1$. The solution near $\xi = 1$ is more of analytical interest, as the boundary-layer concept is not valid. Second, the effect of the viscous exponent ω on the boundary layer depends on the inviscid solutions R and (F/F_o). When $\omega < 1$, the gas viscosity and thermal-conduction effects increase as ω increases. Third, the coupling between the momentum and energy equations is through B and the last term on the right-hand side of Eq. (50) and the second term on the right-hand side of Eq. (51).

It is convenient to rewrite Eqs. (50) and (51) in the general form

$$\alpha_1 W_{\eta\eta} + \alpha_2 W_\eta + \alpha_3 W + \alpha_4 = \alpha_5 W_\xi \qquad (85)$$

where the α_1 are the coefficients and W stand for f_η and g. Equation (85) has the same form as the heat conduction equation. The coefficient α_5, which plays the same role as the thermal diffusivity in the heat-conduction equation, is negative in regions of reverse flow. For axisymmetric boundary-layer flows (i.e., $\sigma = 1$), α_1 becomes very small when $\xi = 1$. It means that the viscosity and thermal conduction effects become very small when $\alpha_1 \doteq 0$. When $\alpha_1 = 0$, Eq. (85) is no longer parabolic, but hyperbolic. Consequently, all numerical methods for solving the boundary-layer equations fail in this case. The simple heat-conduction equation can then be applied.

The unsteady effect on the boundary-layer development can be estimated as follows. Consider the boundary layer induced by a uniform wave (i.e., wave velocity is constant, or $m = 1$). The steady-state boundary-layer equations are:

$$(1-\xi)^{2\sigma_R 1-\omega}\left(\frac{F}{F_o}\right)^{\omega}(Bf_{\eta\eta})_\eta - \varphi f f_{\eta\eta}$$
$$= 2\xi[f\varphi_\xi - \varphi f_\xi]f_{\eta\eta} - \varphi f_\eta^2\left(\frac{\varphi_\xi}{\varphi} + \frac{f_{\eta\xi}}{f_\eta}\right) - \frac{F_\xi g}{R\varphi} \qquad (86)$$

$$(1-\xi)^{2\sigma_R 1-\omega}\left(\frac{F}{F_o}\right)^{\omega}\left[\left(\frac{B}{Pr}\,g_\eta\right)_\eta + \frac{\gamma-1}{\gamma}\frac{R\varphi^2}{F}Bf_{\eta\eta}^2\right] - fg_\eta$$
$$= 2\xi(f\varphi_\xi + \varphi f_\xi)g_\eta - \varphi f_\eta\left(\frac{g_\xi}{g} + \frac{F_\xi}{\gamma F} - \frac{R_\xi}{R}\right)g \qquad (87)$$

Comparing Eqs. (50) and (51) with $m \neq 1$ and Eqs. (86) and (87), it can be shown that the unsteady effect can be neglected only when the following conditions are satisfied:

(1) $(1+2\xi\sigma)\eta \ll |\varphi f + 2\xi(f\varphi_\xi + \varphi f_\xi)|$

(2) $1-\xi \ll \varphi f_\eta$

The nonuniformity of the wave front increases the unsteady effect on the boundary-layer structure. The order of magnitude for the unsteady terms depends on the inviscid flow characteristics and it is difficult to estimate.

4. BOUNDARY-LAYER DEVELOPMENT BEHIND EXPLOSIVE WAVES

4.1 Boundary Layer Behind Strong Blast Waves

Three sets of solutions were obtained. The first set was for the boundary layer induced by a spherical strong blast wave. In order to check the numerical procedure applied here, the case with $\gamma = \gamma_\infty = 1.4$, $\omega = 1$, $b = 1$, $g_w = 0$ and $Pr = 0.72$ behind a spherical blast wave was examined. Results were obtained beyond $\xi = 0.95$. Figures 10 and 11 show the normalized velocity and temperature profiles. For comparison, the corresponding results obtained by Liu and Mirels [Ref. 23] are shown in Fig. 12. It can be seen that agreement between the two sets of results is excellent. Further tabular comparisons are given in Tables 5 and 6. Agreement of the present results with the series expansion results [Ref.18] for the wall derivatives at $\xi = 0$ is better than those obtained by Liu and Mirels [Ref. 23].

The thermal boundary-layer thickness is larger than the velocity boundary-layer thickness since $Pr < 1$ was applied. As ξ increases, the velocity gradient increases at a rate which is larger than that for the temperature gradient. Consequently, a velocity overshoot occurs. Results of other cases with different Pr indicate that (1) the velocity overshoot decreases as Pr increases, (2) there is no flow reversal when the Pr is varied from 0.72 to more than 3, because the density decreases rapidly with ξ. It can be seen from Figs. 10 and 11 that the velocity and thermal boundary-layer thicknesses decrease with η_e as ξ increases (the actual thickness increases with ξ). They become zero at the origin ($\xi = 1$). Therefore, $f_\eta = 1$ for all η at $\xi = 1$.

4.2 Boundary Layer Behind C-J Detonation Waves

A second set of solutions was determined for the C-J detonation wave in a stoichiometric mixture of hydrogen-oxygen with $\omega = 0.75$, $Pr = 2.26$, $T_w = T_\infty = 300°K$, $\gamma = 1.14$, $\gamma_\infty = 1.4$ and $p_\infty = 13.6$ atm for different flow geometries. The distance used from the origin to the wave front is 10 cm (corresponding to the implosion chamber wall) and the wave velocity is 2982 m/s. Figures 13 to 20 show the normalized velocity and temperature distributions across the boundary layer for the planar, cylindrical and spherical inviscid flows. The wall derivatives are shown in Table 7 and in Figs. 21 to 24. From the results presented above, the following observations are made: (1) Flow reversal occurs for all cases with $Pr = 2.26$ when ξ is greater than 0.4. The magnitude of the flow reversal increases as $\bar{\sigma}$ and σ increase. As a result, it has a maximum flow reversal for the spherical flow geometry, i.e., for $\bar{\sigma} = 2$ and $\sigma = 1$. (2) The velocity gradient at the wall increases as ξ increases and reaches a maximum value at ξ between 0.2 and 0.25 and then decreases with ξ increasing. (3) For the case with $\sigma = 1$, the wall temperature gradient increases at a rate

greater than for $\sigma = 0$, as ξ increases. (4) The thickness of the velocity boundary layer is greater than that of the thermal boundary layer.

A third set of solutions was obtained for a spherical C-J detonation wave in a stoichiometric mixture of hydrogen-oxygen ($T_\infty = 300°K$, $\gamma = 1.14$, $\gamma_\infty = 1.4$ and $p_\infty = 13.6$ atm) with different thermal properties.

As mentioned before, for Pr > 1, flow reversal exists when $\xi > 0.3$. In order to examine the effect of the Prandtl number on the flow structure, other cases with Pr = 1.5, Pr = 1.0 and Pr = 0.72 were also studied. Figures 25 to 30 show the normalized velocity and temperature for different Prandtl numbers. From these figures, including Fig. 19, it can be seen that for Pr > 1, the magnitude of the flow reversal decreases with Pr decreasing, whereas for Pr < 1, the flow reversal disappears and a velocity overshoot occurs. The magnitude of velocity overshoot increases as the Pr decreases. It is clearly shown in Fig. 27 that for Pr = 1 neither a flow reversal nor a velocity overshoot exists. Figures 31 and 32 show the wall derivatives of velocity and temperature, respectively. It can be seen from Fig. 31 that when Pr < 1, $f_{\eta\eta}(\xi,0)$ increases monotonically with ξ increasing. However, when Pr > 1, $f_{\eta\eta}(\xi,0)$ increases at first and reaches a maximum value at about $\xi = 0.23$, then decreases to a negative value. Separation is said to occur when the derivative $f_{\eta\eta}(\xi,0)$ changes from a positive to a negative value. The boundary-layer thicknesses of velocity and temperature are shown in Fig. 33. It is shown that when Pr > 1, the velocity boundary layer thickness increases slightly as Pr increases, whereas the thermal boundary-layer thickness decreases considerably. It implies that when Pr > 1, more kinetic energy of flow is lost from the mainstream than when Pr < 1. Due to imbalance between the velocity and thermal boundary-layer thicknesses, the flow is forced to separate at the wall or to have a velocity overshoot at the edge of the boundary layer. This separation is not observed in the blast-wave case.

Table 8 shows the variation of the thicknesses of velocity and temperature with Pr. It was found that the ratio of the velocity boundary-layer thickness to the thermal boundary-layer thickness is proportional to the square root of the Prandtl number, as shown for a steady plane boundary-layer flow [Ref. 27]. For the spherical C-J detonation wave, it can be seen from Table 8 that when Pr > 1, the velocity boundary-layer thickness is greater than for the temperature layer. When Pr < 1, the converse statement is true and when Pr = 1, the two thicknesses are identical.

The effect of the viscous exponent and the surface temperature on the boundary-layer flow was also investigated. The normalized velocity and temperature profiles are shown in Figs. 34 and 35 for the case of $\omega = 1$, and in Figs. 36 and 37 for the case of $T_w = 0$, respectively. The effects of ω and T_w on the velocity and temperature gradients are shown in Table 9 and in Figs. 38 to 41. It can be seen from Table 9 and Figs. 38 to 41 that: (1) when ω changes from 0.75 to 1, the velocity and temperature gradients on the wall increase by a factor of nearly 1.8. (2) The wall-temperature effect on the wall gradients is not significant.

The thermal boundary-layer thickness growing on the wall of the major diameter of the UTIAS hemispherical implosion chamber was obtained numerically from Eqs. (50) and (51), and analytically from Eq. (83). Figure 42 shows the variation of the thermal boundary-layer thickness with ξ just when the detonation wave reaches the hemispherical wall of the implosion chamber at 34 μsec from initiation, and Fig. 43 shows the variation with time at the origin for the case of $T_\infty = 300°K$, b = 1.26, F = 0.1511, R = 0.67, $u_s = 2982$ m/s and $x_s = 10$ cm. The predicted thermal boundary-layer thickness using the analytical solution is about 0.054 mm at the origin, which is very close to 0.058 mm predicted numerically.

4.3 Some Discussions on Boundary-Layer Thickness

Figure 44 shows the variation of boundary-layer thicknesses for C-J spherical and planar detonation waves in $2H_2+O_2$, and strong spherical and planar blast waves in air under the same initial conditions and wave velocity u_s and wave position x_s. For a comparison, the constant speed nonstationary planar shock-wave case in air is also shown in Fig. 44. The initial conditions are: $p_\infty = 13.6$ atm, $T_\infty = 300°K$, wave speed $u_s = 2981.7$ m/sec, and wave position $x_s = 10$ cm. It can be seen from Fig. 44 that the variation of the boundary-layer thickness with distance behind the wave behaves quite differently for a C-J detonation wave, a strong blast wave and a constant speed planar shock wave. It is helpful to recall the relation for the boundary-layer thickness, Eq. (67),

$$\delta = \left[\frac{u_s^{2\omega-1} x_s}{\rho_\infty} \mu_\infty \left(b \frac{\rho_\infty}{p_\infty} F_o \right)^\omega \right]^{1/2} \frac{(2\xi)^{1/2}}{(1-\xi)^\sigma R} \int_0^{\eta_e} g\,d\eta \quad (67)$$

in order to understand these variations. We can see from Eq. (67) that the density ratio plays a very important role in the development of the boundary layer behind a given wave front. For a C-J detonation wave when $\xi > 0.5$, the velocity of the inviscid flow becomes very small, but it does not matter because the density and pressure remain at reasonable levels. For a constant speed planar shock wave, $\sigma = 0$, R = constant and $\int_0^{\eta_e} g\,d\eta$ is also constant (that is, similarity exists and the boundary-layer profiles are identical anywhere), therefore the boundary-layer thickness δ can be expressed as

$$\delta = c\sqrt{\xi}$$

where c is a constant. For the strong blast wave, however, when $\xi > 0.5$, the density ratio becomes very small (as shown in Table 1 and Fig. 2). It means that when $\xi > 0.5$, the inviscid flow is so rarefied that the boundary layer gets comparatively thick (as shown in Fig. 44). Consequently, the assumptions made in derivation of the boundary-layer equations would cease to apply and the plots in Fig. 44 for these cases for larger distances from the wave are no longer of physical interest.

4.4 Heat Transfer to the Wall behind a Detonation Wave in $2H_2+O_2$ Mixture

The relation for calculating wall heat transfer

behind a C-J detonation wave moving into a stationary mixture of $2H_2+O_2$ is given by (see Appendix D)

$$q_w = -B_1 \cdot B_2(t)^{-0.5} \tag{68}$$

where

$$B_1 = \frac{\gamma}{\gamma-1} \frac{g_w^{\omega-1}(g_\eta)_w}{\sqrt{2}\ Pr} \left\{ F^{2+\omega} \left(\frac{TT}{F_o R} \right)^{\omega} \right\}^{1/2} (1-\xi)^{\sigma} \tag{69}$$

$$B_2 = u_{CJ}^2 (\rho_\infty \mu_\infty)^{0.5} \tag{70}$$

It can be seen that B_1 is a function of ξ only. It decreases as ξ increases from 0 to 1. For planar flow with $\sigma = 0$ it reduces to the following form

$$B_1 = \frac{\gamma}{\gamma-1} \frac{g_w^{\omega-1}(g_\eta)_w}{\sqrt{2}\ Pr} \left\{ F^{2+\omega} \left(\frac{TT}{R_o R} \right)^{\omega} \right\}^{1/2} \tag{71}$$

while B_2 represents the effects of the initial conditions. For the structure-independent detonation u_{CJ} is a function of the initial conditions only. From the expression for B_1, it can be seen that q_w is also a function of position. For a given position x, ξ can be expressed as

$$\xi = \frac{u_{CJ}t}{x+u_{CJ}t} \tag{72}$$

where x is the distance of the point considered from the initiation position. Figure 45 shows the variation of heat transfer to the wall with time t, at different positions for plane flow. Also shown in Fig. 45 are the experimental results from Ref. 28. The agreement between the analytical-numerical results and the experimental data is satisfactory. A better relation for the temperature-viscosity might even improve the agreement.

To check the influence of the initial conditions on heat transfer, calculations were also done for the variation of the average heat transfer over given periods of time for different pressures p_∞, and is shown in Fig. 46. The crosses, closed and open circles shown in Fig. 46 represent similar experimental results from Ref. 29. It can be seen from Fig. 46 that the relation between heat transfer and initial pressure is not linear and does not justify the conclusion in Ref. 29 that it is linear.

As shown in Ref. 8, the structure-independent detonation inviscid flow properties in a $2H_2+O_2$ mixture are very insensitive to the initial conditions. For example, the detonation speed changes from 2.59 km/sec to 3.08 km/sec, the temperature from 2934 K to 4645 K, and the pressure ratio from 16 to 21.8 even when the initial pressure changes from 0.01 atm to 100 atm at an initial temperature of 298.15 K. To simplify the procedure of calculation an average value of B_1 was taken in calculating the heat transfer with reasonable approximation. Figure 47 shows a comparison of the present results with experimental and other analytical results from Ref. 15. It can be seen that present analysis is in very good agreement with the experimental data of Ref. 27 over the entire 200 μsec. However, it only agrees well with the data of Ref. 15 from about 150 to 200 μsec. For structure-independent detonations, as shown in Fig. 49, velocity, pressure and density behind the wave front decrease rapidly, then the values of p and ρ level off to a finite value at about $\xi = 0.5$. However, the velocity after $\xi = 0.5$ becomes so small that only conduction heat transfer becomes dominant. That may be the main reason why the present laminar boundary-layer analysis gives a good representation of the variation of heat transfer to the wall with time behind C-J detonation waves.

5. CONCLUSIONS

A modification to the transformed coordinates of Mirels and Hamman [Ref. 18] makes it possible to apply the transformed equations to flows behind either blast or Chapman-Jouguet detonation waves. It was shown that the Prandtl number controls a reversed-flow phenomenon at the wall and a velocity overshoot near the edge of the boundary layer. No flow reversal occurs in the blast-wave case. The effect of Prandtl number on flow reversal in the blast-wave case is not as significant as in the detonation-wave case. The magnitude of the velocity overshoot for the Chapman-Jouguet detonation-wave case is larger than that for the blast-wave case. The viscous exponent ω has a significant effect on the wall skin friction and heat transfer. For $\omega < 1$, the value of wall derivatives reduces by a factor of $(F/RF_o)^{1-\omega}$ as ω decreases. The effect of wall temperature T_w is found to be small. At lower wall temperatures the flow reversal is delayed to some extent, compared to the higher wall temperature.

To test the analysis, the results of heat transfer to the wall behind a planar detonation wave moving into a stationary mixture of $2H_2+O_2$ were computed and the variation of heat transfer with time was compared with experimental data at different positions from the initiation point. Very good agreement was obtained between the present numerical results and the experimental data. This lends confidence to the present analytical-numerical work which is less restrictive in its assumptions and models the actual flow more realistically than has been done previously.

The boundary layer behind a detonation wave may undergo transition to a turbulent one. Consequently, a complete boundary-layer solution through the transition and turbulent flow is very difficult and must be done in stages, as noted in the Introduction. For the strong blast wave, the density behind the wave front decreases so rapidly that the inviscid flow becomes very rarefied and the boundary-layer thickness increases very quickly in a short distance (say, $0 < \xi < 0.3$) away from the wave front. Consequently, the boundary-layer concept may no longer be valid in the region beyond $\xi > 0.3$. To illustrate this point several boundary-layer profiles have been plotted (Fig. 44) and discussed. The present report represents the first of several stages as noted above in the solution of the boundary layer in the UTIAS implosion chamber. Nevertheless, the results are applicable to many other problems.

REFERENCES

1. Glass, I. I. and Sagie, D., "Application of Explosive-Driven Implosions to Fusion", Phys. Fluids, Vol. 25, No. 2, Feb. 1982, pp. 269-270.

2. Kennedy, J. E. and Glass, I. I., "Multipoint Initiated Implosions from Hemispherical Shells of Sheet Explosive", UTIAS Tech. Note No. 99, 1966.

3. Flagg, R. F., "Explosive-Driven, Spherical Implosion Waves", Phys. Fluids, Vol. 11, No. 10, Oct. 1968, pp. 2282-2284. Also UTIAS Report No. 125, June 1967.

4. Elsenaar, A., "A Numerical Model for a Combustion-Driven Spherical Implosion Wave", UTIAS Tech. Note No. 144, 1969.

5. Macpherson, A. K., "A Preliminary Study of Spherical Detonation Wave Symmetry in Stoichiometric Hydrogen-Oxygen Mixtures", UTIAS Tech. Note No. 154, 1970.

6. Macpherson, A. K., "A Preliminary Monte-Carlo Analysis of the Reflection of an Imploding Hemispherical Shock Wave Similar to that Generated in the UTIAS Implosion-Driven Hypervelocity Launcher or Shock Tube", UTIAS Report No. 152, 1970.

7. Glass, I. I., "Shock and Combustion Wave Dynamics in an Implosion-Driven Hypervelocity Launcher", UTIAS Review No. 25, 1965.

8. Saito, T., "An Experimental, Analytical and Numerical Study of Temperature Near Hemispherical Implosion Foci", UTIAS Report No. 260 (to be published).

9. Taylor, G., "The Formation of a Blast Wave by a Very Intense Explosion (I. Theoretical Discussion)", Proc. Royal Society A, Vol. 201, March 22, 1950.

10. Latter, R., "A Similarity Solution for a Spherical Shock Wave", J. Appl. Phys., Vol. 26, No. 8, 1955.

11. Sedov, L. I., "Similarity and Dimensional Methods in Mechanics", Academic Press, 1959.

12. Mirels, H., in Advances in Applied Mechanics, 7, Academic Press, New York, 1962.

13. Lee, J. H., Knystautas, R. and Bach, G. G., "Theory of Explosions", MERL Report 69-10, AFOSR 69-3090 TR, Nov. 1969.

14. Sichel, M., "Modeling of Gaseous and Heterogeneous Detonation Phenomena", Trans. 27th Conf. of Army Mathematicians, 1982.

15. Ragland, K. W., "The Propagation and Structure of Two Phase Detonations", University of Michigan, Ph.D. Thesis, 1967.

16. Paillard, C., et al, "Pressure and Wall Heat Transfer Behind a Hydrogen/Azide Detonation Wave in Narrow Tubes", Gasdynamics of Detonations and Explosions, AIAA, New York, 1981, pp. 134-149.

17. Sichel, M., "A Hydrodynamic Theory for the Propagation of Gaseous Detonations Through Charges of Finite Width", AIAA J., Vol. 4, No. 2, Feb. 1966.

18. Mirels, H. and Hamman, J., "Laminar Boundary Layer Behind Strong Shock Moving with Nonuniform Velocity", J. Phys. Fluids 5, 1962, pp. 91-96.

19. Chen, C. J. and Chang, L. M., "Unsteady Compressible Laminar Boundary Layer Flow Behind a Plane Blast Wave", AIAA 11th Thermophysics Conf., San Diego, California, July 1976.

20. Sichel, M. and David, T. S., "Transfer Behind Detonations in $2H_2+O_2$ Mixtures", AIAA J., Vol. 4, No. 6, 1966, pp. 1089-1090.

21. Mirels, H., "The Wall Boundary Layer Behind a Moving Shock Wave", Symposium, Aug. 26-29, 1957, pp. 283-293.

22. Hartunian, R. A., Russo, A. L. and Marrone, P. V., "Boundary Layer Transition and Heat Transfer in Shock Tubes", J. Aerospace Sci., 27, 1960, pp. 587-594.

23. Liu, S. W. and Mirels, H., "Numerical Solutions for Unsteady Laminar Boundary Layer Behind Blast Waves", Phys. Fluids, Vol. 23(4), 1980, pp. 681-688.

24. Benoit, A., "Properties of Chapman-Jouguet Detonations in Stoichiometric Hydrogen-Oxygen Mixtures Diluted with Helium and Hydrogen", UTIAS Tech. Note No. 104, 1966.

25. Glass, I. I. and Liu, W. S., "Effects of Hydrogen Impurities on Shock Structure and Stability in Ionizing Monatomic Gases. Part 1, Argon", J. Fluid Mech. Vol. 84, Part 1, 1978, pp. 55-77.

26. Blottner, F. G., "Finite Difference Methods of Solution of the Boundary Layer Equations", AIAA J. 8, 1970, pp. 193-205.

27. Schlichting, H., "Boundary Layer Theory", McGraw Hill Book Co. Inc., New York, 1968, pp. 99-102.

28. Laderman, A. J., Hecht, G. J. and Oppenheim, A. K., "Thin Film Thermometry in Detonation Research", Temperature - Its Measurement and Control, in Science and Industry, Vol. 3, Part 2, 1962.

29. Edwards, D. H., Brown, D. R., Hooper, G. and Jones A. T., "The Influence of Wall Heat Transfer on the Expansion Following a C-J Detonation Wave", J. Phys. D: Appl. Phys. 3, 1970, pp. 365-376.

30. Bird, R. B. et al, "Transport Phenomena", John Wiley and Son Inc., New York, 1963.

31. Carslaw, H. S. and Jaeger, J. C., "Conduction of Heat in Solids", Oxford University Press, London, 1950.

Table 1

Inviscid Flow Solution Behind a Strong Spherical Blast Wave

ξ	$\bar{\sigma} = 2$, $m = 2/5$		
	φ	F	R
0.00	0.8333	0.8333	6.0000
0.10	0.68486	0.4231	1.2318
0.20	0.58374	0.33714	0.39251
0.30	0.50309	0.31324	0.13251
0.40	0.42927	0.30656	0.40661×10^{-1}
0.50	0.35738	0.30495	0.10284×10^{-1}
0.60	0.28596	0.30464	0.19214×10^{-2}
0.70	0.21472	0.30460	0.22055×10^{-3}
0.80	0.14384	0.30460	0.10238×10^{-4}
0.90	0.075392	0.30460	0.40588×10^{-7}

Table 2

Flow Derivatives Behind a Strong Spherical Blast Wave

ξ	$\bar{\sigma} = 2$, $m = 2/5$		
	φ_ξ	F_ξ	R_ξ
0.00	1.8056	13.028	125.000
0.10	1.1956	2.2153	15.560
0.20	0.87500	0.58514	4.2368
0.30	0.75925	0.16773	1.4782
0.40	0.72435	0.43694×10^{-1}	0.51333
0.50	0.71549	0.9187×10^{-2}	0.15468
0.60	0.71326	0.13726×10^{-2}	0.36112×10^{-1}
0.70	0.71136	0.11818×10^{-3}	0.55426×10^{-2}
0.80	0.70435	0.36594×10^{-5}	0.39075×10^{-3}
0.90	0.63478	0.73131×10^{-8}	0.35366×10^{-5}

The derivatives are all negative.

Table 3

Solution for Inviscid Flow Field Behind C-J Detonation Wave

	$\bar{\sigma} = 0$, m = 1			$\bar{\sigma} = 1$, m = 1			$\bar{\sigma} = 2$, m = 1		
ξ	Φ	F	R	Φ	F	R	Φ	F	R
0.00	0.4544	0.47752	1.8328	0.4544	0.47752	1.8328	0.45440	0.4775	1.8328
0.05	0.40772	0.43301	1.6821	0.34050	0.36820	1.4595	0.30781	0.33779	1.3534
0.10	0.36105	0.39234	1.5430	0.28650	0.32261	1.3000	0.24717	0.28807	1.1773
0.15	0.31437	0.35527	1.4146	0.24088	0.28807	1.1773	0.19961	0.25350	1.0527
0.20	0.26769	0.32151	1.2962	0.19917	0.25966	1.0750	0.15871	0.22697	0.9556
0.25	0.22101	0.29077	1.1870	0.15984	0.23552	0.98700	0.12222	0.20576	0.8769
0.30	0.17434	0.26281	1.0865	0.12234	0.21474	0.91035	0.089251	0.18851	0.8122
0.35	0.12766	0.23738	0.99388	0.086556	0.19684	0.84356	0.059572	0.17450	0.7591
0.40	0.08098	0.21428	0.90866	0.052765	0.18155	0.78591	0.033490	0.16146	0.7092
0.45	0.034304	0.19329	0.83026	0.021685	0.16881	0.73742	0.012032	0.15504	0.6845

Table 4

Derivatives of Inviscid Parameters Behind C-J Detonation Wave

	$\bar{\sigma} = 0$, m = 1			$\bar{\sigma} = 1$, m = 1			$\bar{\sigma} = 2$, m = 1		
ξ	Φ_ξ	F_ξ	R_ξ	Φ_ξ	F_ξ	R_ξ	Φ_ξ	F_ξ	R_ξ
0.00	0.93356	0.93355	3.1361	$-\infty$ (53.840)	$-\infty$ (53.827)	$-\infty$ (180.92)	$-\infty$ (75.720)	$-\infty$ (75.702)	$-\infty$ (254.51)
0.05	0.93356	0.85156	2.8958	1.2399	1.1030	3.8274	1.4515	1.2615	4.4247
0.10	0.93356	0.77633	2.6727	0.97132	0.77469	2.7328	1.0467	0.8045	2.8783
0.15	0.33356	0.70735	2.4655	0.86560	0.62075	2.2208	0.87356	0.59808	2.1741
0.20	0.93356	0.64412	2.2732	0.80745	0.52153	1.8902	0.76941	0.47150	1.7377
0.25	0.93356	0.58620	2.0949	0.76743	0.44701	1.6399	0.69293	0.38147	1.4232
0.30	0.93356	0.53317	1.9295	0.73318	0.38556	1.4309	0.62663	0.31085	1.1725
0.35	0.93356	0.48465	1.7763	0.69719	0.33137	1.2432	0.55954	0.25079	0.95509
0.40	0.93356	0.44028	1.6344	0.65220	0.28050	1.0630	0.48058	0.19507	0.74903
0.45	0.93356	0.39972	1.5030	0.58542	0.22807	0.87216	0.36919	0.13595	0.52541

The derivatives are all negative.

Table 5

Comparison of Wall Derivatives Obtained by Three Different Numerical Methods

	$f_{\eta\eta}(\xi,0)$			$G_{\eta}(\xi,0)$		
ξ	Series Expansion Method	Liu and Mirels Solution	Present	Series Expansion Method	Liu and Mirels Solution	Present
0.0	0.66141	0.66198	0.66147	0.89693	0.89864	0.89735

Table 6

Comparison of Wall Derivatives of Liu and Mirels (1980) and Present Work for a Boundary Layer Behind a Strong Blast Wave

	$f_{\eta\eta}(\xi,0)$		$g_{\eta}(\xi,0)$	
ξ	Liu and Mirels	Present	Liu and Mirels	Present
0.00	0.66198	0.66147	0.89864	0.89735
0.10	0.99598	0.99520	0.71326	0.70950
0.20	1.4215	1.4210	0.6506	0.6486
0.30	2.0170	2.0170	0.67915	0.6789
0.40	2.8813	2.8800	0.8664	0.8692
0.50	4.03096	4.0240	1.2942	1.2980
0.60	5.52177	5.5090	1.8290	1.8400
0.70	7.94119	7.9040	2.61496	2.6490
0.80	12.7369	12.570	4.o957	4.3220
0.90	27.2309	25.26	9.0235	9.770

Table 7

Comparison of Wall Derivatives for Different Cases Behind a Chapman-Jouguet Wave

(T_w = 300 K, γ = 0.75, Pr = 2.26)

	$\bar{\sigma}$ = 0	σ = 0	$\bar{\sigma}$ = 1	σ = 0	$\bar{\sigma}$ = 1	σ = 1	$\bar{\sigma}$ = 2	σ = 1
ξ	$f_{\eta\eta}(\xi,0)$	$g_\eta(\xi,0)$	$f_{\eta\eta}(\xi,0)$	$g_\eta(\xi,0)$	$f_{\eta\eta}(\xi,0)$	$g_\eta(\xi,0)$	$f_{\eta\eta}(\xi,0)$	$g_\eta(\xi,0)$
0.0	0.4023	0.6354	0.4023	0.6354	0.4023	0.6354	0.4023	0.6354
0.05	0.4149	0.6506	0.4421	0.6883	0.4673	0.7269	0.4800	0.7482
0.10	0.4292	0.6699	0.4586	0.7191	0.5145	0.8043	0.5275	0.8369
0.20	0.4467	0.7101	0.4656	0.7742	0.5943	0.9806	0.5882	1.0330
0.30	0.4293	0.7587	0.4083	0.8314	0.6069	1.2120	0.5190	1.2830
0.40	0.2145	0.8194	0.05685	0.8947	0.1353	1.5320	-0.3740	1.6190
0.45	-0.5084	0.8537	-0.9738	0.9248	-1.7140	1.7410	-3.6520	1.8320
0.50	-0.1279	0.8895	-0.4341	0.9596	-0.8039	1.9860	-2.3680	2.0820
0.60	0.2235	0.9310	0.04352	0.9994	0.2114	2.6110	-0.9636	2.7320
0.70	0.4271	0.9585	0.3287	1.0270	1.2560	3.6320	0.3380	3.7980
0.80	0.5605	0.9783	0.5208	1.0470	2.9270	5.7040	2.2290	5.9640
0.90	0.6513	0.9933	0.6577	1.0620	7.6860	12.1500	7.3090	12.690
0.95	0.6836	0.9996	0.7111	1.0690	17.360	24.350	17.430	25.250

Table 8

Ratios of Boundary Layer Thicknesses for Different Prandtl Number, Pr

	Pr=0.72	Pr=1.0	Pr=1.5	Pr=2.256
ξ	δ_V/δ_T	δ_V/δ_T	δ_V/δ_T	δ_V/δ_T
0.00				
0.10	0.8644	1.000	1.377	1.791
0.20	0.7695	1.000	1.303	1.749
0.30	0.6486	1.000	1.364	1.702
0.40	0.3456	1.000	1.454	1.833
0.50	0.2129	1.000	1.541	1.862
0.60	0.2676	1.000	1.490	1.858
0.70	0.2677	1.000	1.522	1.812
0.80	0.4186	1.000	1.514	1.941
0.90	0.6416	1.000	1.278	2.263
0.95	0.7407	1.000	1.5120	2.158

Table 9

Wall Derivatives for Different Flow Conditions Behind a Chapman-Jouguet Wave

($\bar{U}$ = 2, σ = 1)

	T_w=300 K		T_w=300 K		T_w=300 K		T_w=0.0	
	ω=0.75	Pr=2.256	ω=0.75	Pr=0.72	ω=1.00	Pr=2.256	ω=1.0	Pr=2.256
ξ	$f_{\eta\eta}(\xi,0)$	$g_\eta(\xi,0)$	$f_{\eta\eta}(\xi,0)$	$g_\eta(\xi,0)$	$f_{\eta\eta}(\xi,0)$	$g_\eta(\xi,0)$	$f_{\eta\eta}(\xi,0)$	$g_\eta(\xi,0)$
0.0	0.4023	0.6354	0.4171	0.3352	0.7281	1.115	0.7281	1.195
0.05	0.4800	0.7482	0.5296	0.4038	0.8675	1.309	0.8774	1.412
0.10	0.5275	0.8369	0.6125	0.4558	0.9505	1.456	0.9716	1.577
0.20	0.5882	1.0330	0.7985	0.5699	1.061	1.785	1.123	1.941
0.30	0.5190	1.2830	1.058	0.7147	0.9547	2.199	1.123	2.400
0.40	-0.3740	1.6190	1.567	0.9091	-0.5231	2.751	0.0631	3.007
0.45	-3.652	1.8320	2.540	1.032	-0.6002	3.1010	-0.4284	3.389
0.50	-2.368	2.0820	3.138	1.172	-4.079	3.500	-3.203	3.821
0.60	-0.9636	2.7320	3.541	1.525	-1.834	4.526	-1.318	4.935
0.70	0.3380	3.7980	4.152	2.101	0.2729	6.161	0.6444	6.714
0.80	2.2290	5.9640	5.533	3.67	3.247	9.322	3.538	10.161
0.90	7.3090	12.690	10.15	6.928	10.52	18.08	10.76	19.70
0.95	17.430	25.250	19.72	14.57	22.85	31.75	23.04	34.59

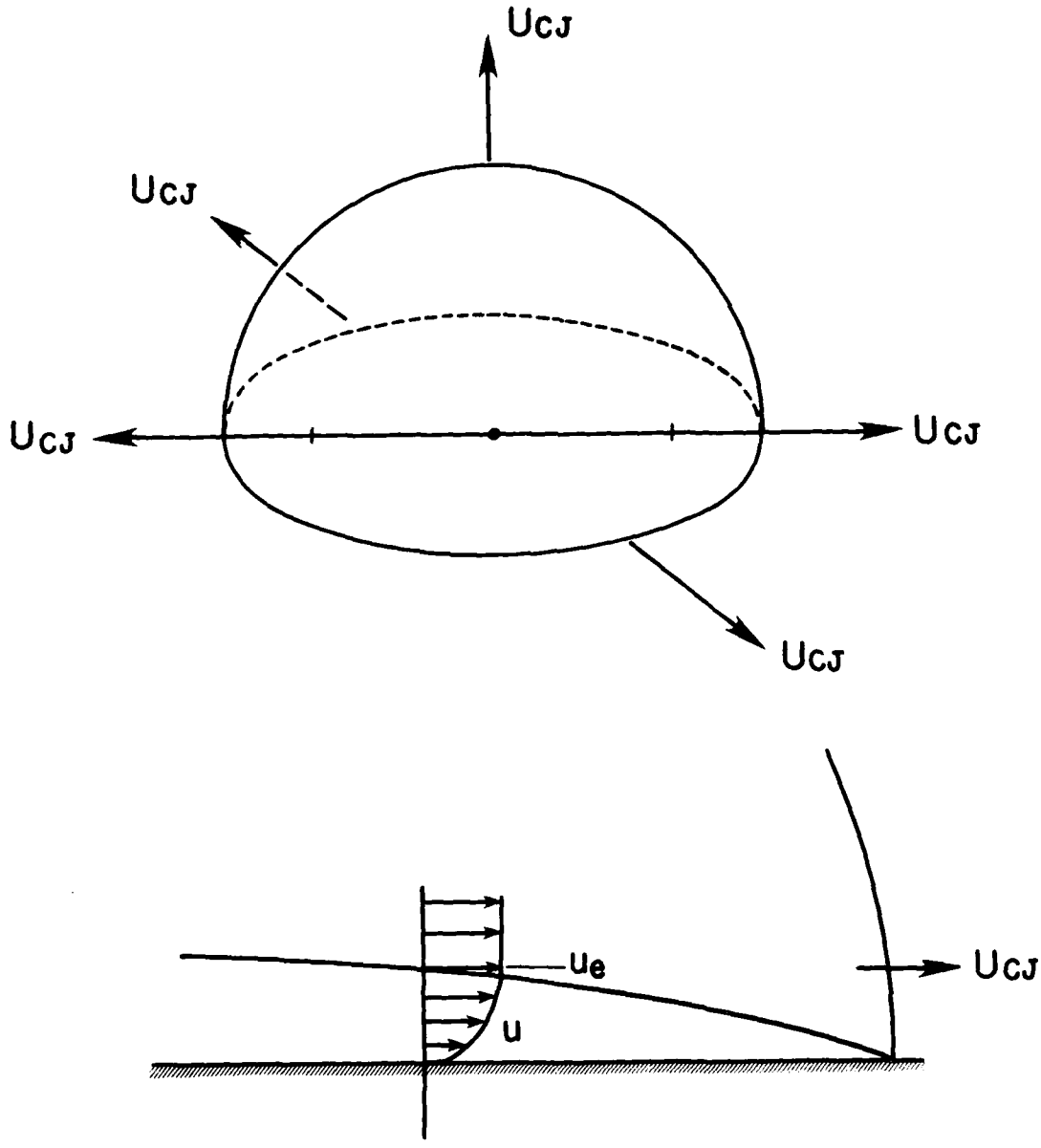

FIG. 1 SKETCH OF BOUNDARY LAYER INDUCED BY HEMISPHERICAL DETONATION WAVE ON THE MAJOR DIAMETER OF UTIAS IMPLOSION CHAMBER.

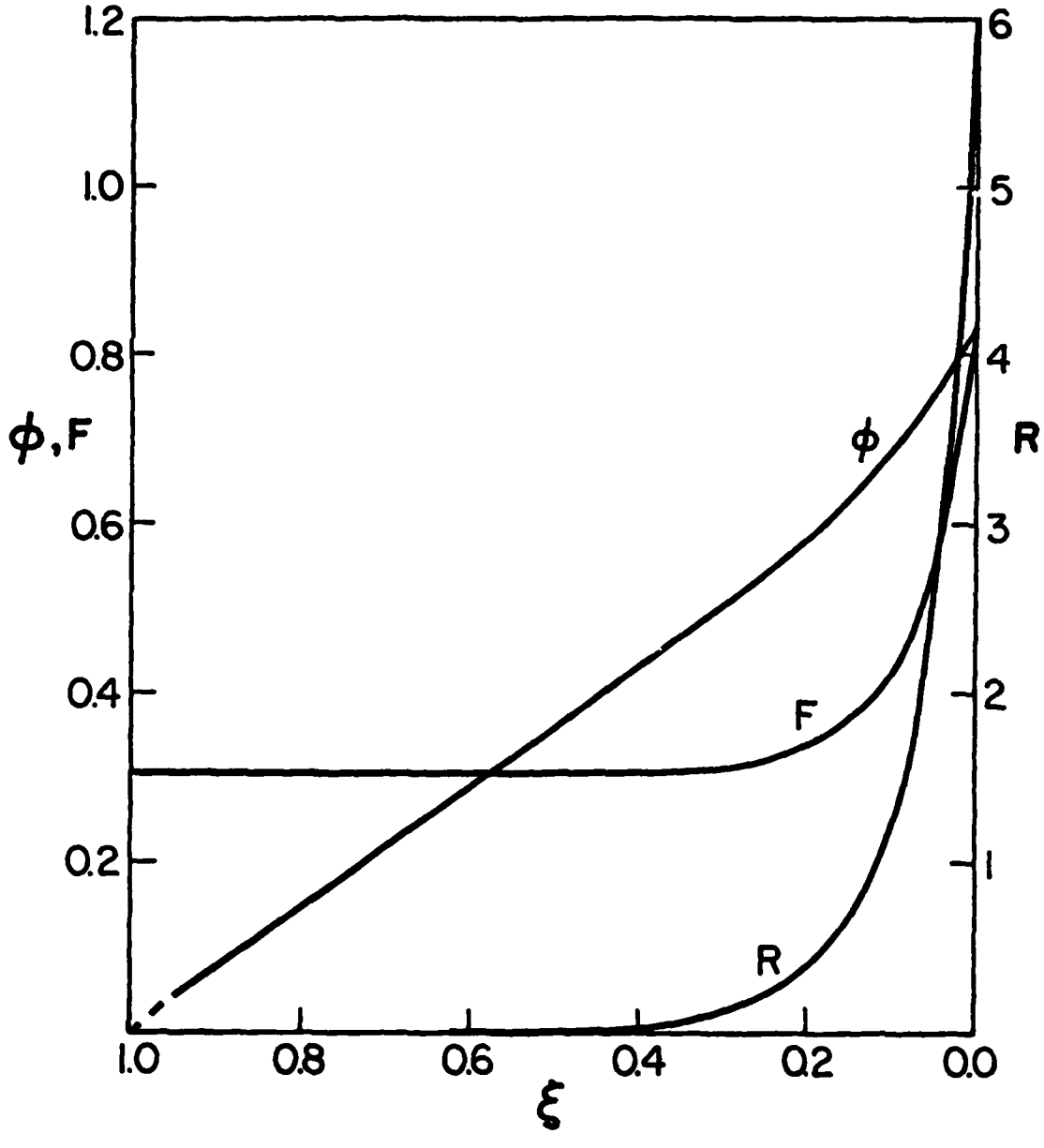

FIG. 2 NORMALIZED INVISCID FLOW PROFILE [illegible] A STRONG SPHERICAL BLAST WAVE FOR DENSITY R, PRESSURE [illegible] AND FLOW VELOCITY φ WITH DISTANCE ξ.

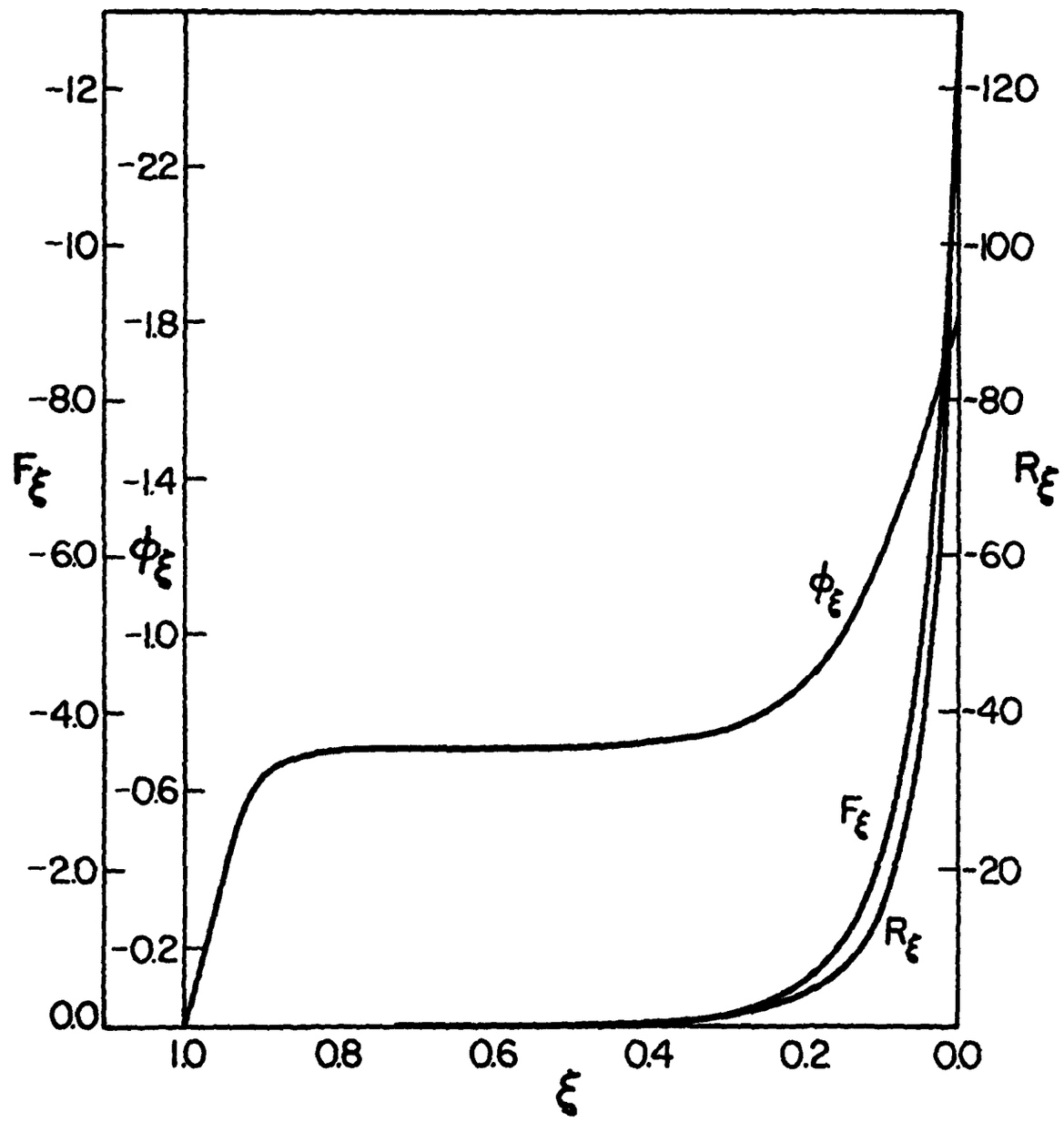

FIG. 3 NORMALIZED PRESSURE DERIVATIVE F_ξ, VELOCITY DERIVATIVE φ_ξ AND DENSITY DERIVATIVE R_ξ FOR INVISCID FLOW BEHIND A STRONG SPHERICAL BLAST WAVE WITH DISTANCE ξ AT $\xi = 0$, $\varphi_\xi = 1.8056$, $F_\xi = 13.028$, $R_\xi = 1.25$.

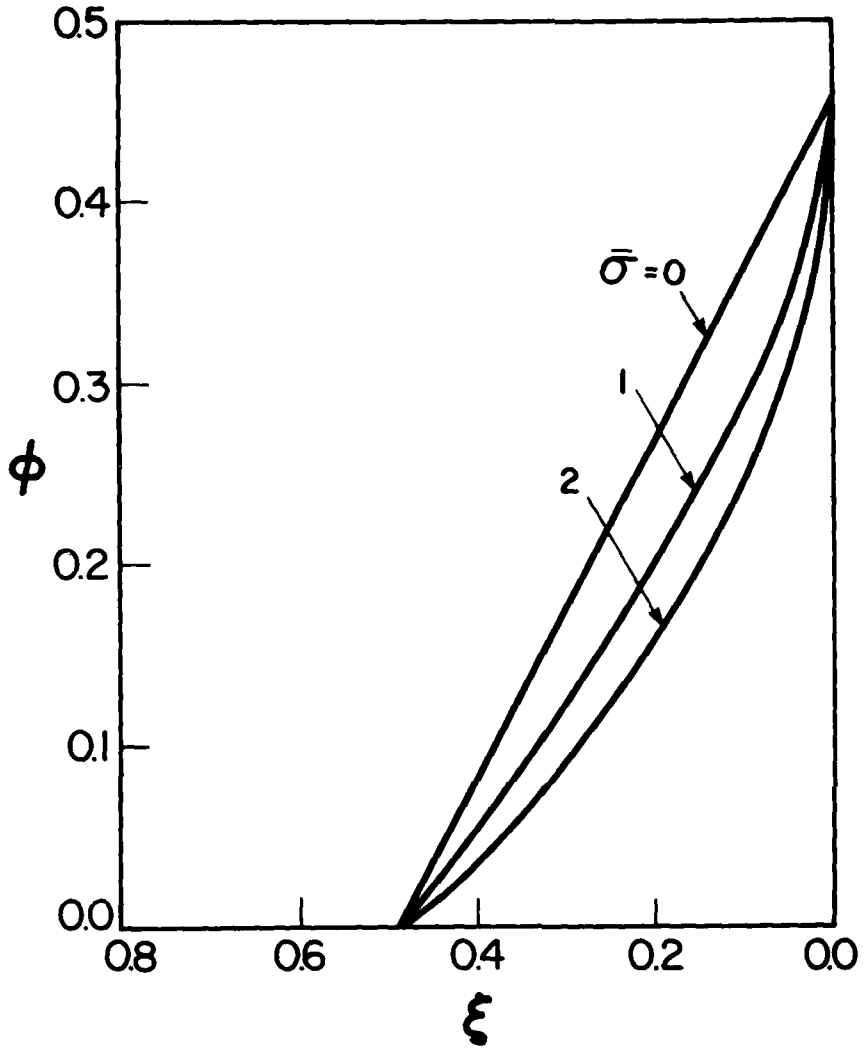

FIG. 4 NORMALIZED INVISCID FLOW VELOCITY PROFILES φ BEHIND C-J DETONATION WAVES WITH DISTANCE ξ FOR PLANAR ($\bar{\sigma}$ = 0), CYLINDRICAL ($\bar{\sigma}$ = 1) AND HEMISPHERICAL ($\bar{\sigma}$ = 2) FLOWS.

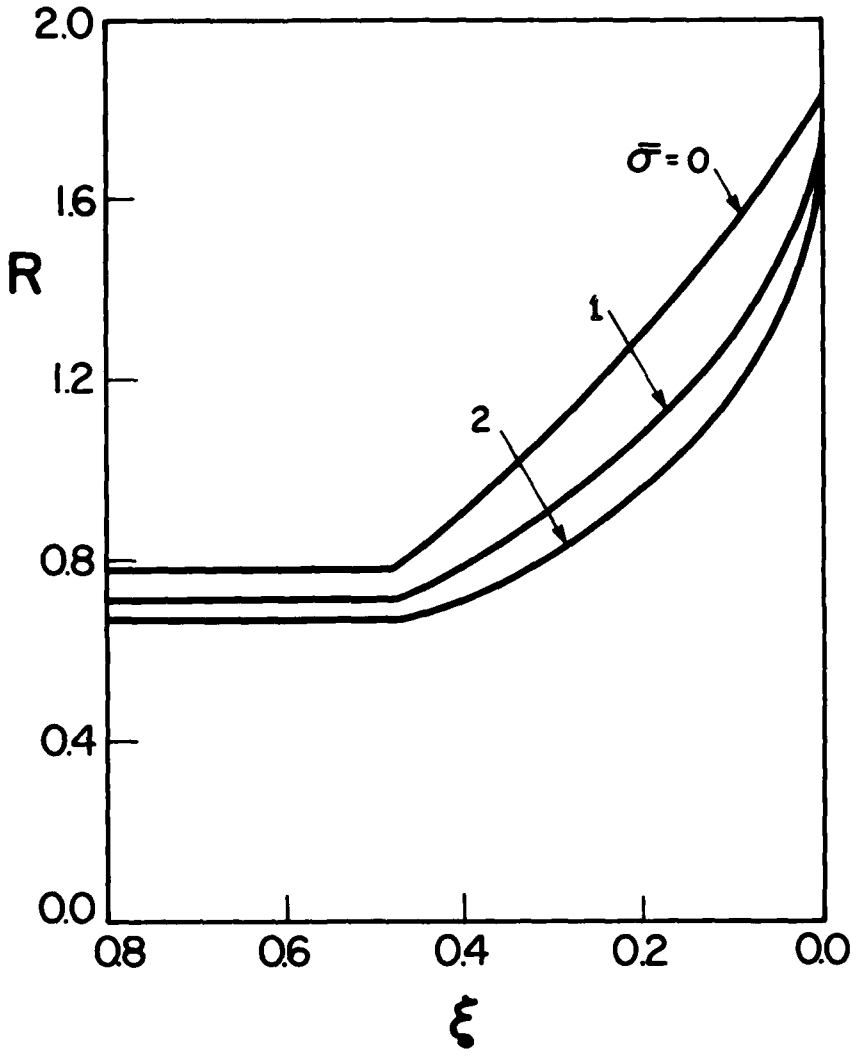

FIG. 5 NORMALIZED INVISCID FLOW DENSITY PROFILES R BEHIND C-J DETONATION WAVES WITH DISTANCE ξ FOR PLANAR ($\bar{\sigma}$ = 0), CYLINDRICAL ($\bar{\sigma}$ = 1) AND SPHERICAL ($\bar{\sigma}$ = 2) FLOWS.

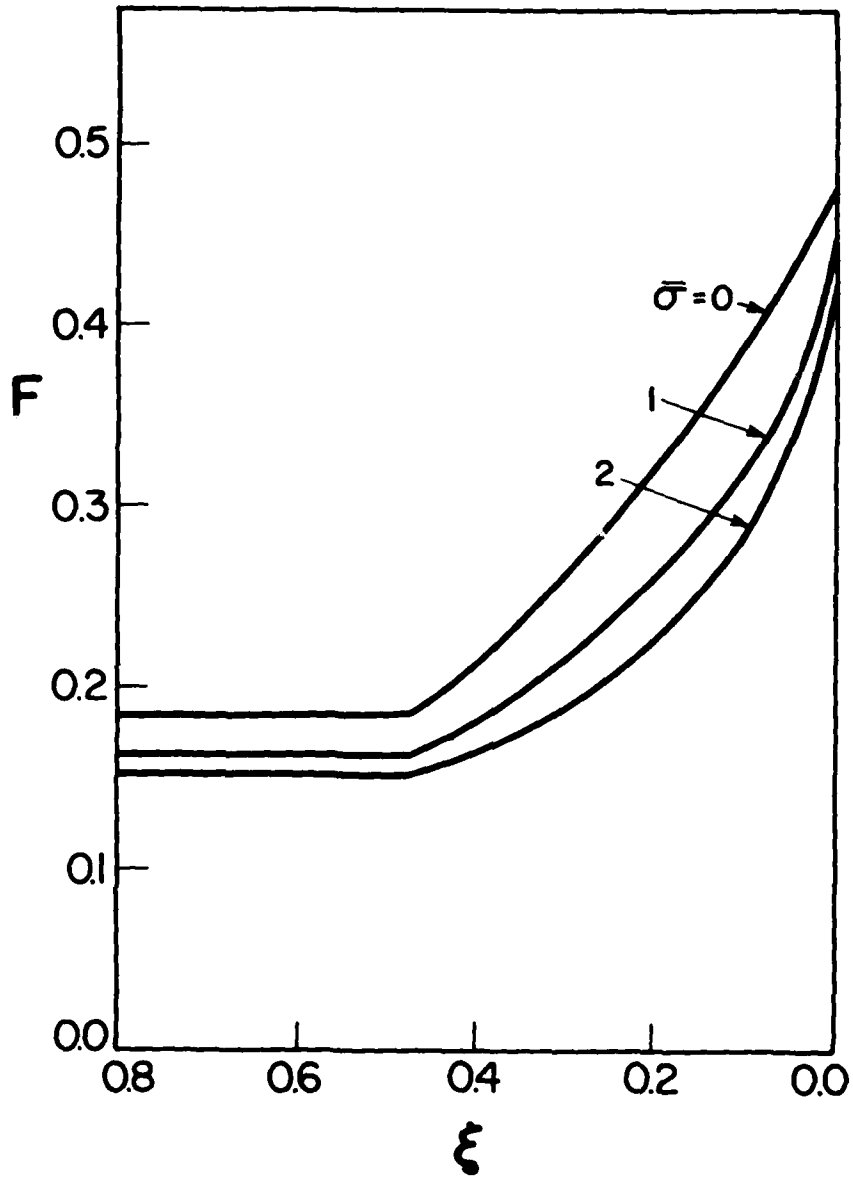

FIG. 6 NORMALIZED INVISCID FLOW PRESSURE PROFILES F BEHIND C-J DETONATION WAVES WITH DISTANCE ξ FOR PLANAR ($\bar{\sigma}$ = 0), CYLINDRICAL ($\bar{\sigma}$ = 1) AND SPHERICAL ($\bar{\sigma}$ = 2) FLOWS.

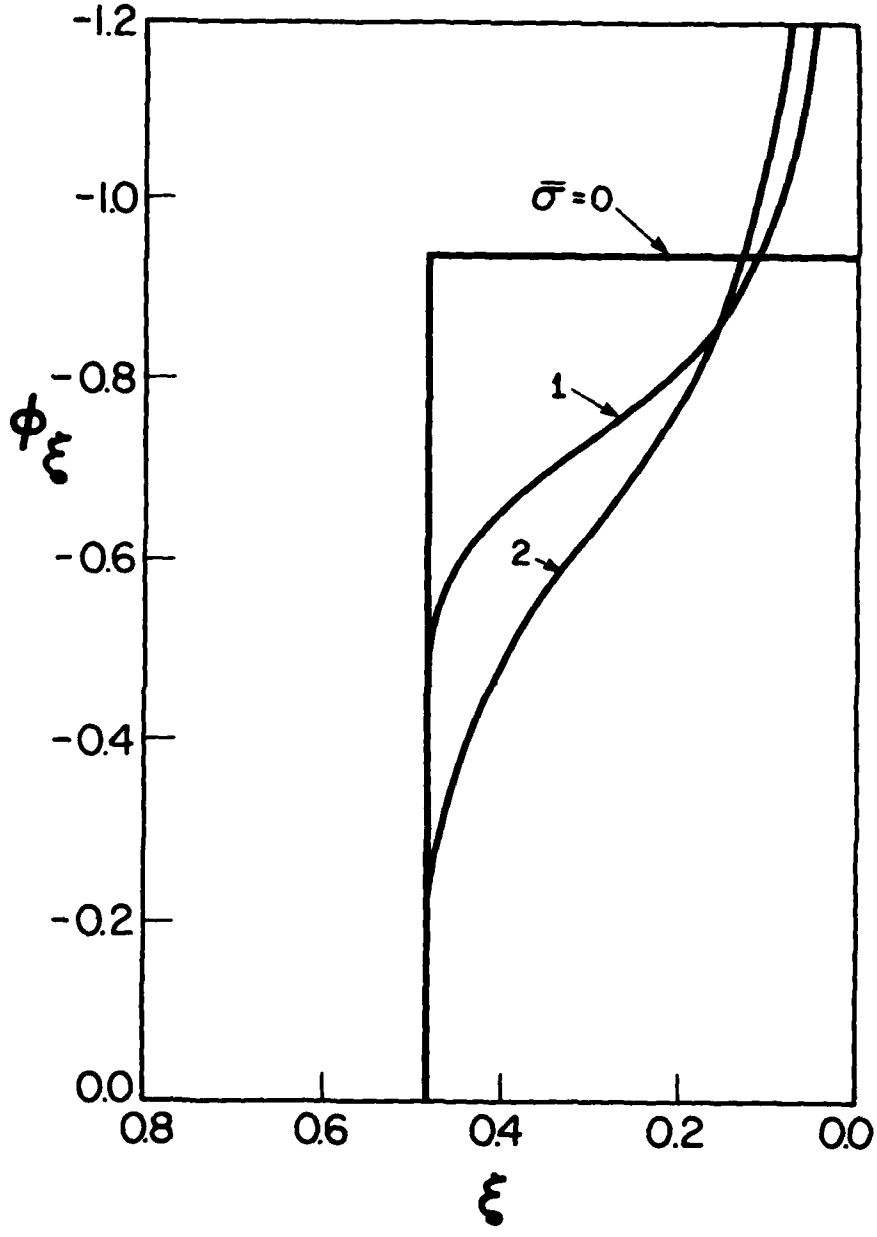

FIG. 7 NORMALIZED INVISCID FLOW DERIVATIVES Φ_ξ FOR VELOCITY BEHIND C-J DETONATION WAVES WITH DISTANCE ξ FOR PLANAR ($\bar{\sigma}$ = 0), CYLINDRICAL ($\bar{\sigma}$ = 1) AND SPHERICAL ($\bar{\sigma}$ = 2) FLOWS.

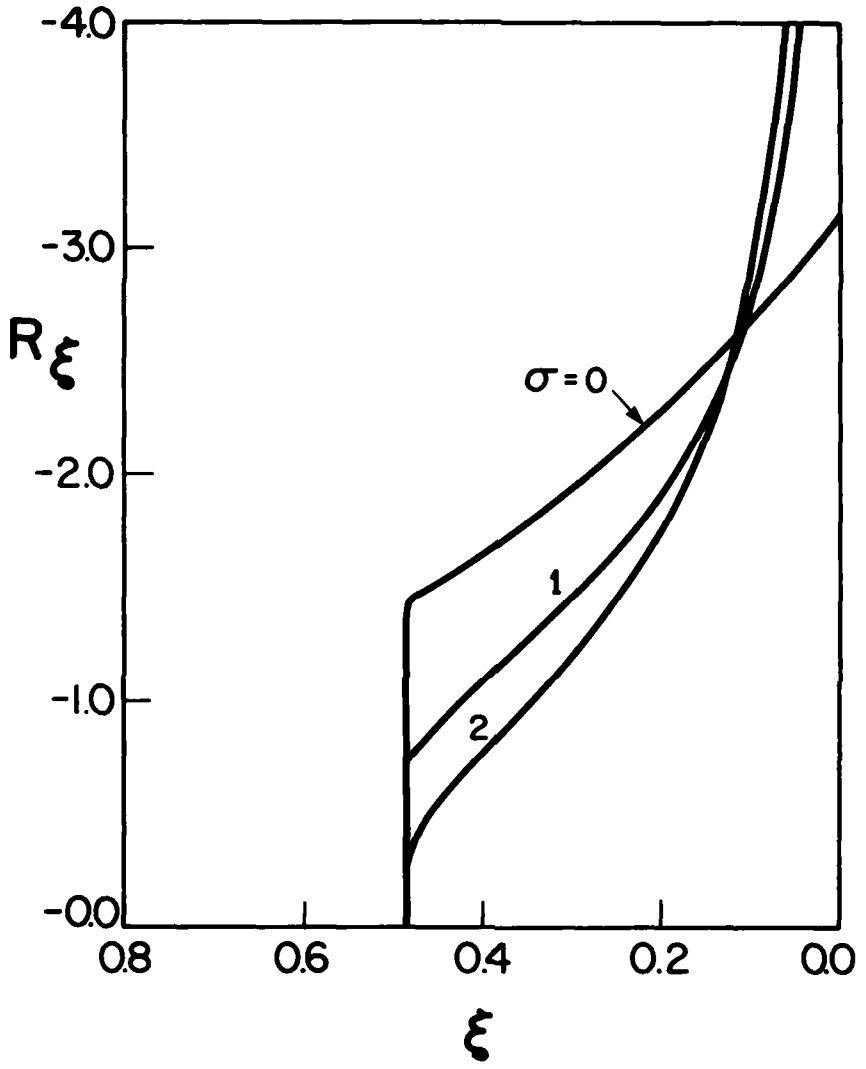

FIG. 8 NORMALIZED INVISCID FLOW DERIVATIVES R_ξ FOR DENSITY BEHIND C-J DETONATION WAVES WITH DISTANCE ξ FOR PLANAR ($\bar{\sigma} = 0$) CYLINDRICAL ($\bar{\sigma} = 1$) AND SPHERICAL ($\bar{\sigma} = 2$) FLOWS.

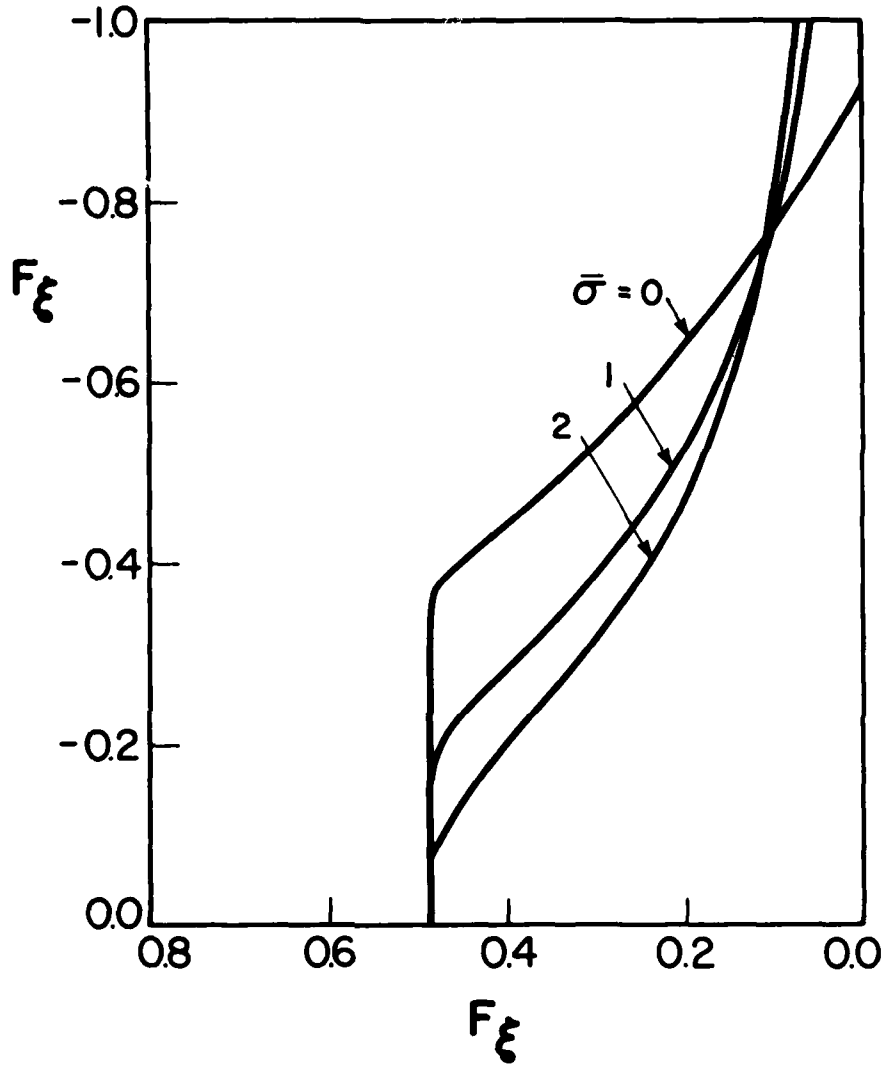

FIG. 9 NORMALIZED INVISCID FLOW DERIVATIVES F_ξ FOR PRESSURE BEHIND C-J DETONATION WAVES WITH DISTANCE ξ FOR PLANAR ($\bar{\sigma} = 0$), CYLINDRICAL ($\bar{\sigma} = 1$) AND SPHERICAL ($\bar{\sigma} = 2$) FLOWS.

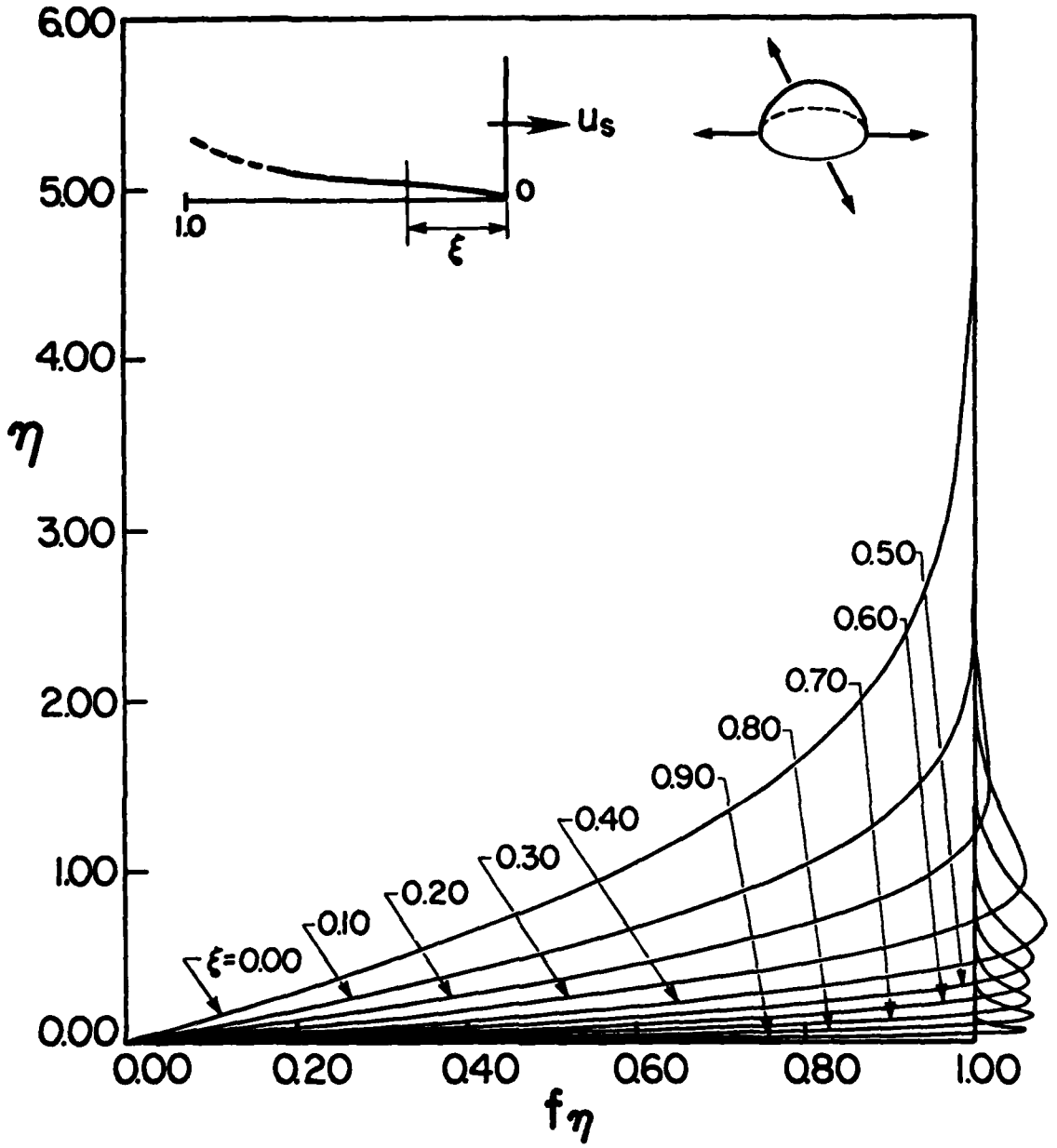

FIG. 10 NORMALIZED VELOCITY PROFILES f_η OF BOUNDARY LAYER WITH DISTANCES η AND ξ FOR A STRONG SPHERICAL BLAST WAVE, Pr = 0.72, γ= 1.4.

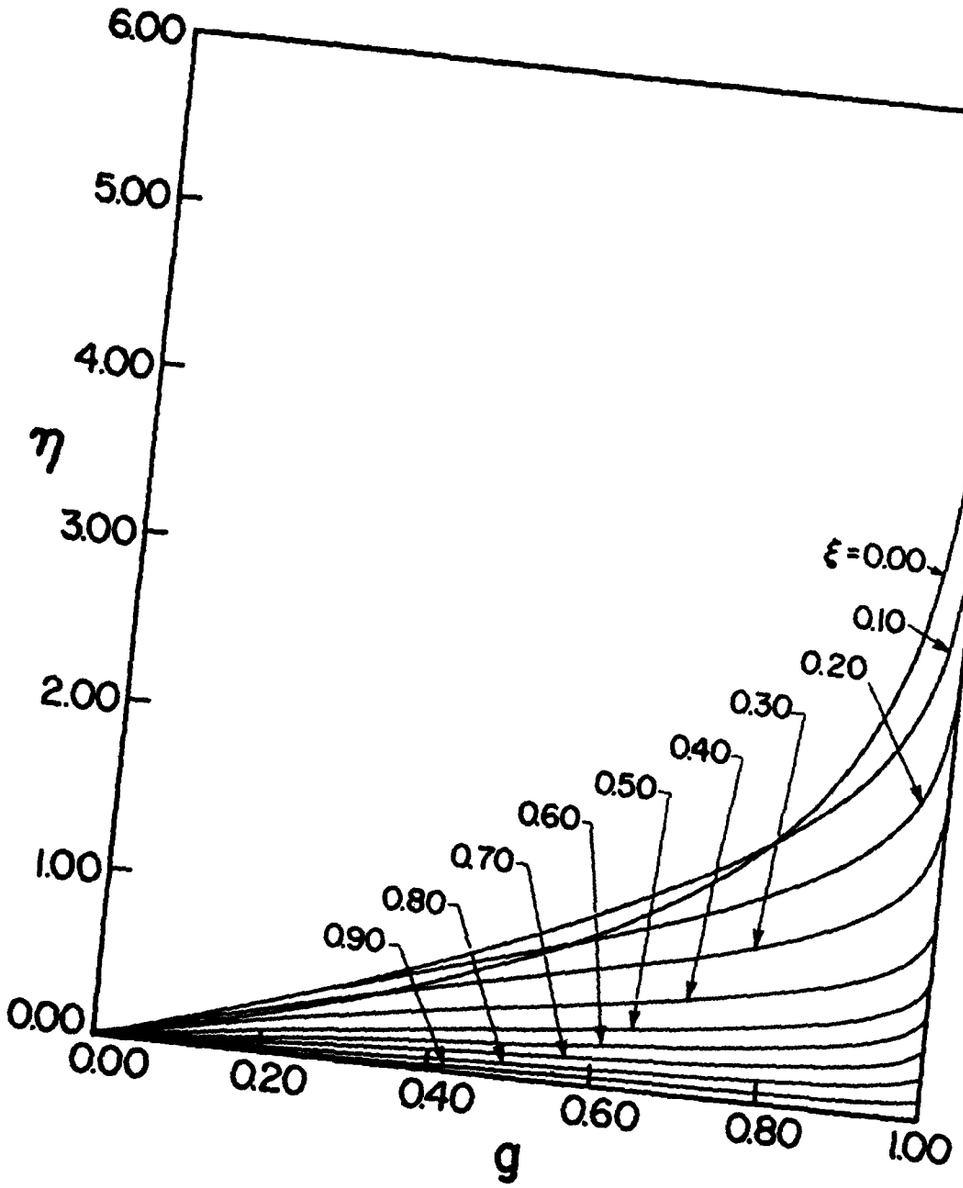

FIG. 11 NORMALIZED TEMPERATURE PROFILE g OF BOUNDARY LAYER WITH DISTANCE η AND ξ FOR A STRONG SPHERICAL BLAST WAVE, Pr = 0.72, γ = 1.4.

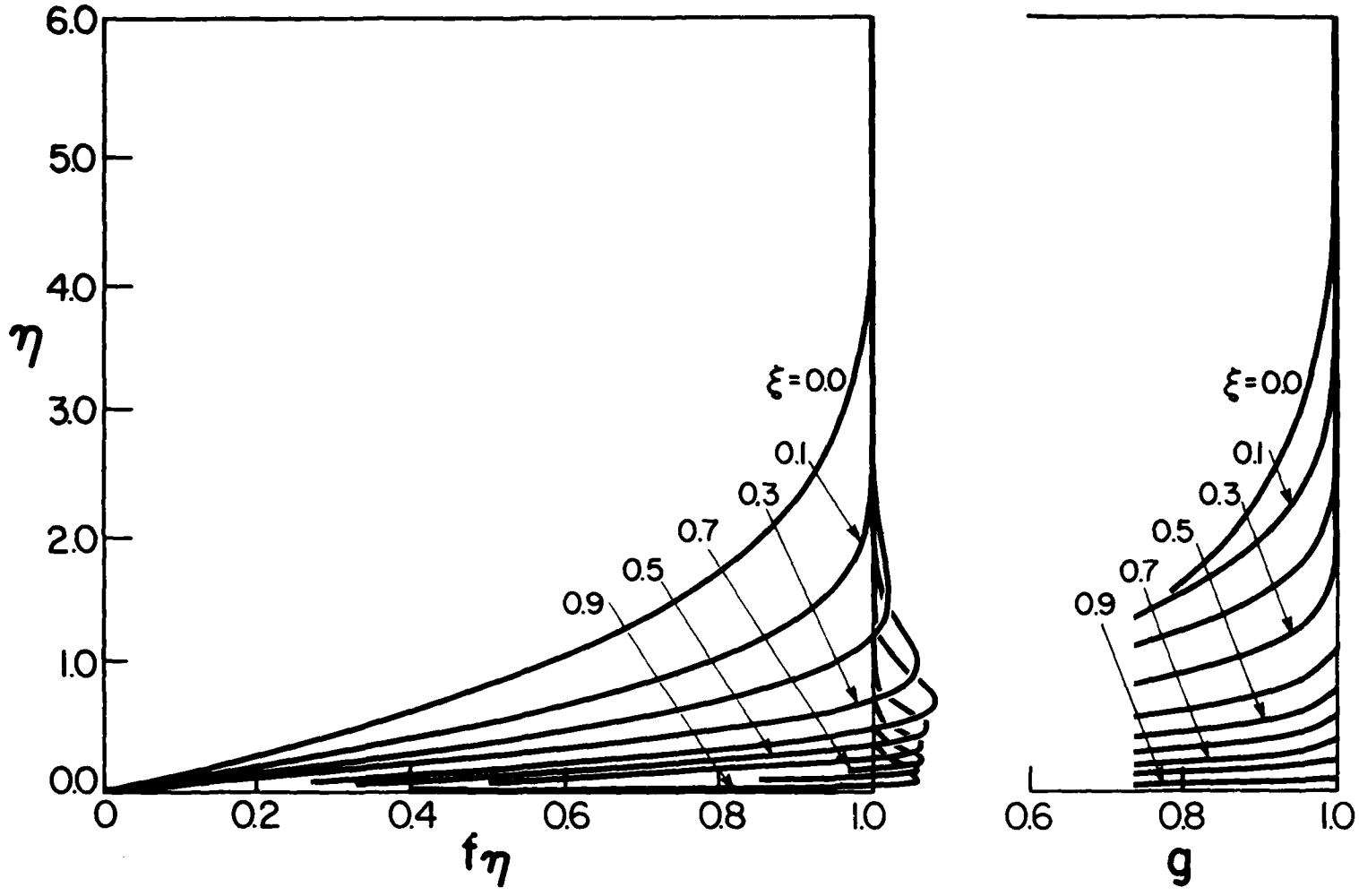

FIG. 12 NORMALIZED VELOCITY f_η AND TEMPERATURE g PROFILES WITH DISTANCES η AND ξ (FROM REF. 23). $\gamma = 1.4$, Pr = 0.72, $\bar{\sigma} = 2$, $\sigma = 1$.

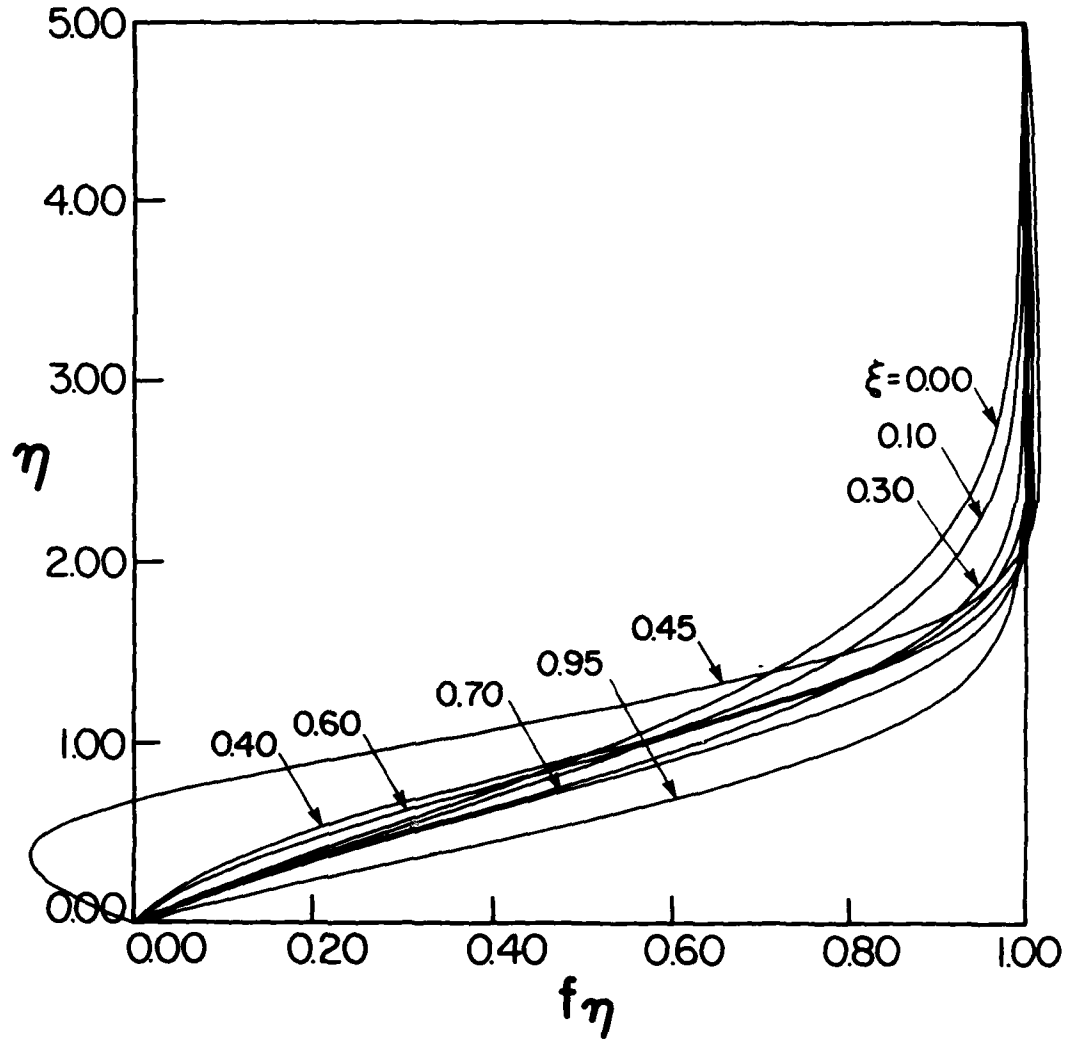

FIG. 13 NORMALIZED VELOCITY PROFILE f_η OF BOUNDARY LAYER WITH DISTANCES η AND ξ BEHIND PLANAR C-J DETONATION WAVE. Pr = 2.26, ω = 0.75, T_w = 300 K, $\bar{\sigma}$ = 0, σ = 0.

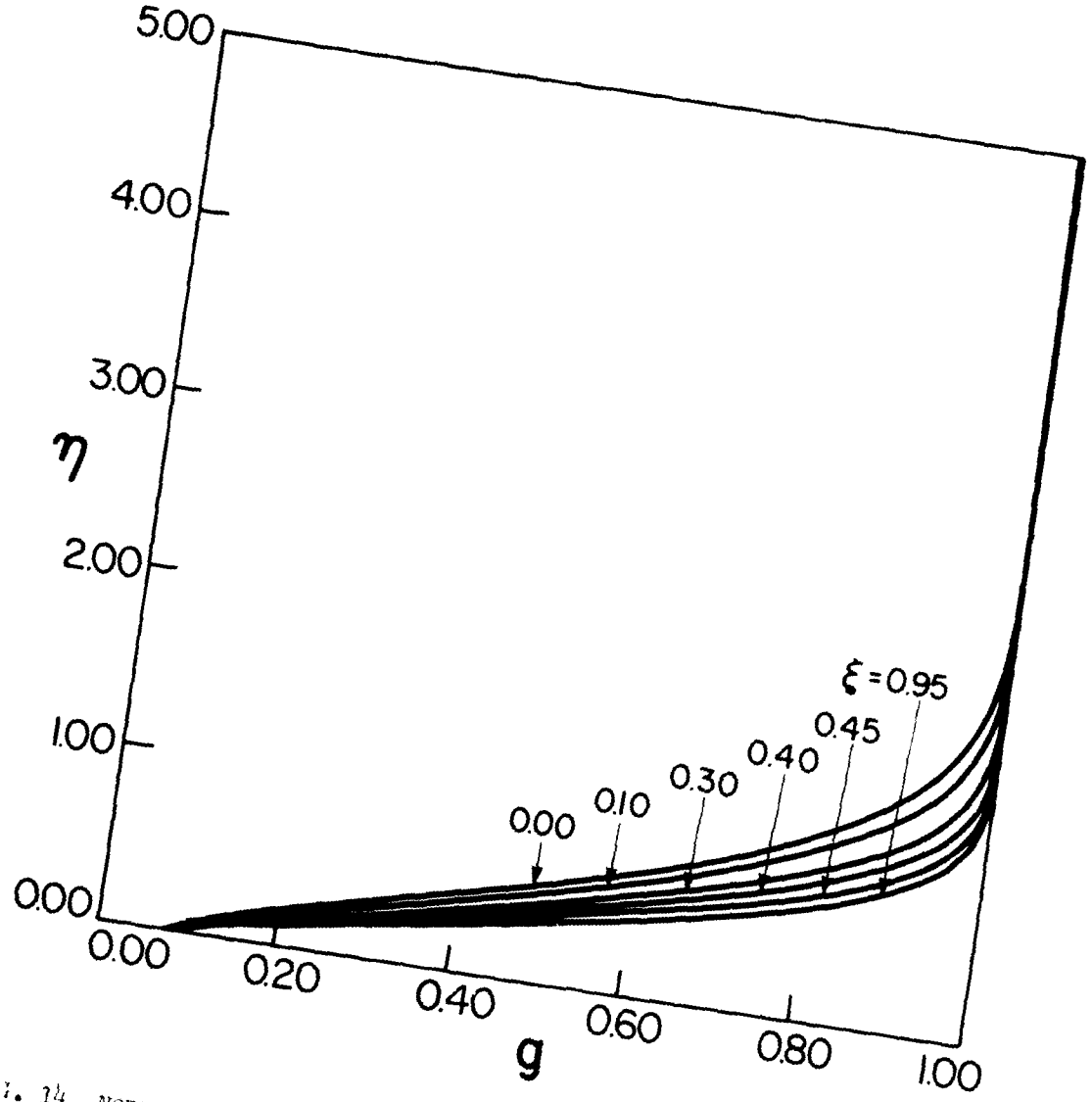

FIG. 14 NORMALIZED TEMPERATURE PROFILE θ OF BOUNDARY LAYER WITH DISTANCES η AND ξ BEHIND PLANAR C-J DETONATION WAVE. Pr = 0.36, γ = 0.75. T_w = 300 K, $\bar{\sigma}$ = 0, σ = 0.

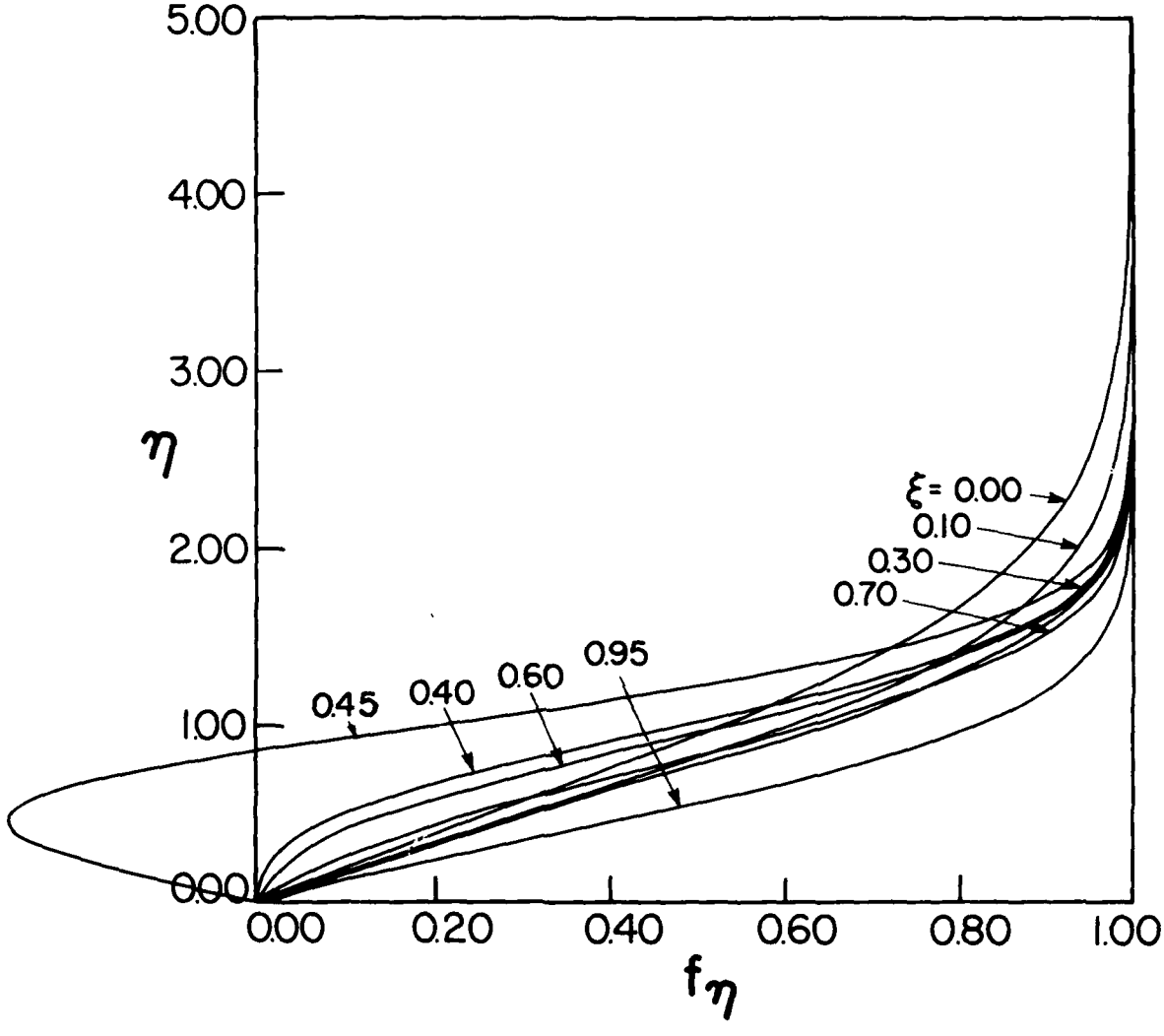

FIG. 15 NORMALIZED VELOCITY PROFILES f_η OF BOUNDARY LAYER WITH DISTANCES η AND ξ BEHIND CYLINDRICAL C-J DETONATION WAVE. Pr = 2.26, ω = 0.75, T_w = 300 K, $\bar{\sigma}$ = 1, σ = 0.

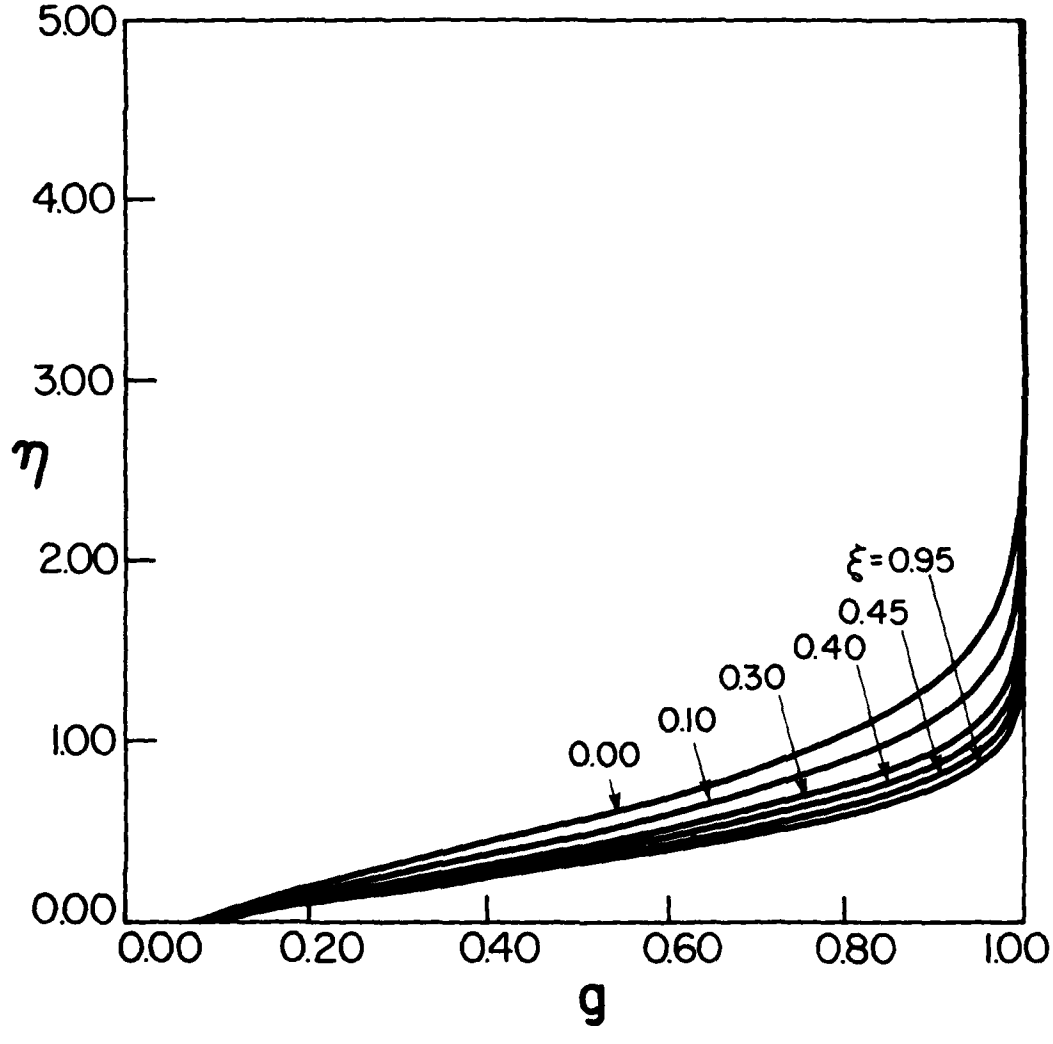

FIG. 16 NORMALIZED TEMPERATURE PROFILES g OF BOUNDARY LAYER WITH DISTANCES η AND ξ BEHIND CYLINDRICAL C-J DETONATION WAVE. Pr = 2.26, ω = 0.75, T_w = 300 K, $\bar{\sigma}$ = 1, σ = 0.

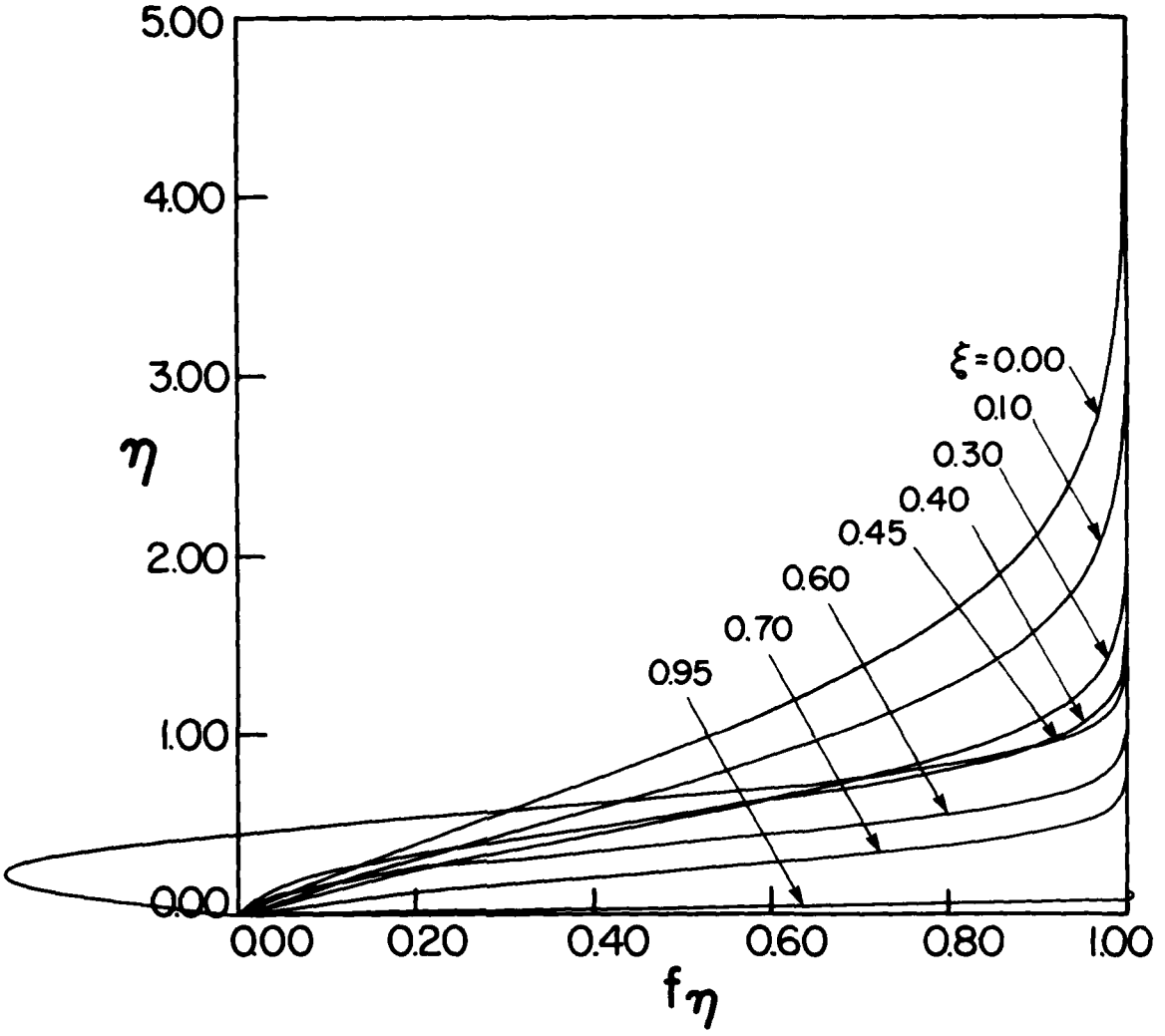

FIG. 17 NORMALIZED VELOCITY PROFILES f_η OF BOUNDARY LAYER WITH DISTANCES η AND ξ BEHIND CYLINDRICAL C-J DETONATION WAVE. Pr = 2.26, $\omega \doteq 0.75$, T_w = 300 K, $\bar{\sigma}$ = 1, σ = 1.

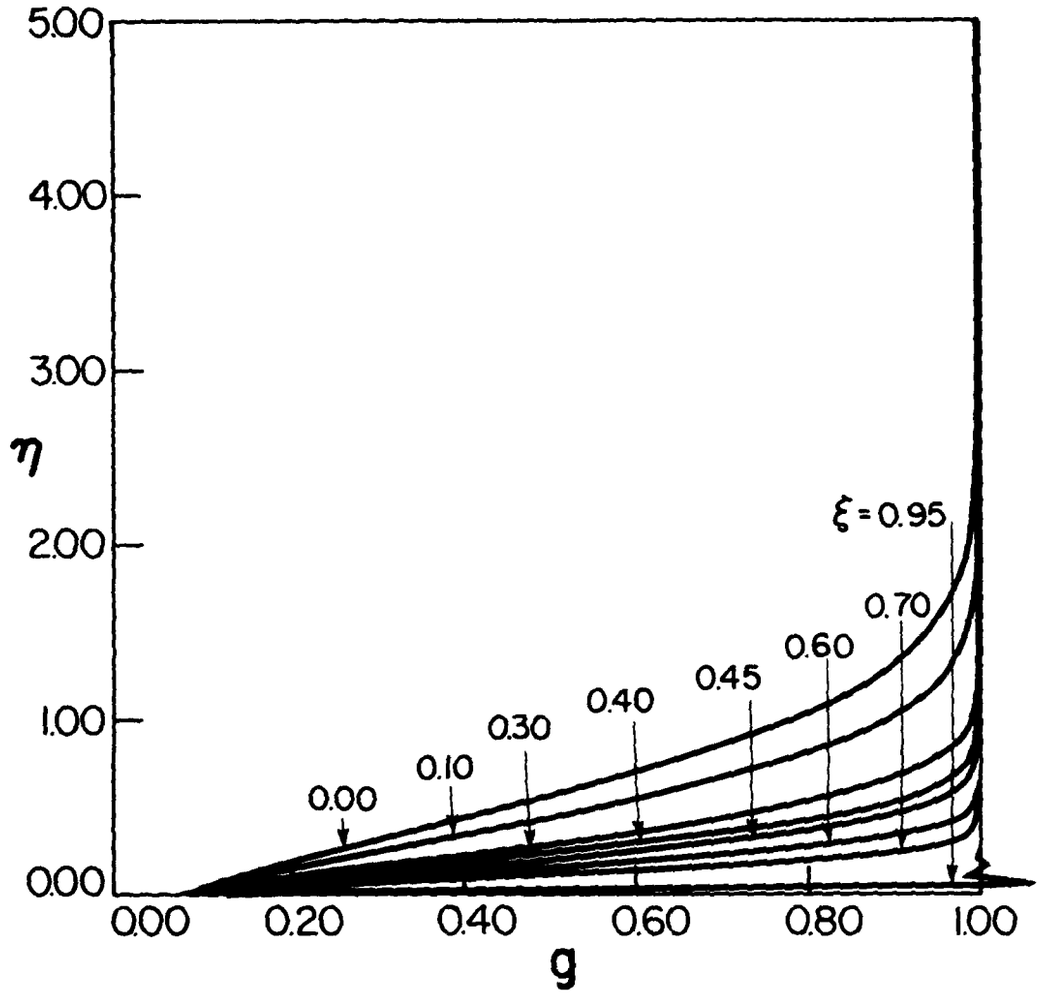

FIG. 18 NORMALIZED TEMPERATURE PROFILES g OF BOUNDARY LAYER WITH DISTANCES η AND ξ BEHIND CYLINDRICAL C-J DETONATION WAVE. Pr = 2.26, $\omega = 0.75$, $T_w = 300$ K, $\bar{\sigma} = 1$, $\sigma = 1$.

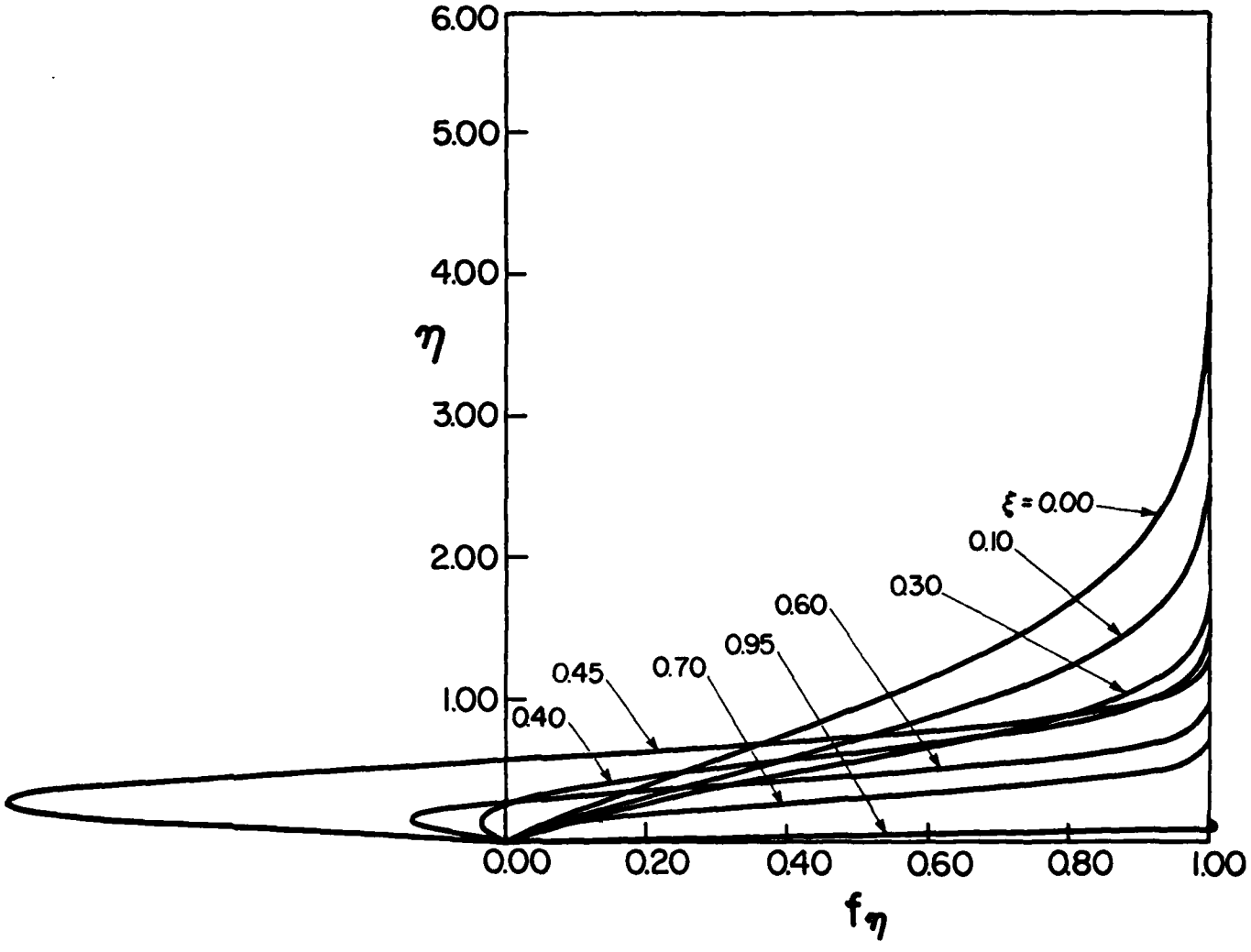

19 NORMALIZED VELOCITY PROFILE f_η OF BOUNDARY LAYER WITH DISTANCES η AND ξ BEHIND SPHERICAL C-J DETONATION WAVE. Pr = 2.26, ω = 0.75, T_w = 300 K, $\bar{\sigma}$ = 2, σ = 1.

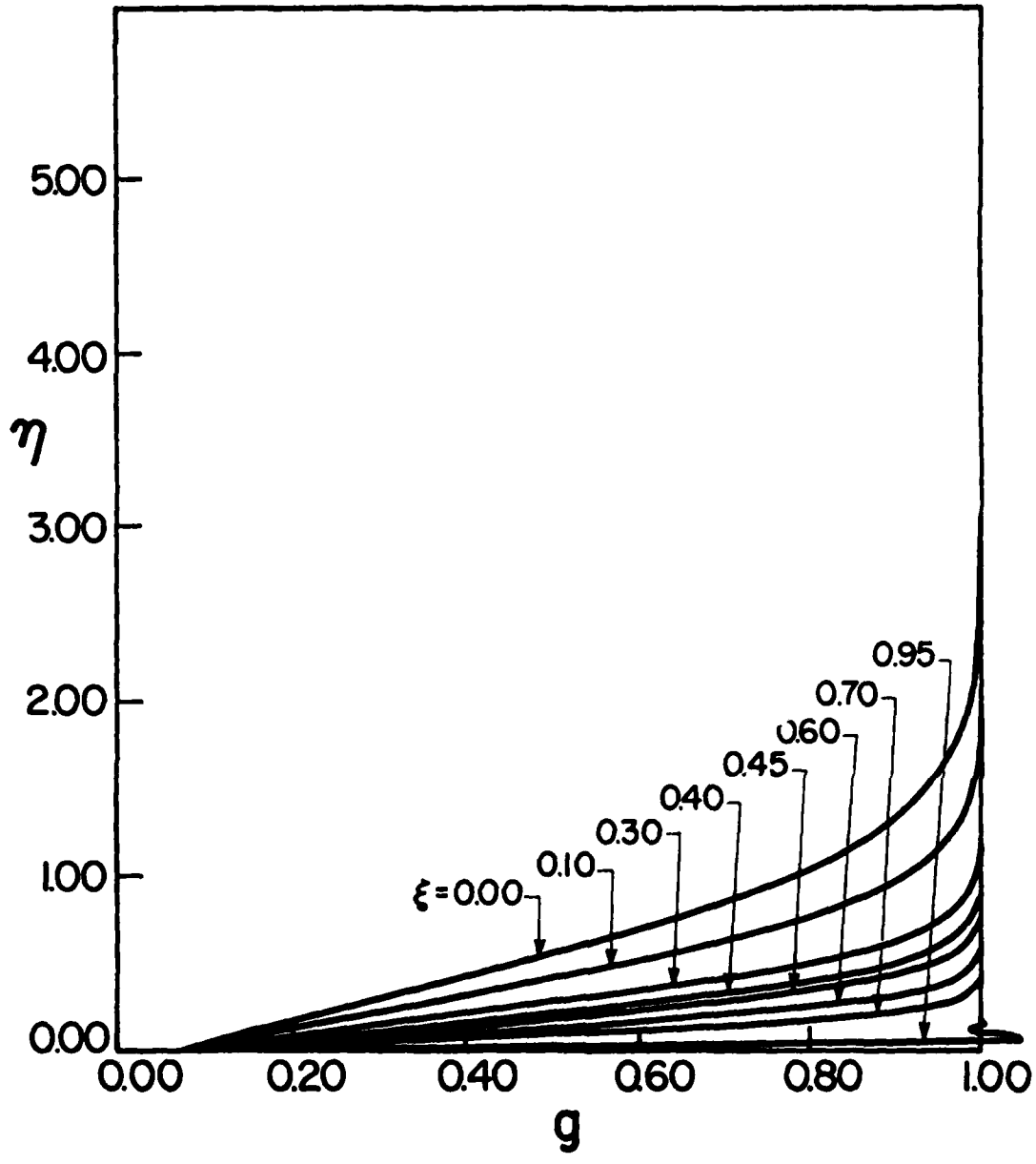

FIG. 20 NORMALIZED TEMPERATURE PROFILES g OF BOUNDARY LAYER WITH DISTANCES η AND ξ BEHIND SPHERICAL C-J DETONATION WAVE. Pr = 2.26, = 0.75, T_w = 300 K, $\bar{\sigma}$ = 2, σ = 1.

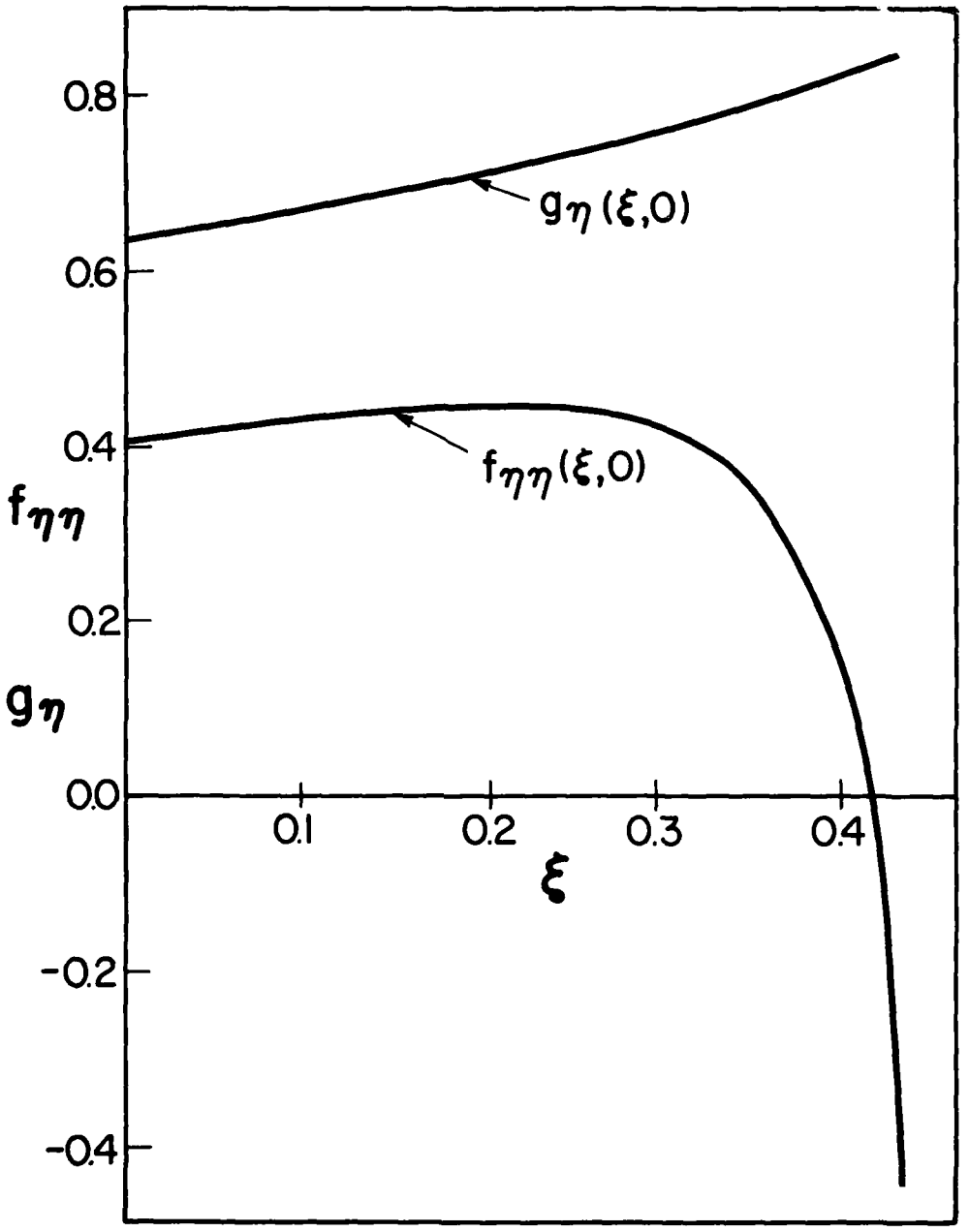

FIG. 21 VARIATION OF NORMALIZED VELOCITY DERIVATIVE $f_{\eta\eta}(\xi,0)$ AND TEMPERATURE DERIVATIVE $g_\eta(\xi,0)$ WITH DISTANCE ξ FOR PLANAR C-J DETONATION WAVE. Pr = 2.26, ω = 0.75, T_w = 300 K, $\bar{\sigma}$ = 0, σ = 0.

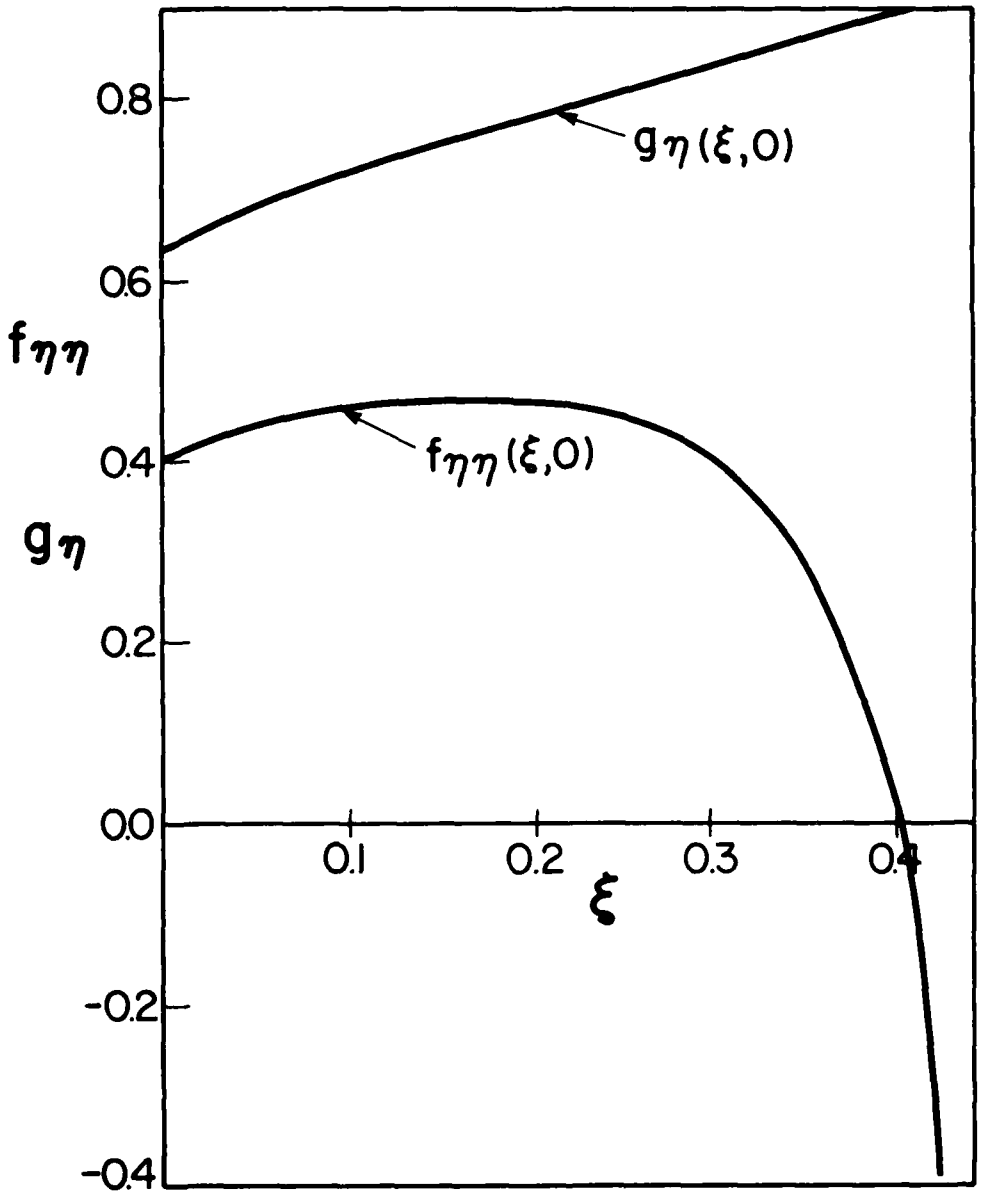

FIG. 22 VARIATION OF NORMALIZED VELOCITY DERIVATIVES $f_{\eta\eta}(\xi,0)$ AND TEMPERATURE DERIVATIVE $g_\eta(\xi,0)$ WITH DISTANCE ξ FOR CYLINDRICAL C-J DETONATION WAVE. Pr = 2.26, ω = 0.75, T_w = 300 K, $\bar{\sigma}$ = 1, σ = 0.

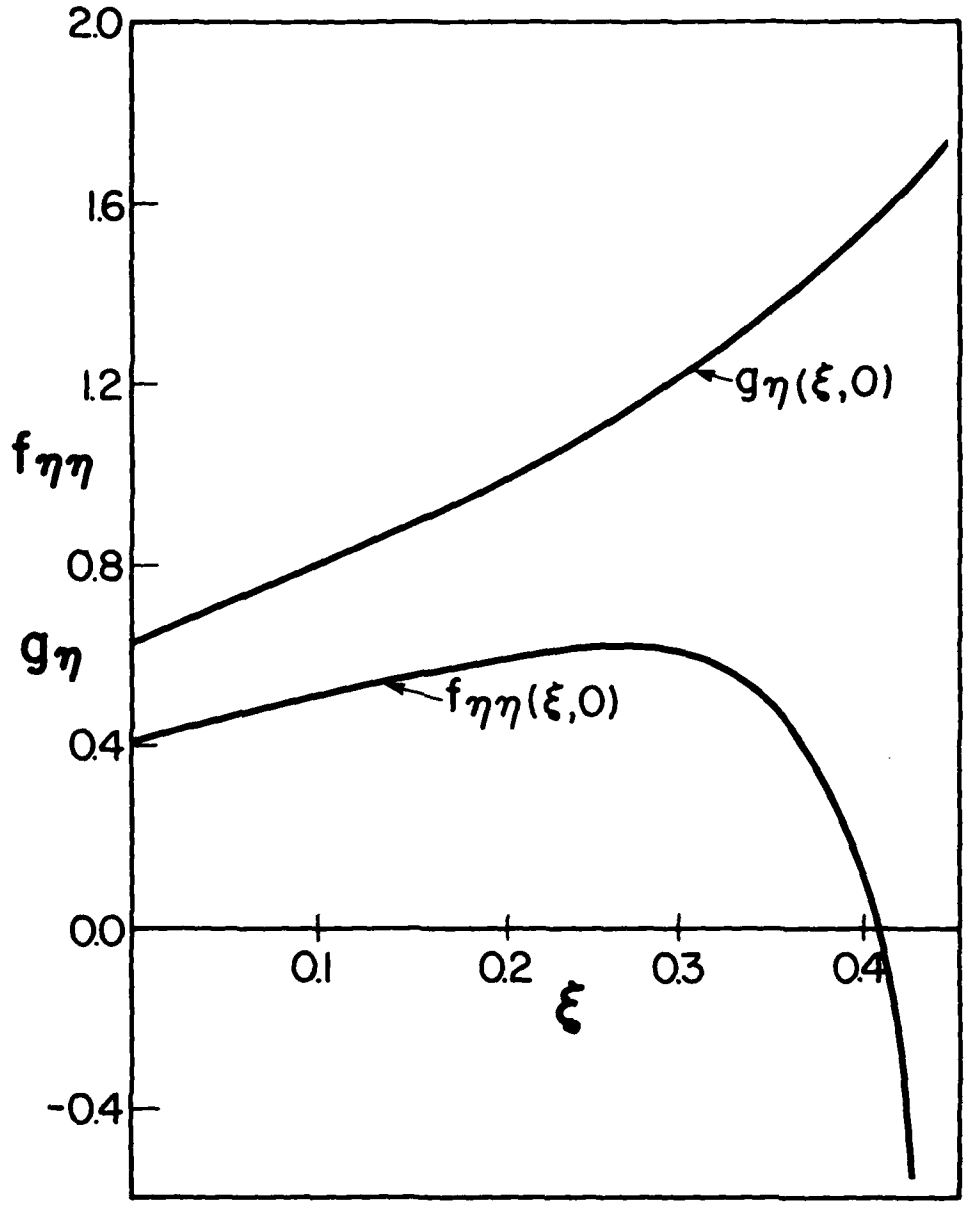

FIG. 23 VARIATION OF NORMALIZED VELOCITY DERIVATIVES $f_{\eta\eta}(\xi,0)$ AND TEMPERATURE DERIVATIVES $g_\eta(\xi,0)$ WITH DISTANCE ξ FOR CYLINDRICAL C-J DETONATION WAVE. Pr = 2.26, ω = 0.75, T_w = 300 K, $\bar{\sigma}$ = 1, σ = 1.

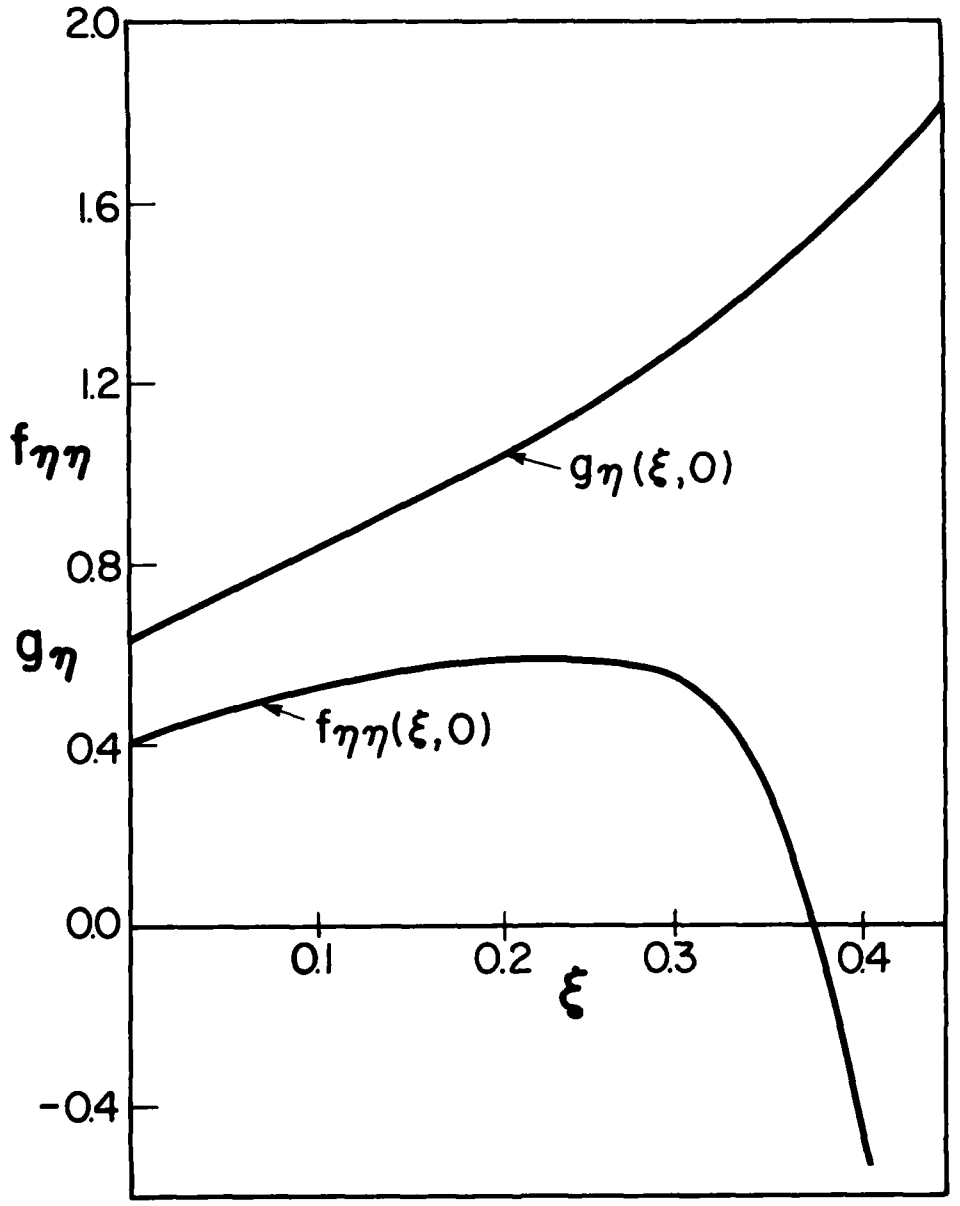

FIG. 24 VARIATION OF NORMALIZED VELOCITY DERIVATIVES $f_{\eta\eta}(\xi,0)$ AND TEMPERATURE DERIVATIVES $g_\eta(\xi,0)$ WITH DISTANCE ξ FOR SPHERICAL C-J DETONATION WAVE. Pr = 2.26, ω = 0.75, T_w = 300 K, $\bar{\sigma}$ = 2, σ = 1.

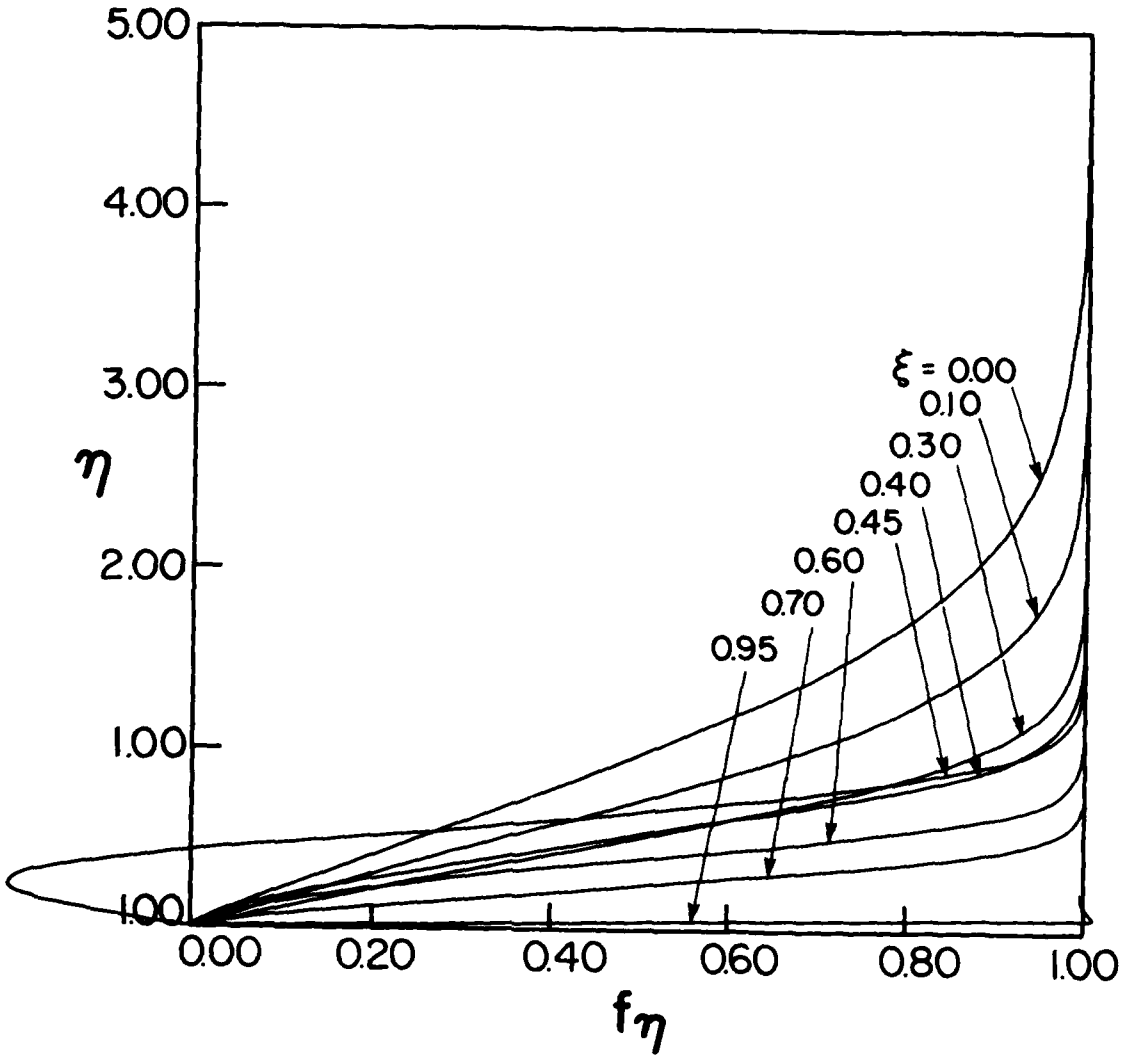

FIG. 25 NORMALIZED VELOCITY PROFILES f_η OF BOUNDARY LAYER WITH DISTANCES ξ AND η BEHIND SPHERICAL C-J DETONATION WAVE. Pr = 1.5, ω = 0.75, T_w = 300 K, $\bar{\sigma}$ = 2, σ = 1.

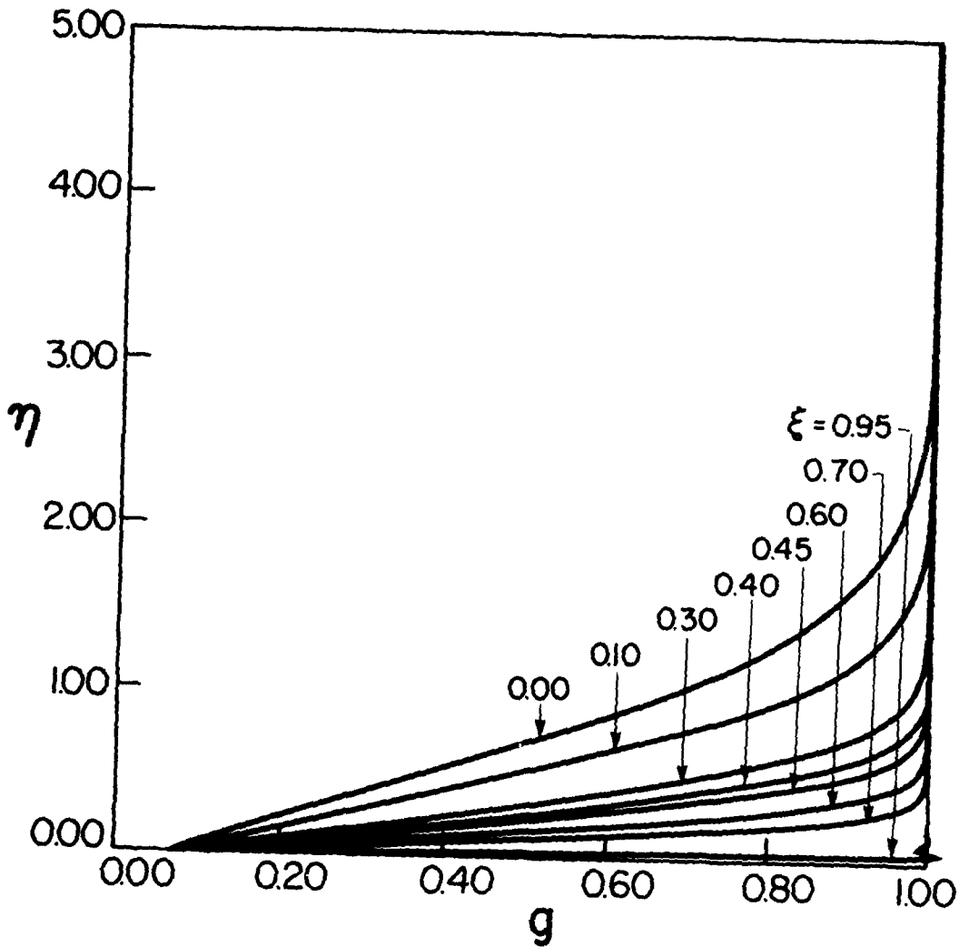

FIG. 26 NORMALIZED TEMPERATURE PROFILES g OF BOUNDARY LAYER WITH DISTANCES ξ AND η BEHIND SPHERICAL C-J DETONATION WAVE. Pr = 1.50, ω = 0.75, T_w = 300 K, $\tilde{\sigma}$ = 2, σ = 1.

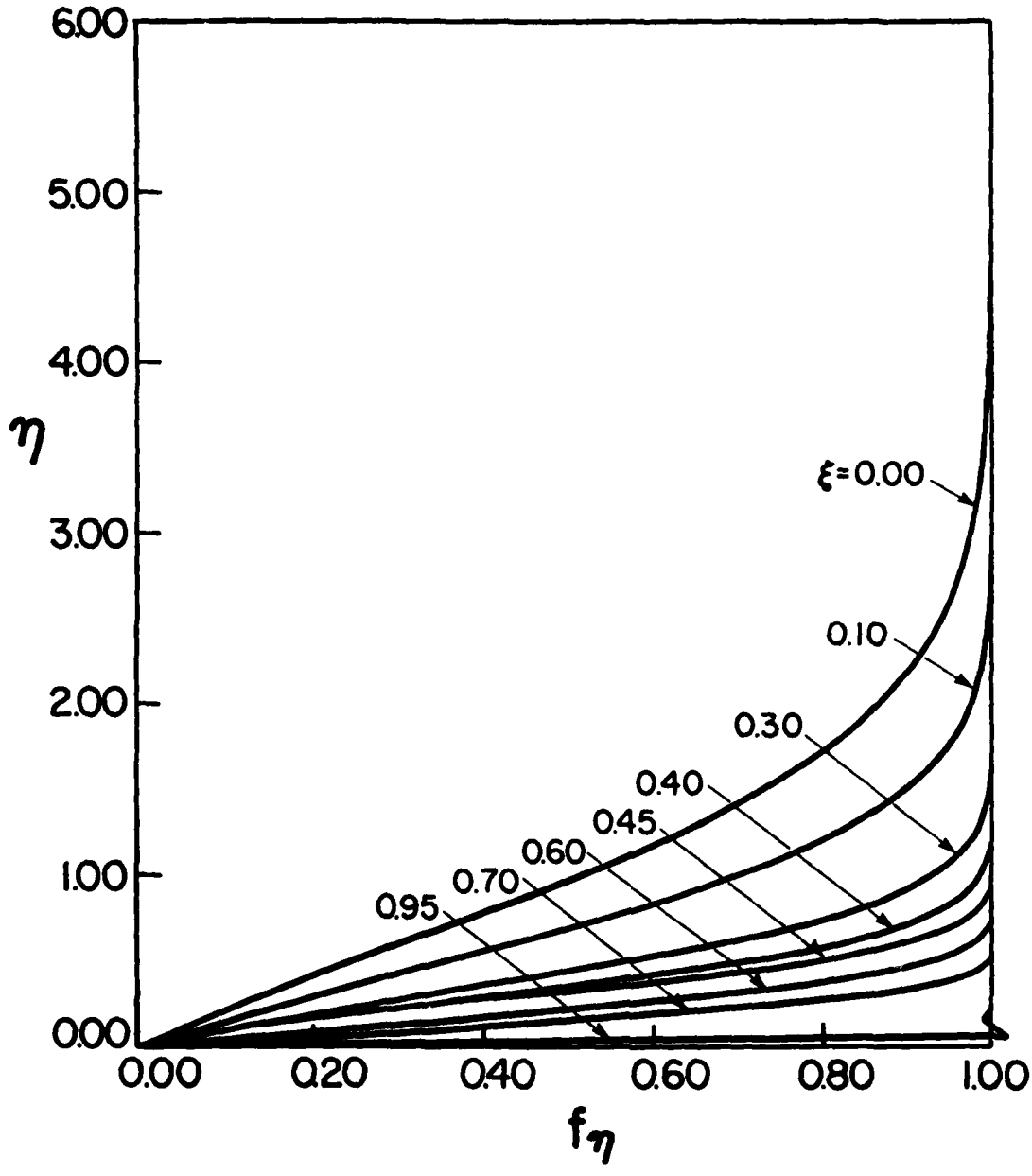

FIG. 27 NORMALIZED VELOCITY PROFILE f_η OF BOUNDARY LAYER WITH DISTANCES ξ AND η BEHIND SPHERICAL C-J DETONATION WAVE. Pr = 1, ω = 0.75, T_w = 300 K, $\bar{\sigma}$ = 2, σ = 1.

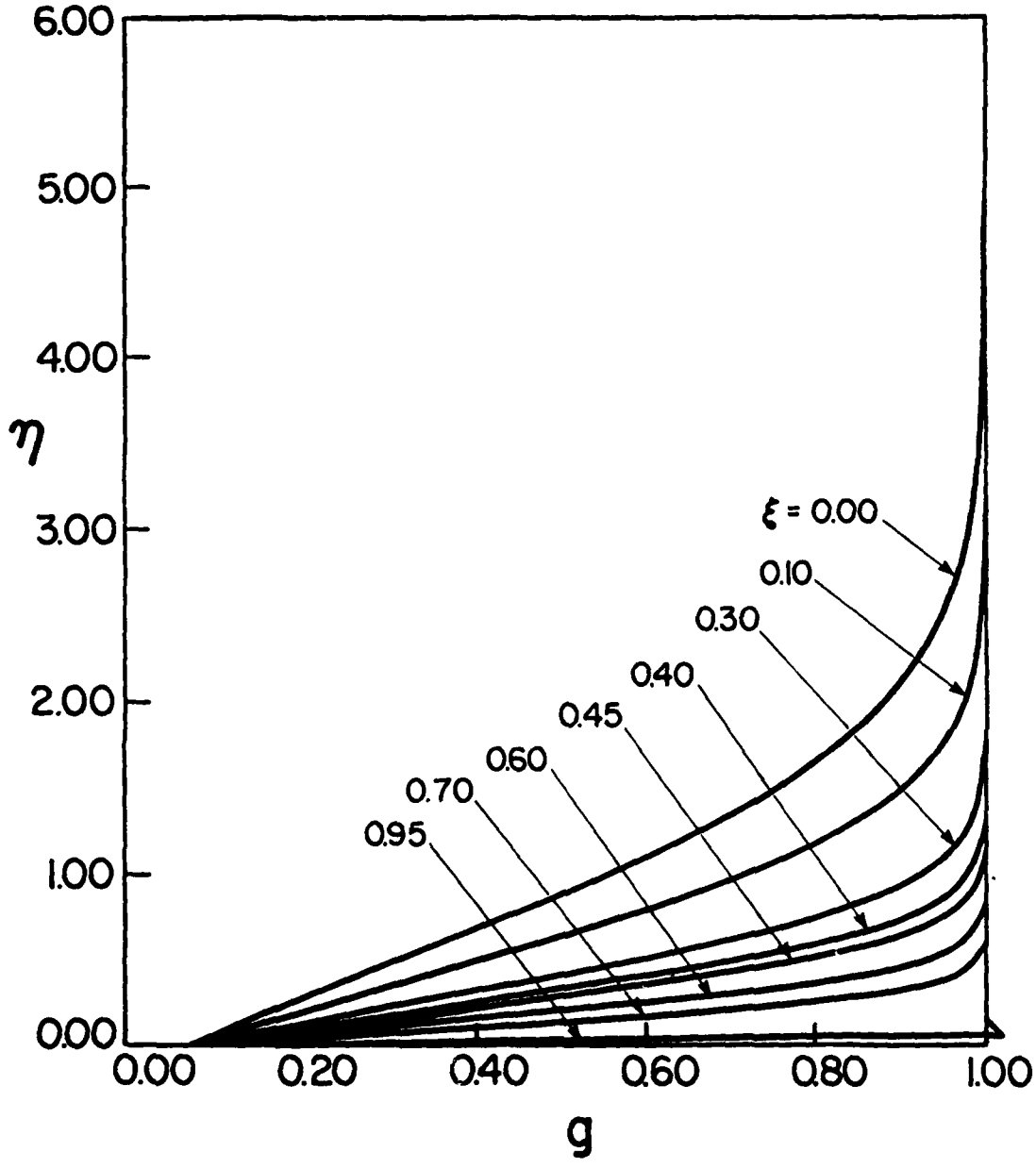

FIG. 28 NORMALIZED TEMPERATURE PROFILES OF BOUNDARY LAYER WITH DISTANCES η AND ξ BEHIND SPHERICAL C-J DETONATION WAVE. Pr = 1, ω = 0.75, T_w = 300 K, $\bar{\sigma}$ = 2, σ = 1.

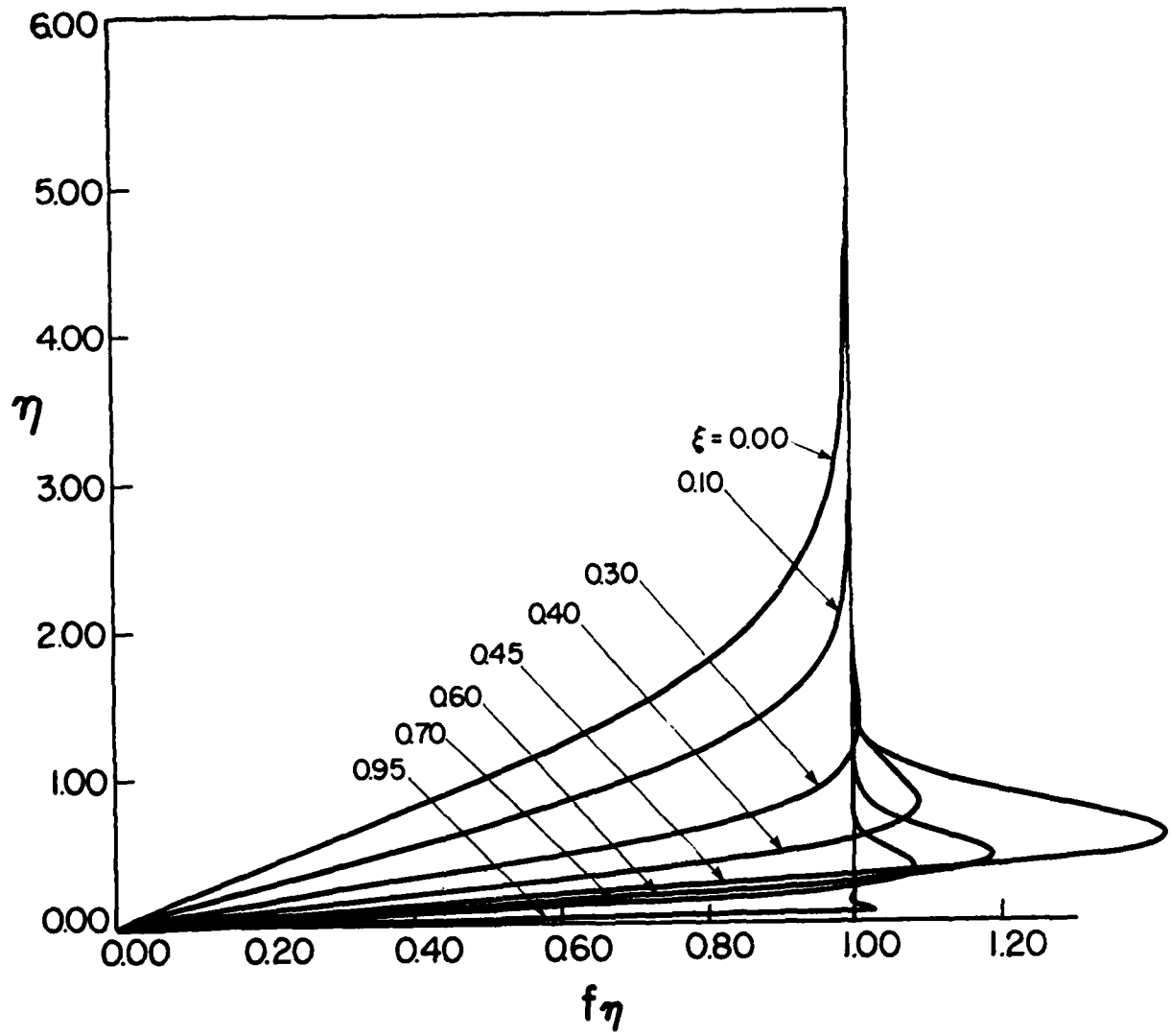

FIG. 29 NORMALIZED VELOCITY PROFILES f_η OF BOUNDARY LAYER WITH DISTANCES η AND ξ BEHIND SPHERICAL C-J DETONATION WAVE. Pr = 0.72, ω = 0.75, T_w = 300 K, $\bar{\sigma}$ = 2, σ = 1.

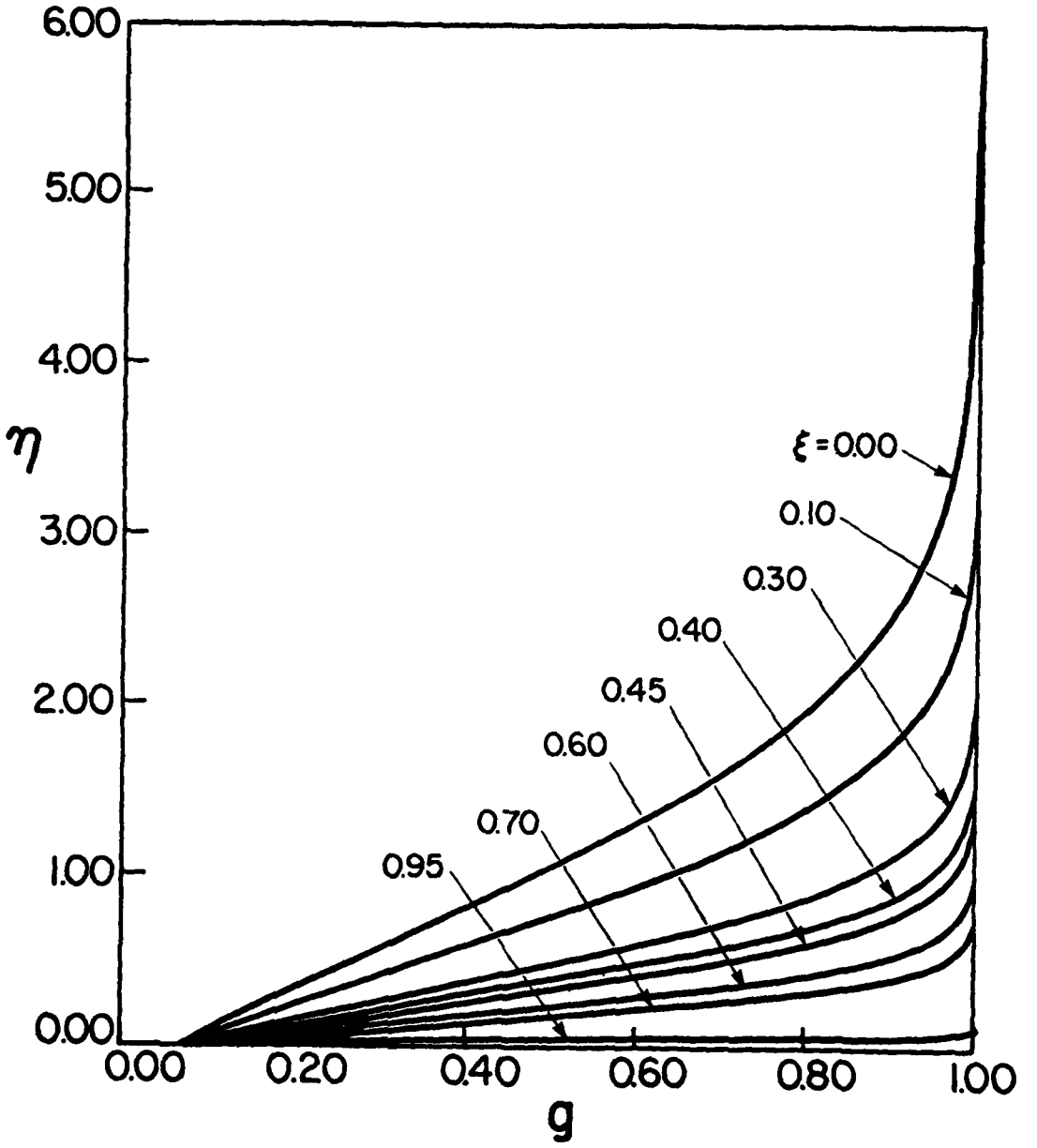

FIG. 30 NORMALIZED TEMPERATURE PROFILES g OF BOUNDARY LAYER WITH DISTANCES η AND ξ BEHIND SPHERICAL C-J DETONATION WAVE. Pr = 0.72, ω = 0.75, T_w = 300 K, $\bar{\sigma}$ = 2, σ = 1.

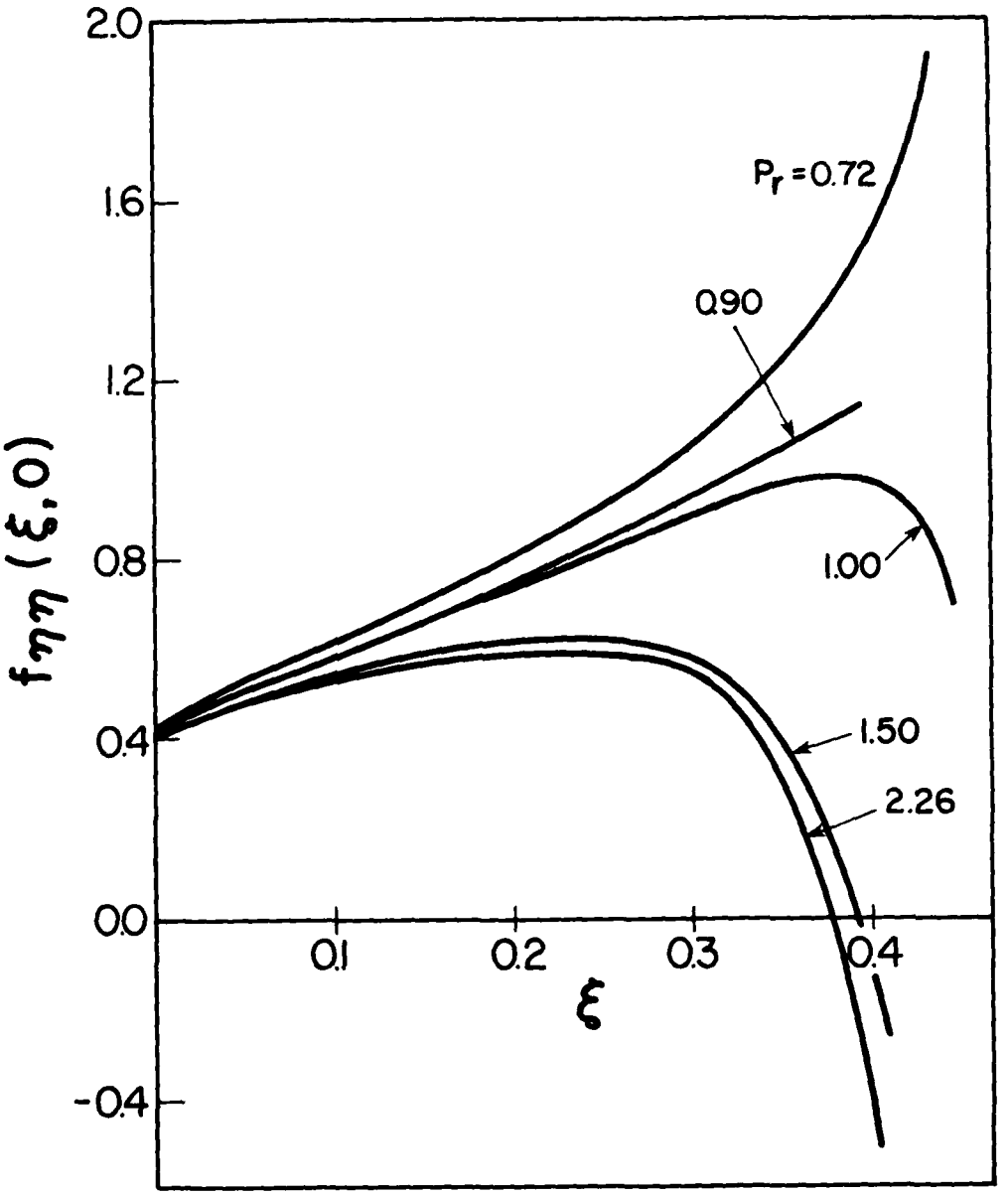

FIG. 31 EFFECT OF Pr ON NORMALIZED VELOCITY DERIVATIVES $f_{\eta\eta}(\xi,0)$ WITH DISTANCE ξ FOR SPHERICAL C-J DETONATION WAVE. $\omega = 0.75$, $T_w = 300$ K, $\bar{\sigma} = 2$, $\sigma = 1$.

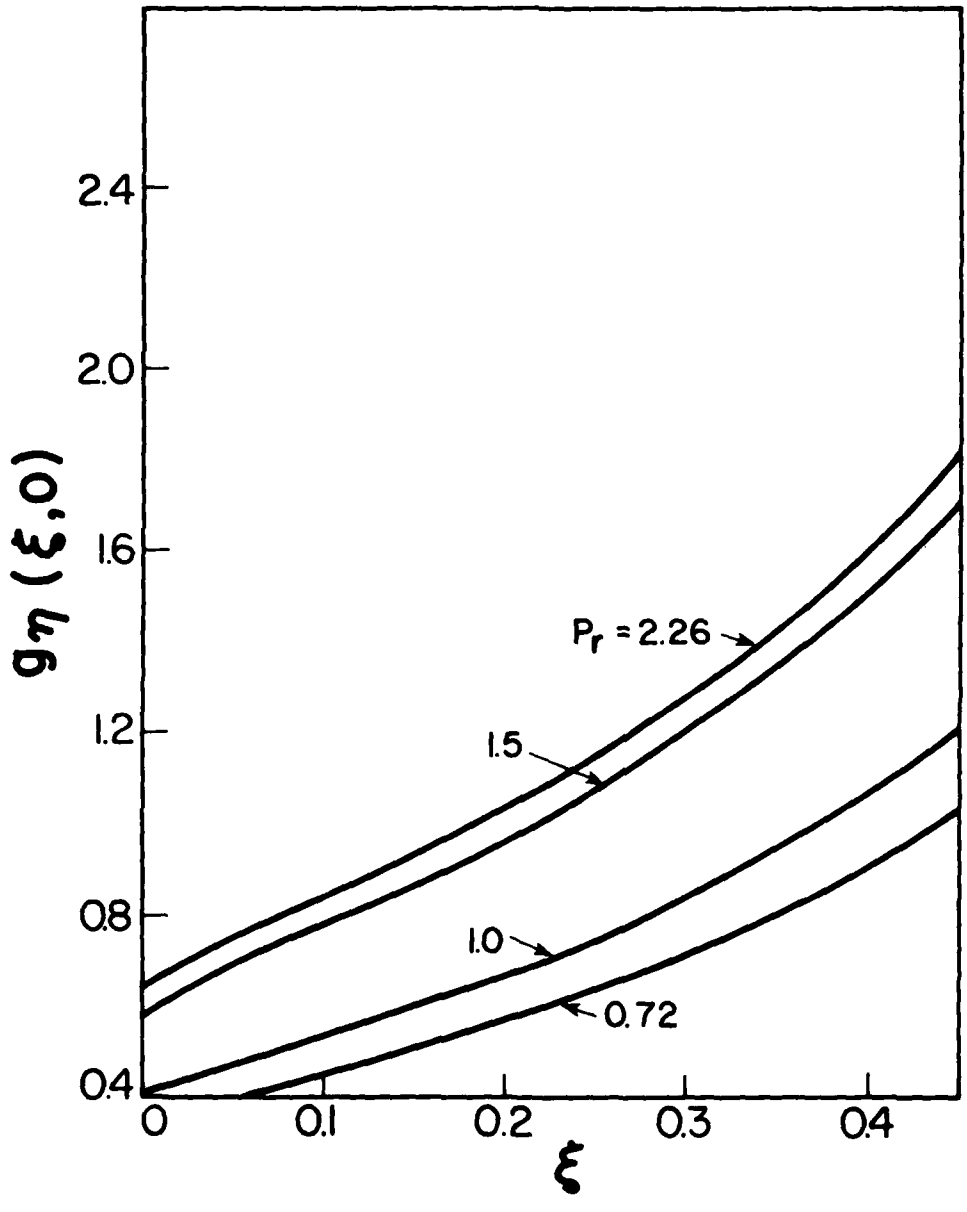

FIG. 32 EFFECT OF Pr ON NORMALIZED TEMPERATURE DERIVATIVES $g_\eta(\xi,0)$ WITH DISTANCE ξ FOR C-J DETONATION WAVE. $\omega = 0.75$, $T_w = 300$ K, $\bar{\sigma} = 2$, $\sigma = 1$.

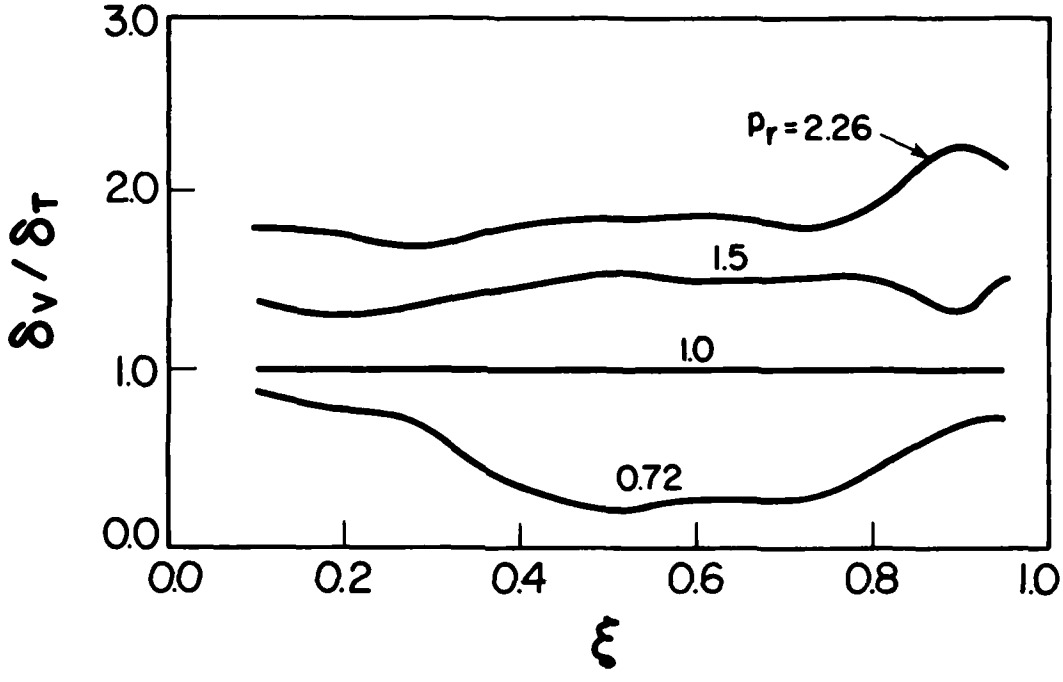

FIG. 33 BOUNDARY-LAYER THICKNESS RATIO OF VELOCITY δ_v AND TEMPERATURE δ_T WITH NORMALIZED DISTANCE ξ FOR DIFFERENT Pr AND FOR SPHERICAL C-J DETONATION WAVE. $\omega = 0.75$, $\bar{\sigma} = 2$, $\sigma = 1$.

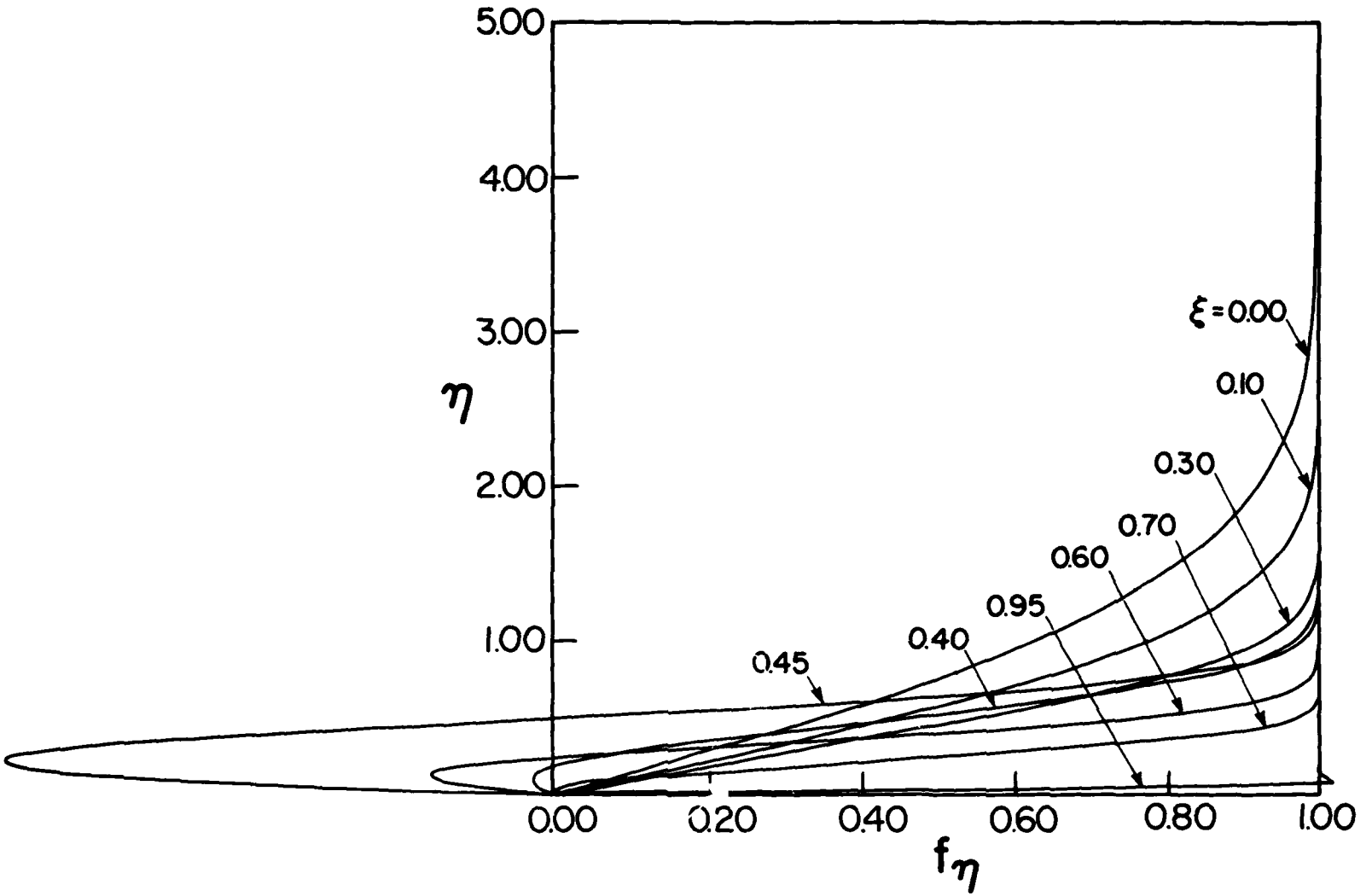

FIG. 34 NORMALIZED VELOCITY PROFILES f_η OF BOUNDARY LAYER WITH DISTANCES η AND ξ BEHIND SPHERICAL C-J DETONATION WAVE. Pr = 2.26, ω = 1, T_w = 300 K, $\bar{\sigma}$ = 2, σ = 1.

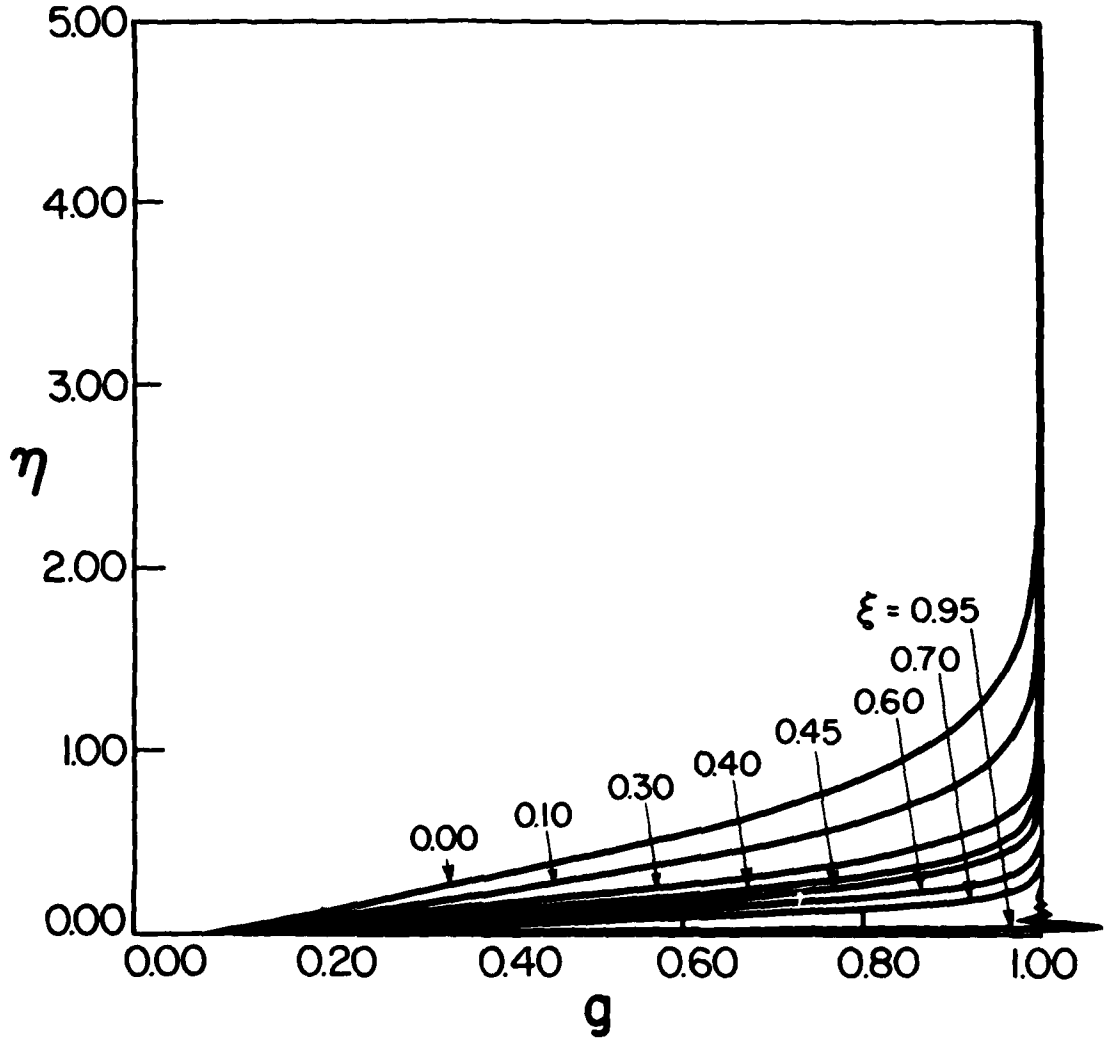

FIG. 35 NORMALIZED TEMPERATURE PROFILES g OF BOUNDARY LAYER WITH DISTANCES η AND ξ BEHIND C-J SPHERICAL DETONATION WAVE. Pr = 2.25, ω = 1, T_w = 300 K, $\bar{\sigma}$ = 2, σ = 1.

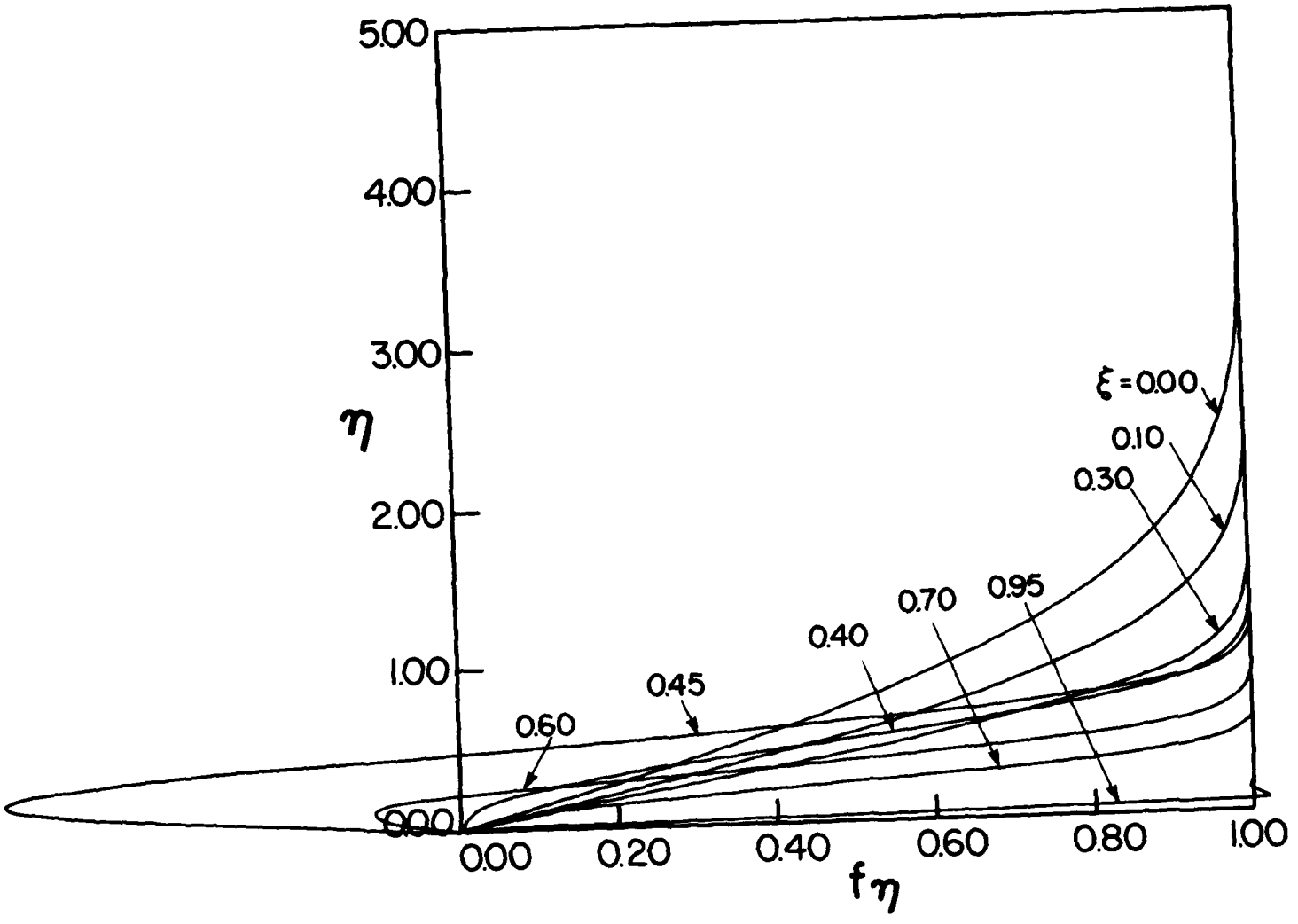

FIG. 36 NORMALIZED VELOCITY PROFILES f_η OF BOUNDARY LAYER WITH DISTANCES η AND ξ BEHIND SPHERICAL C-J DETONATION WAVE. Pr = 2.26, ω = 1, T_w = 0 K, $\tilde{\sigma}$ = 2, σ = 1.

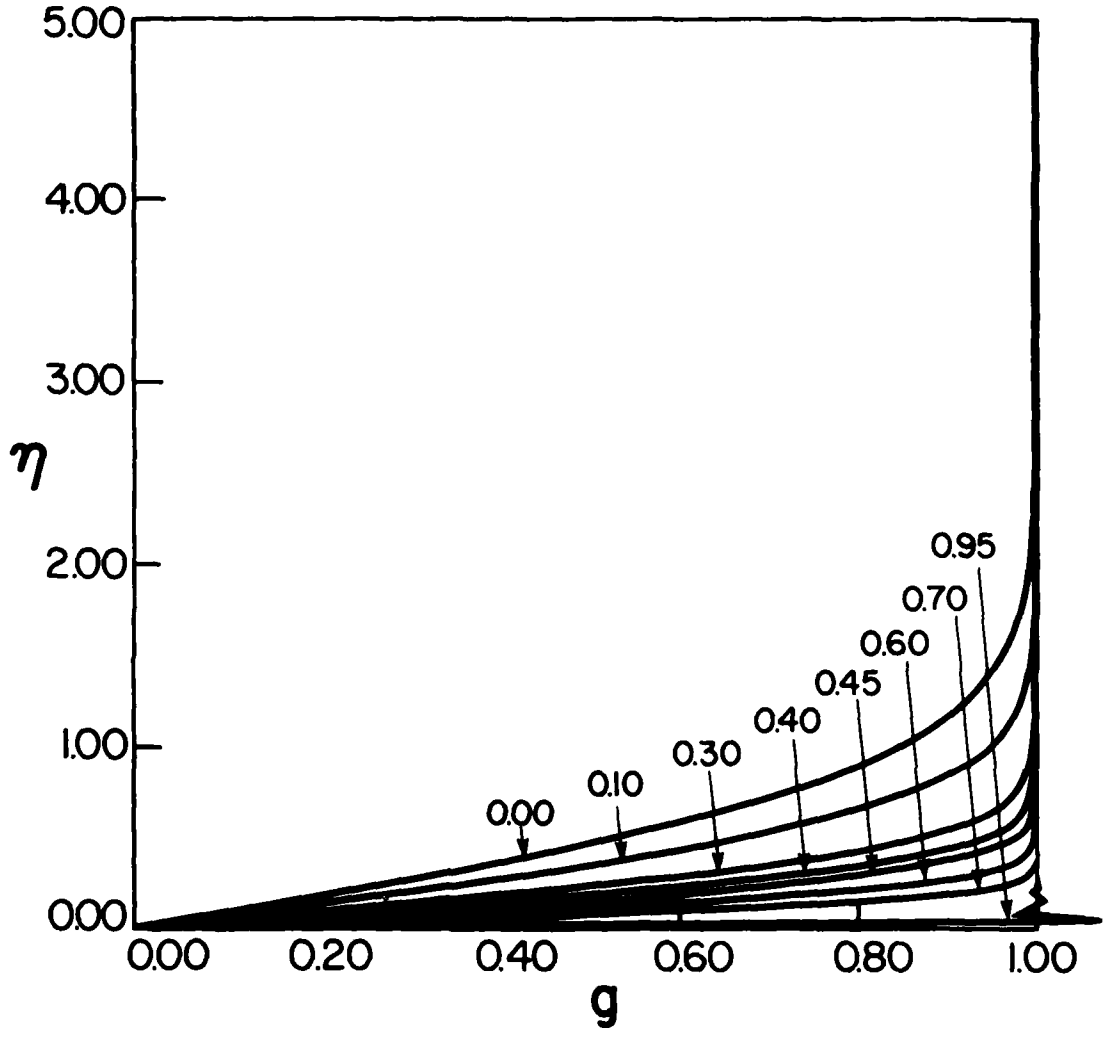

FIG. 37 NORMALIZED TEMPERATURE PROFILES g OF BOUNDARY LAYER WITH DISTANCES η AND ξ BEHIND SPHERICAL C-J DETONATION WAVE. Pr = 2.26, ω = 1, T_w = 0 K, $\bar{\sigma}$ = 2, σ = 1.

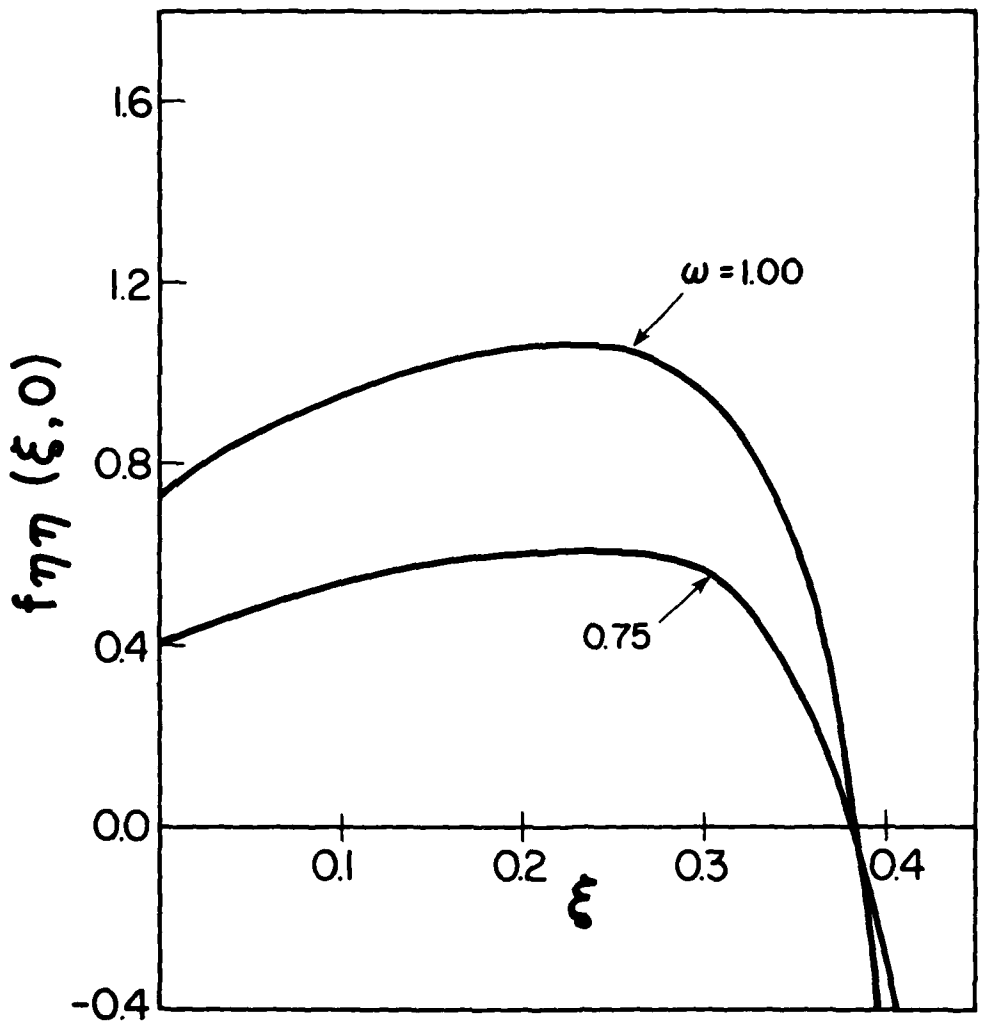

FIG. 38 VARIATION OF NORMALIZED VELOCITY DERIVATIVES $f_{\eta\eta}(\xi,0)$ WITH DISTANCE ξ FOR SPHERICAL C-J DETONATION WAVE. Pr = 2.26, T_w = 300 K, $\bar{\sigma}$ = 2, σ = 1 (FOR DIFFERENT VISCOUS EXPONENT, ω).

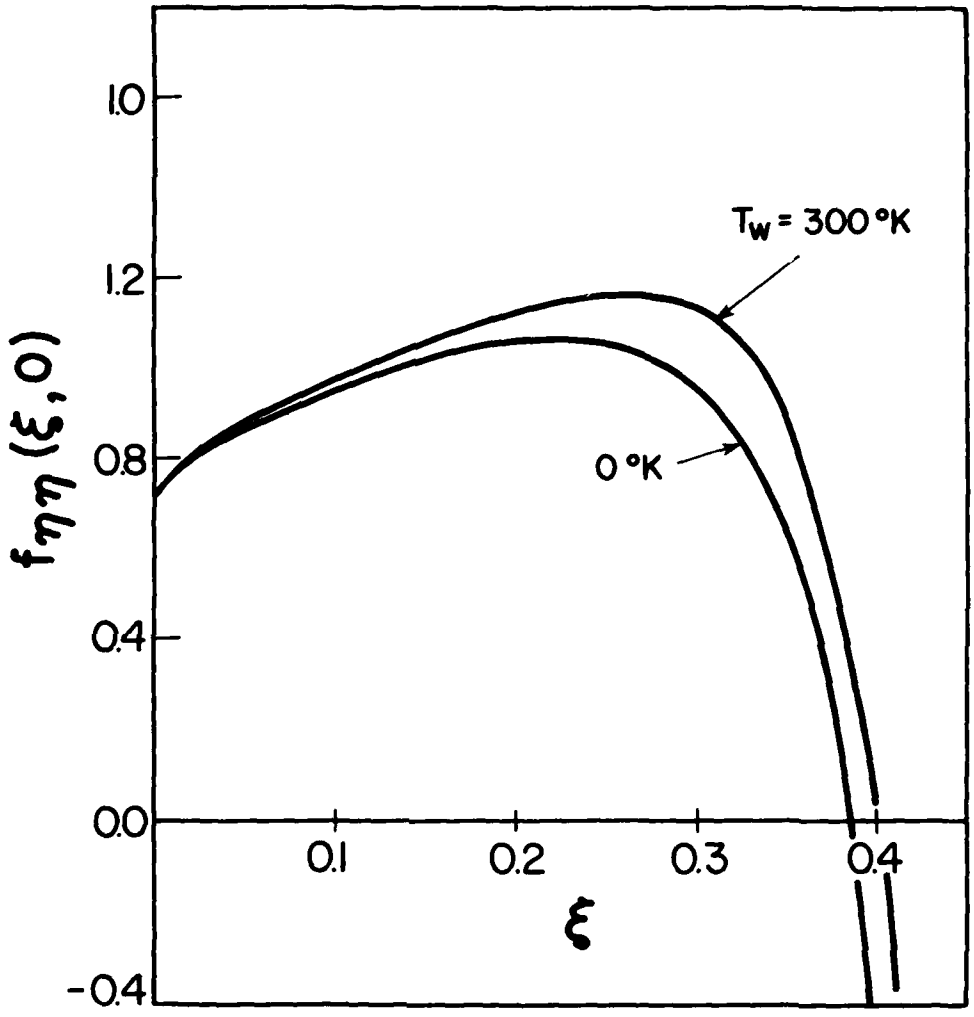

FIG. 39 VARIATION OF NORMALIZED VELOCITY DERIVATIVES $f_{\eta\eta}(\xi,0)$ WITH DISTANCE ξ FOR SPHERICAL C-J DETONATION WAVE. Pr = 2.26, ω = 0.75, $\bar{\sigma}$ = 2, σ = 1 (FOR DIFFERENT WALL TEMPERATURE, T_w).

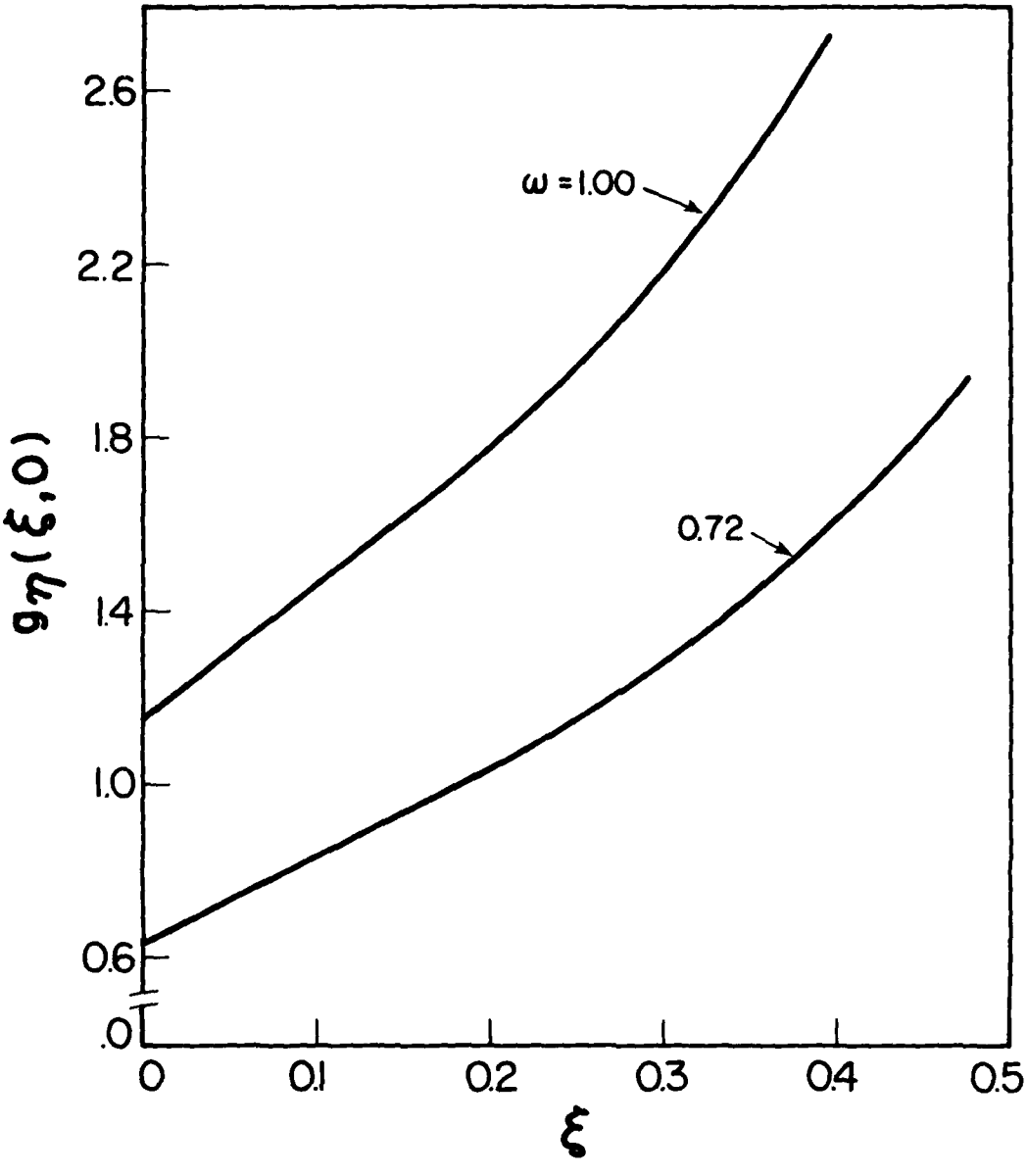

FIG. 40 VARIATION OF NORMALIZED TEMPERATURE DERIVATIVES $g_\eta(\xi,0)$ WITH DISTANCE ξ FOR SPHERICAL C-J DETONATION WAVE. Pr = 2.26, T_w = 300 K, $\bar{\sigma}$ = 2, σ = 1 (FOR DIFFERENT VISCOUS EXPONENT, ω).

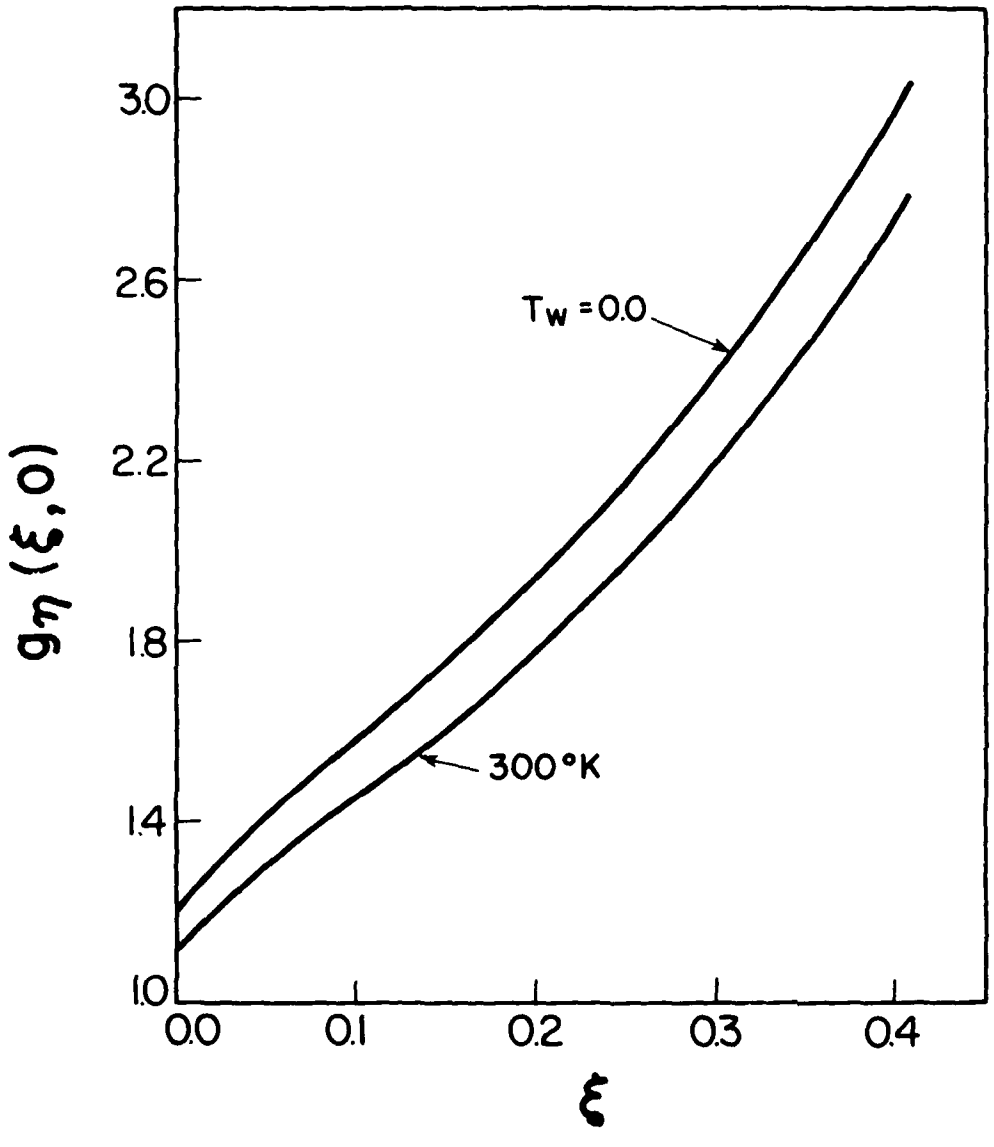

FIG. 41 VARIATION OF NORMALIZED TEMPERATURE DERIVATIVE $g_\eta(\xi,0)$ WITH DISTANCE ξ FOR SPHERICAL C-J DETONATION WAVE. Pr = 2.26, $\omega = 0.75$, $\bar{\sigma} = 2$, $\sigma = 1$ (FOR DIFFERENT WALL TEMPERATURE, T_w).

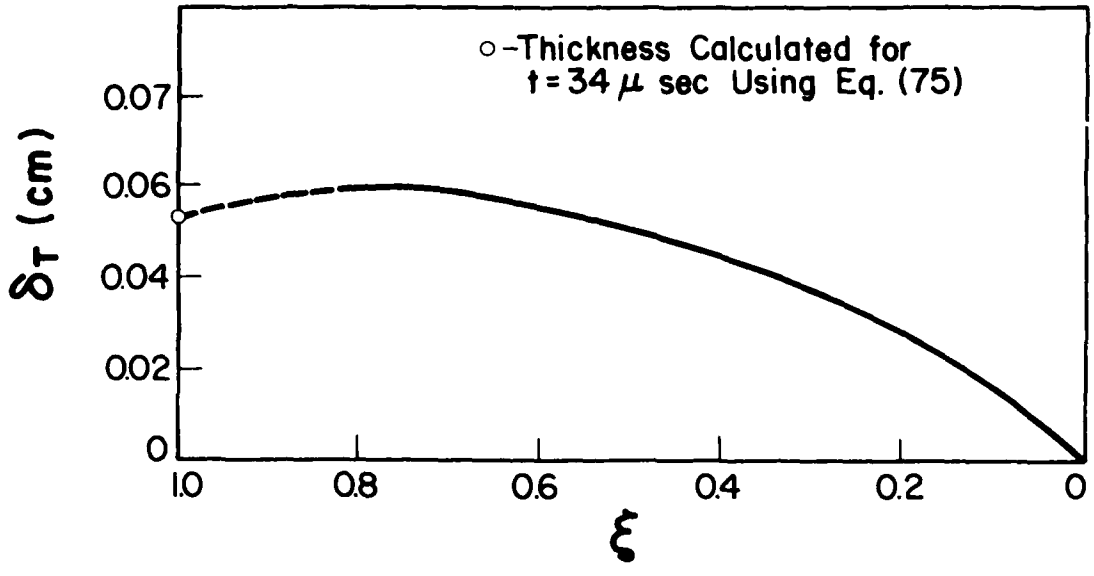

FIG. 42 VARIATION OF THERMAL BOUNDARY-LAYER THICKNESS δ_T WITH DISTANCE ξ FOR UTIAS HEMISPHERICAL IMPLOSION CHAMBER. Pr = 0.26, ω = 0.81, T_w = 300 K, X_s = 10 cm, U_s = 2981 m/sec, $\bar{\sigma}$ = 2, σ = 1.

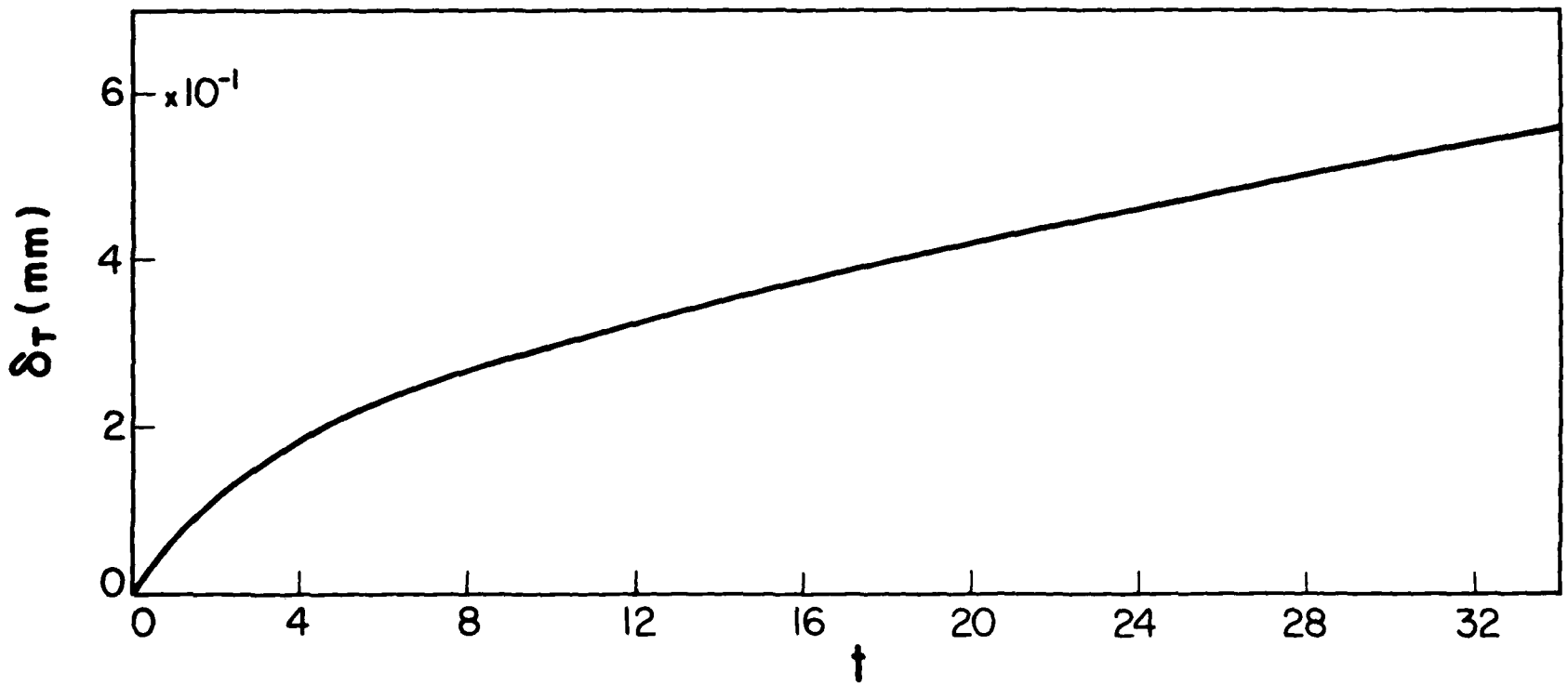

FIG. 43 VARIATION OF THERMAL BOUNDARY-LAYER THICKNESS δ_T WITH TIME AT ORIGIN FOR UTIAS HEMISPHERICAL IMPLOSION CHAMBER.

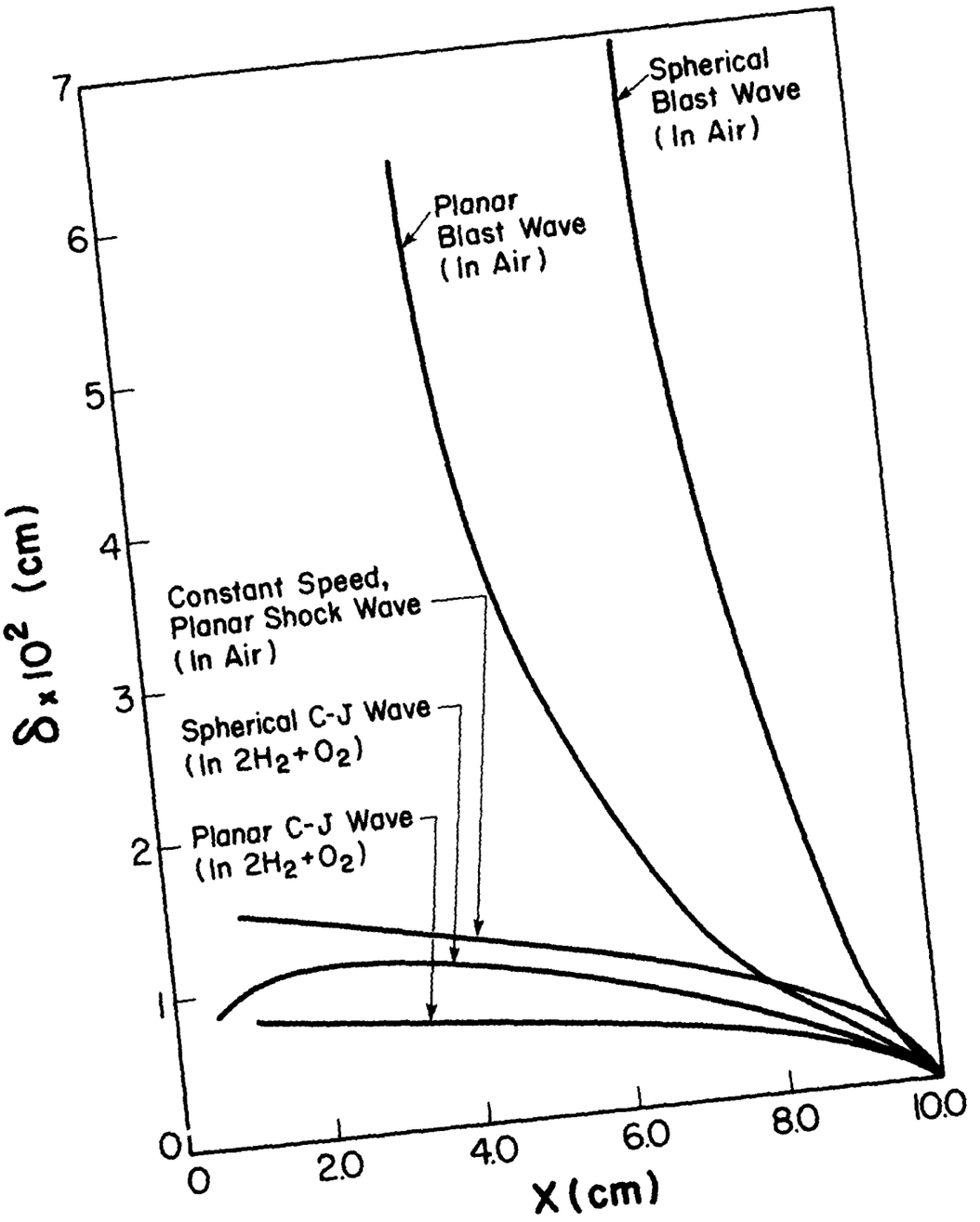

FIG. 44 BOUNDARY-LAYER THICKNESS VARIATIONS δ_V FOR C-J DETONATION WAVES AND STRONG BLAST WAVES (P_∞ = 13.0 kg/cm, T_∞ = 300 K, U_s = 2981 m/sec, X_s = 10 cm) WITH DISTANCE X.

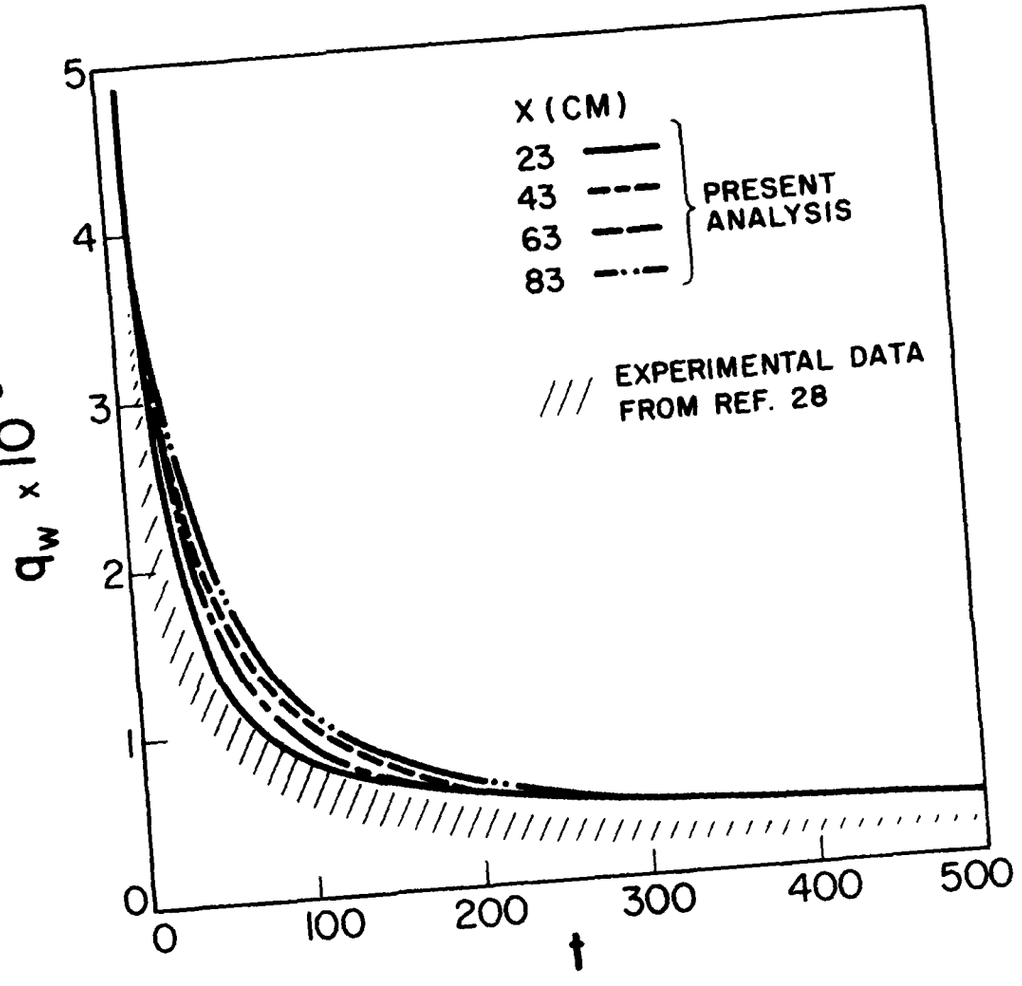

FIG. 45 VARIATION OF ANALYTICAL HEAT TRANSFER q_w (BTU/ft^2 sec) TO THE WALL WITH TIME t (μs) AT DIFFERENT POSITIONS x BEHIND $2H_2+O_2$ GASEOUS DETONATION WAVE AT 1 ATM AND T_∞ = 298.2 K.

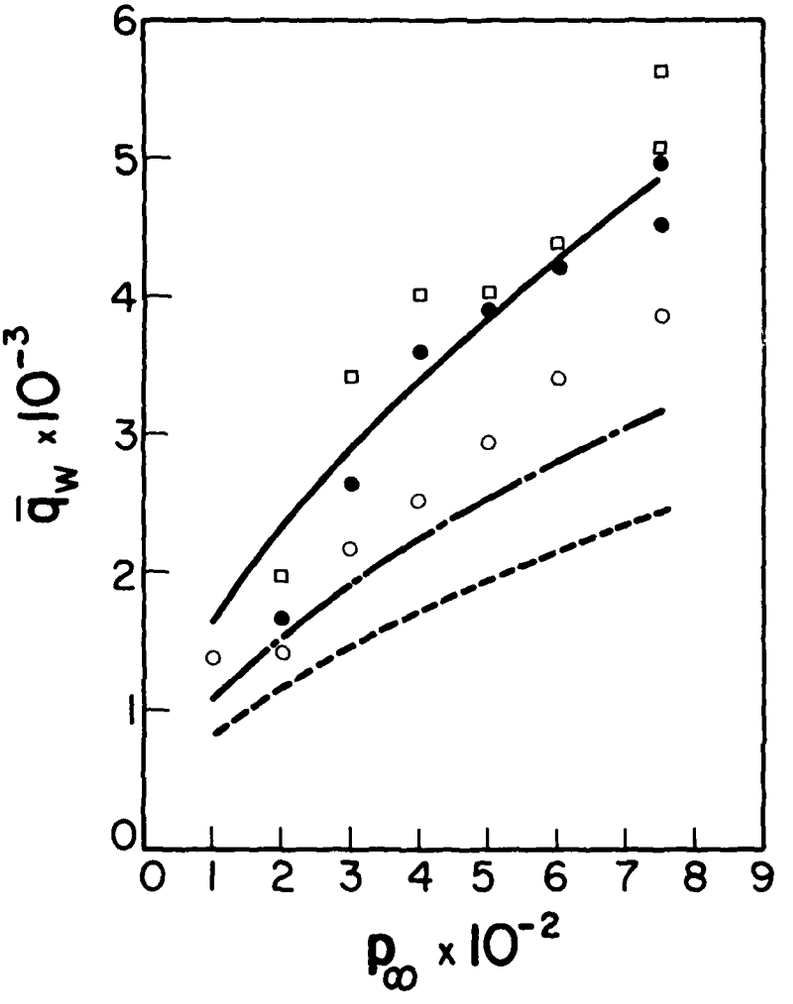

FIG. 46 COMPARISON OF EXPERIMENTAL (□, • AND o FROM REF. 29) AND ANALYTICAL (——, – · – AND – –, PRESENT RESULTS) VARIATIONS OF AVERAGED HEAT TRANSFER, $\bar{q}_w$ (BTU/ft^2 sec) TO THE WALL, OVER 50, 100 AND 150 μs, RESPECTIVELY, WITH INITIAL PRESSURE p_∞ (TORR) BEHIND A HYDROGEN-OXYGEN GASEOUS DETONATION WAVE.

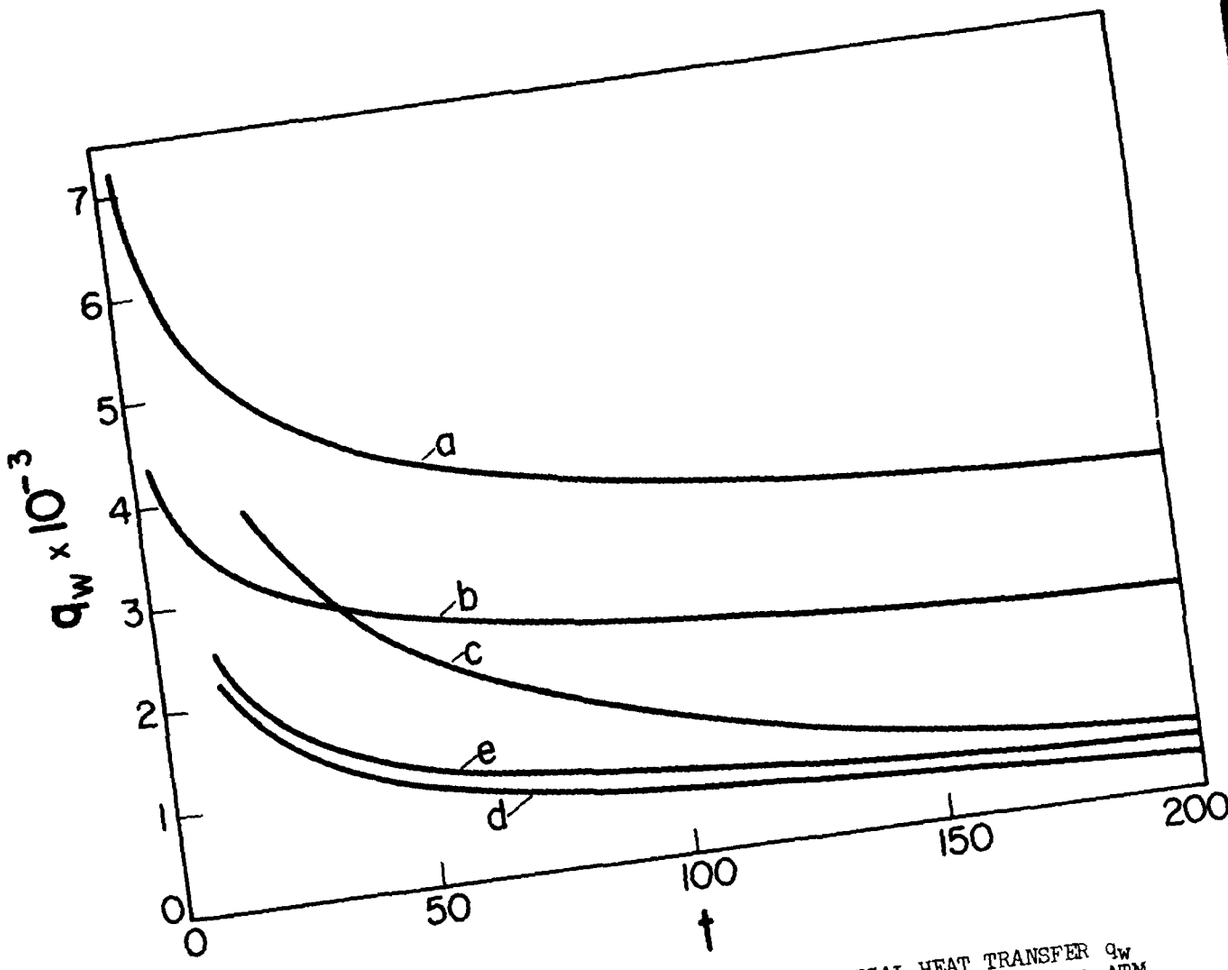

FIG. 47 COMPARISON OF EXPERIMENTAL AND ANALYTICAL HEAT TRANSFER q_w (BTU/ft^2 sec) WITH TIME t (μsec) TO THE WALL BEHIND A 1 ATM HYDROGEN-OXYGEN GASEOUS DETONATION (AFTER REF. 15). (a) EQUILIBRIUM TURBULENT BOUNDARY-LAYER ANALYSIS (SICHEL); (b) FROZEN NON-CATALYTIC TURBULENT BOUNDARY-LAYER ANALYSIS (SICHEL); (c) MEASURED HEAT TRANSFER (RAGLAND); (d) MEASURED HEAT TRANSFER (LADERMAN); (e) EQUILIBRIUM LAMINAR BOUNDARY-LAYER ANALYSIS (PRESENT RESULTS).

APPENDIX A

DERIVATION OF TRANSFORMED BOUNDARY-LAYER EQUATIONS

The unsteady, compressible laminar boundary-layer equations for a perfect gas are:

Continuity:

$$\frac{\partial \rho}{\partial t} + \frac{1}{x^{\sigma}} \frac{\partial (\rho u x^{\sigma})}{\partial x} + \frac{\partial (\rho v)}{\partial y} = 0 \tag{A1}$$

Momentum:

$$\rho \frac{Du}{Dt} = - \frac{\partial p_e}{\partial x} + \frac{\partial}{\partial y} \left(u \frac{\partial u}{\partial y} \right) \tag{A2}$$

Energy:

$$\rho \frac{Dh}{Dt} - \frac{Dp_e}{Dt} = \frac{\partial}{\partial y} \left(\frac{\mu}{Pr} \frac{\partial h}{\partial y} \right) + \mu \left(\frac{\partial u}{\partial y} \right)^2 \tag{A3}$$

State:

$$p = [(\gamma-1)/\gamma] \rho h \tag{A4}$$

To eliminate the explicit dependence on time, Mirels and Hamman [Ref.18] devised a similarity transformation for the lamina boundary-layer induced by a strong blast wave. Only a small modification to their transformation was needed to make it applicable either to blast waves or for detonation waves. The modified transformed coordinates become

$$\tau = t \tag{A5}$$

$$\xi = \left(1 - \frac{x}{x_s} \right) \tag{A6}$$

$$\eta = \frac{x^{\sigma} \int_0^y \frac{\rho}{\rho_{\infty}} dy}{[At^{2m\sigma+2\omega(m-1)+1} \xi]^{1/2}} \tag{A7}$$

For the new variables ξ, η and τ, the derivatives with respect to x, y and t become

$$\frac{\partial}{\partial t} = \frac{\partial \tau}{\partial t} \frac{\partial}{\partial \tau} + \frac{\partial \xi}{\partial t} \frac{\partial}{\partial \xi} + \frac{\partial \eta}{\partial t} \frac{\partial}{\partial \eta} \tag{A8}$$

$$\frac{\partial}{\partial x} = \frac{\partial \xi}{\partial x} \frac{\partial}{\partial \xi} + \frac{\partial \eta}{\partial x} \frac{\partial}{\partial \eta} \tag{A9}$$

$$\frac{\partial}{\partial y} = \frac{\partial \eta}{\partial y} \frac{\partial}{\partial \eta} \tag{A10}$$

For the inviscid flow, we are interested in self-similar motions in the form of

$$x_s = ct^m \tag{A11}$$

Then

$$u_s = cmt^{m-1} \tag{A12}$$

Using Eqs. (A11) and (A12) the derivatives are as follows:

$$\frac{\partial \tau}{\partial t} = 1 \tag{A13}$$

$$\frac{\partial \xi}{\partial x} = - \frac{mt^{-1}}{u_s} \tag{A14}$$

$$\frac{\partial \eta}{\partial y} = \frac{x^{\sigma} \frac{\rho}{\rho_{\infty}}}{[At^{2m\sigma+2\omega(m-1)+1} \xi]^{1/2}} \tag{A15}$$

$$\frac{\partial \xi}{\partial t} = (1-\xi) mt^{-1} \tag{A16}$$

$$\frac{\partial \eta}{\partial t} = \frac{\frac{\partial}{\partial t} \left[x^{\sigma} \int_0^y \frac{\rho}{\rho_{\infty}} dy \right]}{[At^{2m\sigma+2\omega(m-1)+1} \xi]^{1/2}} - \frac{\eta}{2} mt^{-1} \left[2\sigma + \alpha(2\omega-1) + \frac{1}{\xi} \right] \tag{A17}$$

Introducing a scalar stream function defined by

$$u = \frac{\rho_{\infty}}{\rho x^{\sigma}} \frac{\partial \psi}{\partial y} \tag{A18}$$

$$v = - \frac{\rho_{\infty}}{\rho x^{\sigma}} \left[\frac{\partial \psi}{\partial x} + \frac{\partial}{\partial t} \left(x^{\sigma} \int_0^y \frac{\rho}{\rho_{\infty}} dy \right) \right] \tag{A19}$$

substituting Eqs. (A13) to (A19) into Eqs. (A8) to (A10), and adding Eqs. (A10) to (A9), the following derivatives are then obtained

$$\frac{\partial}{\partial t} = \frac{\partial}{\partial \tau} + \frac{\frac{\partial}{\partial t} \left[x^{\sigma} \int_0^y \frac{\rho}{\rho_{\infty}} dy \right]}{[At^{2m\sigma+2\omega(m-1)+1} \xi]^{1/2}} \frac{\partial}{\partial \eta} + (1-\xi) mt^{-1} \frac{\partial}{\partial \xi} - \frac{\eta}{2} mt^{-1} \left[2\sigma + \alpha(2\omega-1) + \frac{1}{\xi} \right] \frac{\partial}{\partial \eta} \tag{A20}$$

$$\frac{\partial}{\partial x} + \frac{\partial}{\partial y} = \frac{\rho_{\infty}}{\rho x^{\sigma}} \frac{\partial \eta}{\partial y} \frac{d\xi}{dx} \left(\frac{\partial \psi}{\partial \eta} \frac{\partial}{\partial \xi} - \frac{\partial \psi}{\partial \xi} \frac{\partial}{\partial \eta} \right) - \frac{\frac{\partial}{\partial t} \left(x^{\sigma} \int_0^y \frac{\rho}{\rho_{\infty}} dy \right)}{[At^{2m\sigma+2\omega(m-1)+1} \xi]^{1/2}} \frac{\partial}{\partial \eta} \tag{A21}$$

Introduce the similarity parameters

$$F(\xi) = \frac{p_e}{\rho_{\infty} u_s^2} \tag{A22}$$

$$\varphi(\xi) = \frac{u_e}{u_s} \tag{A23}$$

$$R(\xi) = \frac{\rho_e}{\rho_{\infty}} \tag{A24}$$

and the temperature ratio

$$\frac{T_e}{T_\infty} = b\,\frac{\rho_\infty}{p_\infty}\,u_s^{\,2}\,\frac{F}{R} \tag{A25}$$

where

$$b = \frac{\gamma(\gamma_\infty-1)C_{p_\infty}}{\gamma_\infty(\gamma-1)C_p}$$

for the inviscid flow. The dimensionless stream function is defined as

$$f(\xi,\eta) = \psi/\{u_e[A\tau^{2m\sigma+2\omega(m-1)+1}\,\xi]^{1/2}\} \tag{A26}$$

The total derivative is defined by

$$\rho\,\frac{D}{Dt} = \rho\,\frac{\partial}{\partial t} + \rho u\,\frac{\partial}{\partial x} + \rho v\,\frac{\partial}{\partial y} \tag{A27}$$

Substituting Eqs. (A22) to (A24) and (A26) into (A20) and (A21), then Eq. (A27) becomes

$$\rho\,\frac{D}{Dt} = -\rho m t^{-1}\left\{\left[\frac{\eta}{2}\,[2\sigma+\alpha(2\omega-1) - (\varphi f_\xi+\varphi_\xi f)\right.\right.$$
$$\left.\left.+\frac{1}{2\xi}\,(\eta-\varphi f)\right]\frac{\partial}{\partial\eta} - (1-\xi-\varphi f_\eta)\,\frac{\partial}{\partial\xi}\right\} + \rho\,\frac{\partial}{\partial\tau} \tag{A28}$$

For the momentum equation, Eq. (A2), the transformation can be done term by term. For $\rho(Du/Dt)$, we have

$$\rho\,\frac{Du}{Dt} = -\rho m t^{-1}u_s\varphi\left\{\left[\frac{\eta}{2}\,(2\sigma+\alpha(2\omega-1) - (\varphi f_\xi+\varphi_\xi f)\right.\right.$$
$$\left.\left.+\frac{1}{2\xi}\,(\eta-\varphi f)\right]f_{\eta\eta} - (1-\xi-\varphi f_\eta)\left(\frac{\varphi_\xi}{\varphi}+\frac{f_{\eta\xi}}{f_\eta}\right)f_\eta - \alpha f_\eta\right\} \tag{A29}$$

For $\partial p_e/\partial x$, using Eqs. (A22) to (A24), the following expression is obtained:

$$-\frac{\partial p_e}{\partial x} = \rho m u_s\varphi t^{-1}\,\frac{g}{R}\,\frac{F_\xi}{\varphi} \tag{A30}$$

where $g = h/h_e = T/T_e$ is the enthalpy or temperature ratio. A new dependent variable is defined as follows:

$$B = \frac{\rho\mu}{\rho_e\mu_e} \tag{A31}$$

With the transformed coordinates, ξ, η, the term $\partial/\partial y[\mu(\partial u/\partial y)]$ can be expressed in the following form

$$\frac{\partial}{\partial y}\left(\mu\,\frac{\partial u}{\partial y}\right) = \frac{x^{2\sigma}\,\frac{\rho}{\rho_\infty}\,u_s\,\rho_e\mu_e\varphi}{[At^{2m\sigma+2(m-1)\omega+1}\xi]}\,(Bf_{\eta\eta})_\eta \tag{A32}$$

Define

$$A = \frac{2C^{2(\sigma+\omega)}\,m^{2\omega-1}\,\mu_\infty}{\rho_\infty}\left[b\,\frac{\rho_\infty}{p_\infty}\,F_o\right]^\omega$$

and note that

$$\frac{x^{2\sigma}}{[At^{2m\sigma+2(m-1)\omega+1}\xi]t^{-1}} = \frac{(1-\xi)^{2\sigma}}{\xi}\,\frac{C^{2(\sigma+\omega)}\,m^{2\omega}}{Au_s^{2\omega}}$$

Substituting Eqs. (A29), (A30) and (A32) into the momentum equation and dividing both sides by $\rho m u_s \varphi t^{-1}$, the following equations are obtained:

$$(1-\xi)^{2\sigma}\,R^{1-\omega}(F/F_o)^\omega(Bf_{\eta\eta})_\eta + (\eta-\varphi f)f_{\eta\eta}$$
$$= 2\xi\left\{\left[f\varphi_\xi + \varphi f_\xi - \frac{\eta}{2}\,[2\sigma+\alpha(2\omega-1)]\right]f_{\eta\eta}\right.$$
$$\left.+\left[\alpha+(1-\xi-\varphi f_\xi)\left(\frac{\varphi_\xi}{\varphi}+\frac{f_{\eta\xi}}{f_\eta}\right)\right]f_\eta - \frac{F_\xi g}{R\varphi}\right\} \tag{A33}$$

for the momentum equation.

The same procedure can be applied to the energy equation, Eq. (A3), term by term:

(1)

$$\rho\,\frac{Dh}{Dt} = -\rho m t^{-1}h_e\left\{\left[\frac{\eta}{2}\,[2\sigma+\alpha(2\omega-1)] - (\varphi f_\xi+\varphi_\xi f)\right.\right.$$
$$\left.\left.+\frac{1}{2\xi}\,(\eta-\varphi f)\right]g_\eta - \left[(1-\xi+\varphi f_\eta)\left(\frac{F_\xi}{F}+\frac{g_\xi}{g}-\frac{R_\xi}{R}\right)\right.\right.$$
$$\left.\left.+2\alpha\right]g\right\} \tag{A34}$$

(2)

$$\frac{Dp_e}{Dt} = -\rho m t^{-1}h_e\,\frac{\gamma-1}{\gamma}\left[(1-\xi+\varphi f_\eta)g\,\frac{F_\xi}{F}+2\alpha g\right] \tag{A35}$$

(3)

$$\frac{\partial}{\partial y}\left(\frac{\mu}{Pr}\,\frac{\partial h}{\partial y}\right) = \frac{x^{2\sigma}\rho h_e\rho_e\mu_e}{[At^{2m\sigma+2(m-1)\omega+1}]\rho_\infty^{\,2}}\left(\frac{B}{Pr}\,g_\eta\right)_\eta \tag{A36}$$

(4)

$$\mu\left(\frac{\partial u}{\partial y}\right)^2 = \frac{x^{2\sigma}\rho u_s^{\,2}\varphi^2\rho_e\mu_e}{[At^{2m\sigma+2(m-1)\omega+1}\xi]\rho_\infty^{\,2}}\,Bf_{\eta\eta}^2 \tag{A37}$$

Noting that

$$\frac{\rho_e\mu_e}{\rho_\infty^{\,2}} = R\,\frac{\mu_\infty}{\rho_\infty}\left[b\,\frac{\rho_\infty}{p_\infty}\,u_s^{\,2}\,\frac{F}{R}\right]^\omega \tag{A38}$$

$$\frac{u_s^{\,2}}{h_e} = \frac{\gamma-1}{\gamma}\,\frac{R}{F} \tag{A39}$$

the transformed energy equation becomes

$$(1-\xi)^{2\sigma}\left\{R^{1-\omega}\left(\frac{F}{F_o}\right)^\omega\left(\frac{B}{Pr}\,g_\eta\right)_\eta + \right. \qquad \text{(Contd.)}$$

$$+ \frac{\gamma-1}{\gamma} \frac{R\varphi^2}{F} R^{1-\omega} \left(\frac{F}{F_o} \right)^{\omega} B f_{\eta\eta}^2 \Big\} + (\eta-\varphi f) g_\eta$$

$$= 2\xi \left\{ \left[f\varphi_\xi + \varphi f_\xi - \frac{\eta}{2} [2\sigma+\alpha(2\omega-1)] \right] g_\eta \right.$$

$$\left. + \left[\frac{2\alpha}{\gamma_1} + (1-\xi-\varphi f_\eta) \left(\frac{g_\xi}{g} + \frac{F_\xi}{\gamma F} - \frac{R_\xi}{R} \right) \right] g \right\} \qquad (A40)$$

APPENDIX B

THERMAL CONDUCTIVITY AND VISCOSITY FOR MULTICOMPONENT GAS MIXTURES

The viscosity μ and thermal conductivity K contained in the momentum and energy equations are estimated by using the following semi-empirical relations given in Ref. 30.

$$\mu = \sum_{i=1}^{n} \frac{N_i \mu_i}{\sum_{j=1}^{n} N_j \phi_{ij}} \qquad (B1)$$

for viscosity of gas mixture, and

$$K = \sum_{i=1}^{n} \frac{N_i K_i}{\sum_{j=1}^{n} N_j \phi_{ij}} \qquad (B2)$$

for thermal conductivity in which

$$\phi_{ij} = \frac{1}{\sqrt{8}} \left(1 + \frac{M_i}{M_j} \right)^{-\frac{1}{2}} \left[1 + \left(\frac{\mu_i}{\mu_j} \right)^{\frac{1}{2}} \left(\frac{M_j}{M_i} \right)^{\frac{1}{4}} \right]^2 \qquad (B3)$$

and n is the number of chemical species in the mixture; N_i and N_j are the mole fractions of species i and j; μ_i and μ_j are the viscosities of species i and j at the system temperature and pressure; and M_i and M_j are the corresponding molecular weights. Note that ϕ_{ij} is dimensionless and when i = j, $\phi_{ij} = 1$. Basically, Eqs. (B1) and (B2) are adequate only at low density. As shown in Figs. B1 and B2, the viscosity and thermal conductivity of a gas approach a definite limit (the low-density limit) as the temperature reaches a very high value at a given pressure. The temperature of the gas mixture behind a C-J wave is about 4000 K. Taking water-steam as an example, the critical temperature is 400 K and the critical pressure is 1 atm. In the region behind a C-J wave, the average pressure is less than 10 atm. Hence, its reduced pressure is less than 10 and its reduces temperature is 10. From Figs. B1 and B2, it can be concluded that the low-density limit is still a good approximation.

APPENDIX C

BOUNDARY LAYER THICKNESS CLOSE TO THE ORIGIN

As pointed out before, the origin is singular for the boundary-layer equations. Near the origin, the solution becomes divergent. Therefore it is necessary to find an alternate way of evaluating the thermal boundary-layer thickness at origin. Since the gas velocity is very small in the middle of the wave behind a C-J detonation, the boundary-layer equations reduce to

$$\rho \frac{\partial h}{\partial t} = \frac{\partial}{\partial y} \left(\frac{\mu}{P_r} \frac{\partial h}{\partial y} \right) \qquad (C1)$$

Assuming that the P_r and C_p are constant, Eq. (C1) can be rewritten in the following form

$$\frac{1}{\alpha} \frac{\partial T}{\partial t} = \frac{\partial^2 T}{\partial y^2} \qquad (C2)$$

where $\alpha \equiv K/\rho C_p$. The corresponding boundary conditions are

$$\begin{aligned} y &= 0, \qquad T = T_w \\ y &\to \infty, \qquad T = T_e \end{aligned} \qquad (C3)$$

The UTIAS implosion chamber is made of steel. Because the thermal conductivity of steel is much

greater than that of the gas and the flow duration of interest is very short, it is reasonable to assume that T_w = constant, that the gas thickness is infinite in the y-direction, its temperature is uniform in the x-direction, and the natural convection heat transfer is negligible. Defininig the temperature difference,

$$\bar{T} = T - T_w \tag{C4}$$

Eq. (C2) can be expressed as

$$\frac{1}{\alpha}\frac{\partial \bar{T}}{\partial t} = \frac{\partial^2 \bar{T}}{\partial y^2} \tag{C5}$$

The boundary conditions of Eq. (C3) become

$$\begin{aligned} y = 0, \quad & \bar{T} = \bar{T}_w = 0 \\ y \to \infty, \quad & \bar{T} = \bar{T}_e = T_e - T_w \end{aligned} \tag{C6}$$

The solution of Eq. C5) is [Ref. 31)

$$\bar{T} = (\bar{T}_e)\,\mathrm{erf}\,\frac{y}{\sqrt{4\alpha t}} \tag{C7}$$

Using the relation of Eq. (C4), the temperature within the thermal boundary layer is

$$T(y,t) = (T_e - T_w)\,\mathrm{erf}\,\frac{y}{\sqrt{4\alpha t}} + T_w \tag{C8}$$

For convention, we define the thermal boundary-layer thickness as $\delta_T = y_e$ at which

$$\frac{T(y_e,t)}{T_e} = 0.99 \tag{C9}$$

According to the previous results for the inviscid flow, the temperature outside the thermal boundary layer can be expressed as

$$T_e = T_\infty \cdot \left(b\,\frac{F}{R}\,\frac{\rho_\infty}{p_\infty}\,u_s^2 \right) \tag{C10}$$

where T_∞ = 298.15 K, b = 1.2594, F = 0.051135, R = 0.669363, u_s = 2981.5 x 10^2 cm/sec, then the temperature is

$$T_e = 12.25\ T_\infty$$

Using these data, the thermal boundary-layer thickness is obtained approximately by

$$\delta_T = y_e = 1.8\ \sqrt{4\alpha t} \tag{C11}$$

According to the definition of $\alpha = K/\rho C_p$, a simple relation holds:

$$\delta_T = 0.94\ \sqrt{t}\ \text{cm} \tag{C12}$$

where t is given in μsec.

APPENDIX D

DERIVATION OF HEAT TRANSFER EXPRESSION

According to the definition of the heat transfer rate to the wall, we can express it as follows:

$$q_w = -K\left(\frac{\partial T}{\partial y}\right)_w \tag{D1}$$

Using the transformed coordinate it then becomes

$$q_w = -\frac{1}{P_r}\,\mu_w \left(\frac{\partial \eta}{\partial y}\right)_w h_e g_\eta(\xi,0) \tag{D2}$$

where

$$\left(\frac{\partial \eta}{\partial y}\right)_w = \frac{x^\sigma \frac{\rho_w}{\rho_\infty}}{\left[A t^{2m\sigma+2\omega(m-1)+1}\xi\right]^{1/2}} \tag{D3}$$

$$t^{2m\sigma+2\omega(m-1)+1} = \frac{x_s^{2\sigma+1}\,u_s^{2\omega-1}}{c^{2(\sigma+\omega)}\,m^{2\omega-1}} \tag{D4}$$

$$A = \frac{2c^{2(\sigma+\omega)}\,m^{2\omega-1}\,\mu_\infty}{\rho_\infty}\left[b\,\frac{\rho_\infty}{p_\infty}\,F_o\right]^\omega \tag{D5}$$

$$h_e = \frac{\gamma}{\gamma-1}\,u_s^2\,\frac{F}{R} \tag{D6}$$

$$TT = \frac{T_e}{T_\infty} = \gamma_\infty b M_s^2\,\frac{F}{R} \tag{D7}$$

$$Re_{\infty s} = \frac{u_s \rho_\infty x_s}{\mu_\infty} \qquad (D8)$$

Putting Eqs. (D3)-(D8) into (D2) and after rearranging, we can get

$$q_w = -\frac{\gamma}{\gamma-1}\frac{1}{P_r}\frac{(1-\xi)^\sigma}{(2\xi)^{1/2}}\left[F^{2+\omega}\left(\frac{TT}{F_o R}\right)^\omega Re_{\infty s}\right]^{1/2} \cdot g^{\omega-1}(\xi,0)g_\eta(\xi,0)\frac{\mu_\infty u_s^2}{x_s} \qquad (D9)$$

If ξ and $Re_{\infty s}$ are replaced by

$$\xi = \frac{u_s t}{x + u_s t}$$

$$Re_{\infty s} = \frac{u_s \rho_\infty x_s}{\mu_\infty}$$

we can get

$$q_w = -\frac{\gamma}{\gamma-1}\frac{g^{\omega-1}(\xi,0)g_\eta(\xi,0)}{\sqrt{2}\,P_r}\left[F^{2+\omega}\left(\frac{TT}{F_o R}\right)^\omega\right]^{1/2} \cdot (1-\xi)^\sigma u_s^2\sqrt{\rho_\infty\mu_\infty}\,(t)^{-0.5} \qquad (D10)$$

Let

$$B_1 = -\frac{\gamma}{\gamma-1}\frac{g^{\omega-1}(\xi,0)g_\eta(\xi,0)}{\sqrt{2}\,P_r}\left[F^{2+\omega}\left(\frac{TT}{F_o R}\right)^\omega\right]^{1/2}(1-\xi)^\sigma$$

and

$$B_2 = u_s^2\sqrt{\rho_\infty\mu_\infty}$$

Finally the heat transfer rate to the wall can be expressed as

$$q_w = -B_1 \cdot B_2 (t)^{-0.5} \qquad (D11)$$

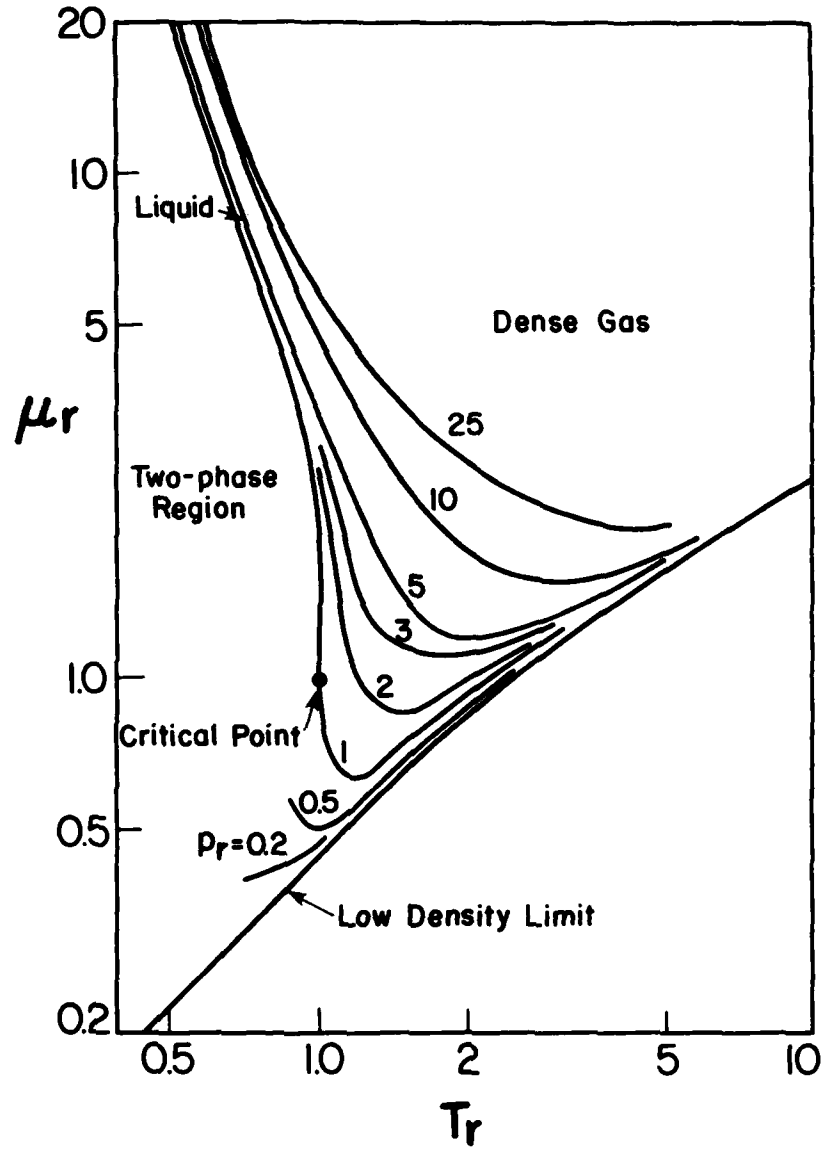

FIG. B1 VARIATION OF NORMALIZED VISCOSITY $\mu_r = \mu/\mu_e$ WITH PRESSURE AND TEMPERATURE $T_r = T/T_e$, $Pr = p/p_e$ (FROM REF. 30).

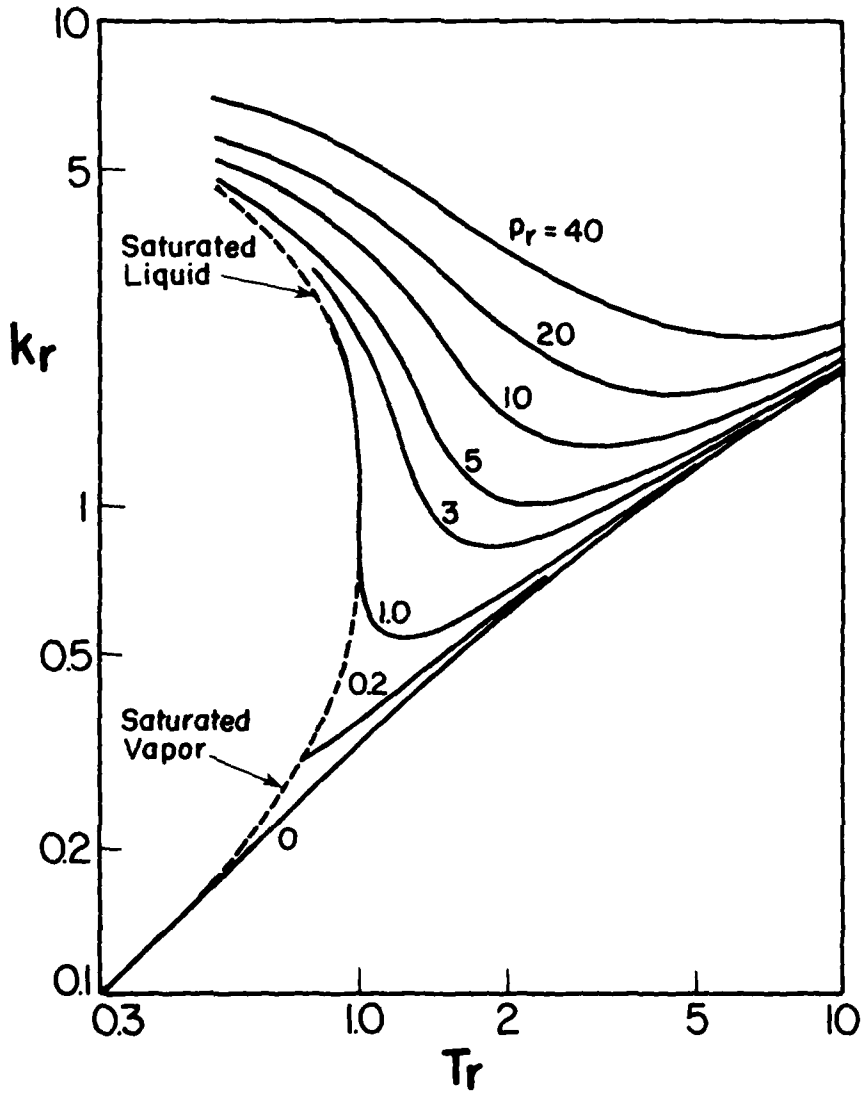

FIG. B2 VARIATION OF CONDUCTIVITY $K_r = K/K_e$ WITH PRESSURE $P_r = P/P_e$ AND TEMPERATURE $T_r = T/T_e$ (FROM REF. 30).

UTIAS Report No. 259

Institute for Aerospace Studies, University of Toronto (UTIAS)
4925 Dufferin Street, Downsview, Ontario, Canada, M3H 5T6

LAMINAR BOUNDARY LAYERS BEHIND BLAST WAVES AND DETONATION WAVES

Du, Xixing; Liu, W. S; Glass, I. I.

1. Blast waves; 2. Detonation waves; 3. Laminar wall-boundary-layers; 4. Comparison with experimental data.

I. Du, Xixing; Liu, W. S; Glass, I. I. II. UTIAS Report No. 259

The transformed coordinates devised by Mirels and Hamman have been modified in such a way that the transformed nonstationary-boundary-layer equations become applicable to boundary-layer flows induced by blast and detonation waves moving with a power-law trajectory in planar, cylindrical and spherical geometries. Investigations were made of boundary-layer flows in air behind nonuniform strong blast waves and in the burned gas of a stoichiometric mixture of hydrogen and oxygen behind uniform Chapman-Jouguet detonation waves. The results show the Prandtl number has a profound influence on the boundary layer flow. For a blast wave and Pr less than unity it controls a boundary-layer velocity overshoot near the wave. The overshoot decreases with increasing Prandtl number. For Chapman-Jouguet detonation waves similar results are obtained for a Pr = 0.71. However, for an actual fluid a Pr = 0.71 is universal and was used. Away from the wave where the inviscid flow velocity approaches a steady state, the results also show that the viscous exponent has a significant effect on the wall shear stress, but not for the heat flux, and that the effect of the wall temperature is small. In order to show a few of the general features of the boundary layers, actual velocity profiles were computed for spherical and cylindrical stoichiometric hydrogen-oxygen and for blast waves in air. It is shown that for a blast wave in air the density behind a blast wave the boundary-layer thickness becomes infinite at the wave. For detonation waves, counterparts at the same wave velocity (but different pressure ratios) the boundary-layer thickness in air behind a quasi-stationary planar shock wave is much greater than that behind a detonation wave at the same wave velocity. In order to test the analyses, the heat flux to the wall behind a planar detonation wave was calculated. The results are in good agreement with other data, and adds confidence to the present analyses for cylindrical and spherical waves.

UTIAS Report No. 259

Institute for Aerospace Studies, University of Toronto (UTIAS)
4925 Dufferin Street, Downsview, Ontario, Canada, M3H 5T6

LAMINAR BOUNDARY LAYERS BEHIND BLAST WAVES AND DETONATION WAVES

Du, Xixing; Liu, W. S; Glass, I. I.

1. Blast waves; 2. Detonation waves; 3. Laminar wall-boundary-layers; 4. Comparison with experimental data.

I. Du, Xixing; Liu, W. S; Glass, I. I. II. UTIAS Report No. 259

The transformed coordinates devised by Mirels and Hamman have been modified in such a way that the transformed nonstationary-boundary-layer equations become applicable to boundary-layer flows induced by blast and detonation waves moving with a power-law trajectory in planar, cylindrical and spherical geometries. Investigations were made of boundary-layer flows in air behind nonuniform strong blast waves and in the burned gas of a stoichiometric mixture of hydrogen and oxygen behind uniform Chapman-Jouguet detonation waves. The results show the Prandtl number has a profound influence on the boundary layer flow. For a blast wave and Pr less than unity it controls a boundary-layer velocity overshoot near the wave. The overshoot decreases with increasing Prandtl number. For Chapman-Jouguet detonation waves similar results are obtained for a Pr = 0.71. However, for an actual fluid a Pr = 0.71 is universal and was used. Away from the wave where the inviscid flow velocity approaches a steady state, the results also show that the viscous exponent has a significant effect on the wall shear stress, but not for the heat flux, and that the effect of the wall temperature is small. In order to show a few of the general features of the boundary layers, actual velocity profiles were computed for spherical and cylindrical stoichiometric hydrogen-oxygen and for blast waves in air. It is shown that for a blast wave in air the density behind a blast wave the boundary-layer thickness becomes infinite at the wave. For detonation waves, counterparts at the same wave velocity (but different pressure ratios) the boundary-layer thickness in air behind a quasi-stationary planar shock wave is much greater than that behind a detonation wave at the same wave velocity. In order to test the analyses, the heat flux to the wall behind a planar detonation wave was calculated. The results are in good agreement with other data, and adds confidence to the present analyses for cylindrical and spherical waves.

Available copies of this report are limited. Return this card to UTIAS, if you require a copy.

UTIAS Report No. 259

Institute for Aerospace Studies, University of Toronto (UTIAS)
4925 Dufferin Street, Downsview, Ontario, Canada, M3H 5T6

LAMINAR BOUNDARY LAYERS BEHIND BLAST WAVES AND DETONATION WAVES

Du, Xixing; Liu, W. S; Glass, I. I.

1. Blast waves; 2. Detonation waves; 3. Laminar wall-boundary-layers; 4. Comparison with experimental data.

I. Du, Xixing; Liu, W. S; Glass, I. I. II. UTIAS Report No. 259

The transformed coordinates devised by Mirels and Hamman have been modified in such a way that the transformed nonstationary-boundary-layer equations become applicable to boundary-layer flows induced by blast and detonation waves moving with a power-law trajectory in planar, cylindrical and spherical geometries. Investigations were made of boundary-layer flows in air behind nonuniform strong blast waves and in the burned gas of a stoichiometric mixture of hydrogen and oxygen behind uniform Chapman-Jouguet detonation waves. The results show the Prandtl number has a profound influence on the boundary layer flow. For a blast wave and Pr less than unity it controls a boundary-layer velocity overshoot near the wave. The overshoot decreases with increasing Prandtl number. For Chapman-Jouguet detonation waves similar results are obtained for a Pr = 0.71. However, for an actual fluid a Pr = 0.71 is universal and was used. Away from the wave where the inviscid flow velocity approaches a steady state, the results also show that the viscous exponent has a significant effect on the wall shear stress, but not for the heat flux, and that the effect of the wall temperature is small. In order to show a few of the general features of the boundary layers, actual velocity profiles were computed for spherical and cylindrical stoichiometric hydrogen-oxygen and for blast waves in air. It is shown that for a blast wave in air the density behind a blast wave the boundary-layer thickness becomes infinite at the wave. For detonation waves, counterparts at the same wave velocity (but different pressure ratios) the boundary-layer thickness in air behind a quasi-stationary planar shock wave is much greater than that behind a detonation wave at the same wave velocity. In order to test the analyses, the heat flux to the wall behind a planar detonation wave was calculated. The results are in good agreement with other data, and adds confidence to the present analyses for cylindrical and spherical waves.

Available copies of this report are limited. Return this card to UTIAS, if you require a copy.

UTIAS Report No. 259

Institute for Aerospace Studies, University of Toronto (UTIAS)
4925 Dufferin Street, Downsview, Ontario, Canada, M3H 5T6

LAMINAR BOUNDARY LAYERS BEHIND BLAST WAVES AND DETONATION WAVES

Du, Xixing; Liu, W. S; Glass, I. I.

1. Blast waves; 2. Detonation waves; 3. Laminar wall-boundary-layers; 4. Comparison with experimental data.

I. Du, Xixing; Liu, W. S; Glass, I. I. II. UTIAS Report No. 259

The transformed coordinates devised by Mirels and Hamman have been modified in such a way that the transformed nonstationary-boundary-layer equations become applicable to boundary-layer flows induced by blast and detonation waves moving with a power-law trajectory in planar, cylindrical and spherical geometries. Investigations were made of boundary-layer flows in air behind nonuniform strong blast waves and in the burned gas of a stoichiometric mixture of hydrogen and oxygen behind uniform Chapman-Jouguet detonation waves. The results show the Prandtl number has a profound influence on the boundary layer flow. For a blast wave and Pr less than unity it controls a boundary-layer velocity overshoot near the wave. The overshoot decreases with increasing Prandtl number. For Chapman-Jouguet detonation waves similar results are obtained for a Pr = 0.71. However, for an actual fluid a Pr = 0.71 is universal and was used. Away from the wave where the inviscid flow velocity approaches a steady state, the results also show that the viscous exponent has a significant effect on the wall shear stress, but not for the heat flux, and that the effect of the wall temperature is small. In order to show a few of the general features of the boundary layers, actual velocity profiles were computed for spherical and cylindrical stoichiometric hydrogen-oxygen and for blast waves in air. It is shown that for a blast wave in air the density behind a blast wave the boundary-layer thickness becomes infinite at the wave. For detonation waves, counterparts at the same wave velocity (but different pressure ratios) the boundary-layer thickness in air behind a quasi-stationary planar shock wave is much greater than that behind a detonation wave at the same wave velocity. In order to test the analyses, the heat flux to the wall behind a planar detonation wave was calculated. The results are in good agreement with other data, and adds confidence to the present analyses for cylindrical and spherical waves.

Available copies of this report are limited. Return this card to UTIAS, if you require a copy.

UTIAS Report No. 259

Institute for Aerospace Studies, University of Toronto (UTIAS)
4925 Dufferin Street, Downsview, Ontario, Canada, M3H 5T6

LAMINAR BOUNDARY LAYERS BEHIND BLAST WAVES AND DETONATION WAVES

Du, Xixing; Liu, W. S; Glass, I. I.

1. Blast waves, 2. Detonation waves, 3. Laminar wall-boundary-layers, 4. Comparison with experimental data
I. Du, Xixing, Liu, W. S, Glass, I. I. II. UTIAS Report No. 259

The transformed coordinates devised by Mirels and Hamman have been modified in such a way that the transformed nonstationary-boundary-layer equations become applicable to boundary-layer flows induced by the blast and detonation waves moving with a power-law trajectory in planar, cylindrical and spherical geometries. Investigations were made of boundary-layer flows in air behind non-uniform strong blast waves and in the burned gas of a stoichiometric mixture of hydrogen and oxygen behind uniform Chapman-Jouguet detonation waves. The results show the Prandtl number has a profound influence on the boundary-layer flow. For a blast wave and Pr less than unity it controls a boundary-layer velocity overshoot as the moves away from the wave. The overshoot decreases with increasing Prandtl number. For a Chapman-Jouguet detonation wave similar results are obtained for a Pr = 0.72. However, for an actual Pr = 0.40, a flow reversal occurs away from the wave where the inviscid flow velocity approaches a small value. The results also show that the viscous exponent has a significant effect on the wall shear stresses and heat transfer, and that the effect of the wall temperature is small. In order to show some of the physical features of the laminar boundary layers, actual velocity profiles were computed for spherical and planar detonation waves in stoichiometric hydrogen-oxygen and for blast waves in air. It is shown that owing to the rapid decrease of density behind a blast wave the boundary-layer thickness becomes very much larger than their detonation wave counterparts at the same wave velocity but different physical conditions. In addition, the velocity boundary-layer thickness in air behind a quasistationary planar shock wave is somewhat more than for a planar detonation wave at the same wave velocity. In order to test the validity of the analysis, the heat transfer to the wall behind a planar detonation wave was calculated. The profile of the variation of the heat transfer with time at any given position behind a C-J detonation wave is in good agreement with the experimental data, and adds confidence to the present analyses for cylindrical and spherical flows as well.

UTIAS Report No. 259

Institute for Aerospace Studies, University of Toronto (UTIAS)
4925 Dufferin Street, Downsview, Ontario, Canada, M3H 5T6

LAMINAR BOUNDARY LAYERS BEHIND BLAST WAVES AND DETONATION WAVES

Du, Xixing; Liu, W. S; Glass, I. I.

1. Blast waves; 2. Detonation waves, 3. Laminar wall-boundary-layers, 4. Comparison with experimental data
I. Du, Xixing; Liu, W. S; Glass, I. I. II. UTIAS Report No. 259

The transformed coordinates devised by Mirels and Hamman have been modified in such a way that the transformed nonstationary-boundary-layer equations become applicable to boundary-layer flows induced by the blast and detonation waves moving with a power-law trajectory in planar, cylindrical and spherical geometries. Investigations were made of boundary-layer flows in air behind non-uniform strong blast waves and in the burned gas of a stoichiometric mixture of hydrogen and oxygen behind uniform Chapman-Jouguet detonation waves. The results show the Prandtl number has a profound influence on the boundary-layer flow. For a blast wave and Pr less than unity it controls a boundary-layer velocity overshoot as the moves away from the wave. The overshoot decreases with increasing Prandtl number. For a Chapman-Jouguet detonation wave similar results are obtained for a Pr = 0.72. However, for an actual Pr = 0.40, a flow reversal occurs away from the wave where the inviscid flow velocity approaches a small value. The results also show that the viscous exponent has a significant effect on the wall shear stresses and heat transfer, and that the effect of the wall temperature is small. In order to show some of the physical features of the laminar boundary layers, actual velocity profiles were computed for spherical and planar detonation waves in stoichiometric hydrogen-oxygen and for blast waves in air. It is shown that owing to the rapid decrease of density behind a blast wave the boundary-layer thickness becomes very much larger than their detonation wave counterparts at the same wave velocity but different physical conditions. In addition, the velocity boundary-layer thickness in air behind a quasistationary planar shock wave is somewhat more than for a planar detonation wave at the same wave velocity. In order to test the validity of the analysis, the heat transfer to the wall behind a planar detonation wave was calculated. The profile of the variation of the heat transfer with time at any given position behind a C-J detonation wave is in good agreement with the experimental data, and adds confidence to the present analyses for cylindrical and spherical flows as well.

Available copies of this report are limited. Return this card to UTIAS, if you require a copy.

UTIAS Report No. 259

Institute for Aerospace Studies, University of Toronto (UTIAS)
4925 Dufferin Street, Downsview, Ontario, Canada, M3H 5T6

LAMINAR BOUNDARY LAYERS BEHIND BLAST WAVES AND DETONATION WAVES

Du, Xixing; Liu, W. S; Glass, I. I.

1. Blast waves, 2. Detonation waves, 3. Laminar wall-boundary-layers, 4. Comparison with experimental data
I. Du, Xixing, Liu, W. S, Glass, I. I. II. UTIAS Report No. 259

Available copies of this report are limited. Return this card to UTIAS, if you require a copy.

UTIAS Report No. 259

Institute for Aerospace Studies, University of Toronto (UTIAS)
4925 Dufferin Street, Downsview, Ontario, Canada, M3H 5T6

LAMINAR BOUNDARY LAYERS BEHIND BLAST WAVES AND DETONATION WAVES

Du, Xixing; Liu, W. S; Glass, I. I.

1. Blast waves, 2. Detonation waves, 3. Laminar wall-boundary-layers, 4. Comparison with experimental data
I. Du, Xixing, Liu, W. S, Glass, I. I. II. UTIAS Report No. 259

Available copies of this report are limited. Return this card to UTIAS, if you require a copy.


DA1
FILM